SYNTHESIS OF GRAPHENE OXIDE/REDUCED GRAPHENE OXIDE-SILVER NANOCOMPOSITES FOR SENSOR APPLICATION

AN 'AMT MOHAMED NOOR

FACULTY OF SCIENCE
UNIVERSITY OF MALAYA
KUALA LUMPUR

2017

SYNTHESIS OF GRAPHENE OXIDE/REDUCED GRAPHENE OXIDE-SILVER NANOCOMPOSITES FOR SENSOR APPLICATION

AN 'AMT MOHAMED NOOR

THESIS SUBMITTED IN FULFILMENT OF THE REQUIREMENTS FOR THE DEGREE OF DOCTOR OF PHILOSOPHY

FACULTY OF SCIENCE
UNIVERSITY OF MALAYA
KUALA LUMPUR

2017

UNIVERSITY OF MALAYA

ORIGINAL LITERARY WORK DECLARATION

Name of Candidate: **AN 'AMT MOHAMED NOOR**

Registration/Matric No: **SHC120063**

Name of Degree: **DOCTOR OF PHILOSOPHY**

Title of Project Paper/Research Report/Dissertation/Thesis ("this Work"):

SYNTHESIS OF GRAPHENE OXIDE/REDUCED GRAPHENE OXIDE-SILVER NANOCOMPOSITES FOR SENSOR APPLICATION

Field of Study: **ADVANCED MATERIALS**

I do solemnly and sincerely declare that:

(1) I am the sole author/writer of this Work;
(2) This Work is original;
(3) Any use of any work in which copyright exists was done by way of fair dealing and for permitted purposes and any excerpt or extract from, or reference to or reproduction of any copyright work has been disclosed expressly and sufficiently and the title of the Work and its authorship have been acknowledged in this Work;
(4) I do not have any actual knowledge nor do I ought reasonably to know that the making of this work constitutes an infringement of any copyright work;
(5) I hereby assign all and every rights in the copyright to this Work to the University of Malaya ("UM"), who henceforth shall be owner of the copyright in this Work and that any reproduction or use in any form or by any means whatsoever is prohibited without the written consent of UM having been first had and obtained;
(6) I am fully aware that if in the course of making this Work I have infringed any copyright whether intentionally or otherwise, I may be subject to legal action or any other action as may be determined by UM.

Candidate's Signature Date: 07 /04/2017

Subscribed and solemnly declared before,

Witness's Signature Date: 07/04/2017

Name:

Designation:

To my wife and sons with love

''Lebatnya hujan seluruh dunia, lebat lagi rahmat dan nikmat Allah''

ABSTRACT

Graphene, a single layer of sp^2-bonded carbon atoms has recently become a huge interest that acts as a potential nanomaterial due to its advantages and unique sensory properties. The incorporation of metal nanoparticles on graphene as nanocomposite has been reported to significantly improved the material properties through surface modification. Hence, the development of the graphene-based nanocomposites has demonstrated excellent potential in the fabrication of highly sensitive sensors. A simple, cheaper, and reproducible technique to prepare graphene-based metal nanocomposites on a large volume is required in order to achieve successful incorporation of metal nanoparticles onto graphene-based materials. Therefore, a novel, easy to handle, less-toxicity, and high yield production of graphene oxide/graphene-based metal nanocomposites has been successfully designed. Herein, the synthesis and characterization have been reported, including the investigation on the relationship between the nanocomposite and the sensor performance. In this thesis, the first part focused on the synthesis of graphene oxide–silver (GO-Ag) nanocomposite which uses a simple ultrasonication irradiation method. The morphology revealed that the spherical Ag nanoparticles with an average size of ~ 12 nm were uniformly distributed on the GO layer. Both the spectral and colorimetric methods were performed on the optical detection of Hg^{2+} ions and the results showed that the limit of detection (LOD) achieved is 0.59 μM. The GO-Ag nanocomposite managed to exhibit good selectivity towards the detection of Hg^{2+} ions in the presence of higher concentration of other environmentally related heavy metal ions. In the electrochemical study, a catalytic current was displayed by the cyclic voltammogram in the reduction of H_2O_2 at the GO-Ag nanocomposite modified glassy carbon electrode (GCE). The nanocomposite modified electrode showed a linear range of 100 μM–11 mM (R^2 =0.988) towards the detection of H_2O_2 by using amperometric *i-t* curve. The LOD was set to be 28.3 μM. On top of that, the

sensor was stable as the current responses were reproducible for the purpose of repeated measurements. The aim for the second part of the study was to synthesize GO-Ag as well as reduced graphene oxide – silver (rGO-Ag) nanocomposite by using microwave irradiation method for the spectrophotometric and surface enhanced raman spectroscopy (SERS) detection of dopamine (DA) including the electrochemical sensing of 4-Nitrophenol (4-NP). The average particle size was found to be ~20 nm, but the size of Ag nanoparticles can be tuned by adjusting the irradiation time. It was also observed that the GO-Ag nanocomposite exhibited good SERS activity on DA substrate with micromolar concentration. Apart from that, the spectrophotometric determination of DA was also studied by using nanocomposite while the response of AgNPs SPR band with the successive addition of DA was linearly increase in absorbance with the red shifting of wavelength of 100 nM to 2 μM concentration range. The LOD was found to be 66.1 nM in determining the DA. In the electrochemical study, the amperometric *i-t* has been used to detect the low concentration of 4-nitrophenol (4-NP). The rGO-Ag nanocomposites modified GCE was also observed to exhibit a notable electrochemical reduction towards 4-NP with a linear range of 1- 10 μM (R^2 = 0.9985) and a detection limit of 0.32 μM. In summary, this work has successfully synthesized GO/rGO-Ag nanocomposites for highly sensitive optical and electrochemical sensor.

ABSTRAK

Graphene, satu lapisan atom karbon terikat secara sp^2 baru-baru ini telah menjadi tarikan minat sebagai bahan nano yang berpotensi kerana kelebihan dan ciri-ciri sensor yang unik. Penyatuan nanopartikel logam pada graphene sebagai nanokomposit telah dilaporkan, meningkatkan sifat bahan melalui pengubahsuaian permukaan. Oleh itu, pembuatan nanokomposit berdasarkan graphene telah menunjukkan potensi yang cemerlang dalam pembuatan sensor yang sangat sensitif. Dalam usaha untuk mencapai kejayaan menyatukan nanopartikel logam pada bahan berasaskan graphene, kaedah yang mudah, murah dan dapat diulang kembali bagi menyediakan graphene berasaskan nanokomposit logam pada jumlah yang besar amat diperlukan. Dengan itu, kaedah yang tulen, mudah untuk dikendalikan, kurang toksik, dan hasil yang tinggi bagi pengeluaran graphene oksida/graphene nanokomposit berasaskan logam telah berjaya dibangunkan. Di sini, sintesis dan pencirian telah dilaporkan termasuk siasatan ke atas hubungan antara nanokomposit dan prestasi sensor. Dalam kajian ini, bahagian pertama akan fokus kepada sintesis nanokomposit graphene oksida-perak (GO-Ag) menggunakan kaedah sinaran ultrasonik. Morfologi menunjukkan nanopartikel Ag berbentuk sfera dengan purata saiz ~ 12 nm telah disebarkan secara seragam di atas lapisan GO. Kaedah spektrum dan kolorimetrik telah dijalankan untuk pengesanan optik pada ion Hg^{2+} dan keputusan menunjukkan had pengesanan (LOD) adalah 0.59μM. Nanokomposit GO-Ag mempamerkan pemilihan tertentu yang baik terhadap pengesanan ion Hg^{2+}dengan kehadiran ion logam berat lain yang berkaitan dengan alam sekitar. Dalam kajian elektrokimia, kitaran voltammogram memaparkan arus pemangkin bagi penurunan H_2O_2 pada elektrod gelas karbon (GCE) ubahsuai dengan nanokomposit GO-Ag. Elektrod ubahsuai dengan nanokomposit menunjukkan julat linear daripada 100 μM-11 mM (R^2 = 0.988) terhadap pengesanan H_2O_2 dengan menggunakannya lekuk amperometric *i-t*. Nilai LOD yang telah dikira ialah 28.3 μM. Dalam pada itu, sensor

adalah stabil dimana respon arus sama bagi setiap ulangan pengukuran dilakukan. Bahagian kedua kajian ini adalah untuk mensintesis nanokomposit GO-Ag dan penurunan graphene oksida - perak (rGO-Ag) dengan menggunakan kaedah penyinaran gelombang mikro untuk spektrofotometri dan spektroskopi raman dipertingkatkan oleh permukaan (SERS) pengesanan terhadap dopamin (DA) dan penderiaan elektrokimia terhadap 4 -Nitrophenol (4-NP). Purata saiz zarah didapati ialah ~ 20 nm, di mana saiz nanopartikel Ag boleh diubah dengan mengubah masa penyinaran. Kami telah mendapati bahawa nanokomposit GO-Ag mempamerkan aktiviti SERS yang baik di atas substrat DA dengan kepekatan micromolar. Penentuan spektrofotometri bagi DA juga telah dikaji menggunakan nanokomposit dan respon jurang bagi AgNPs SPR meningkat dengan penambahan DA secara linear dengan peralihan panjang gelombang merah dalam julat kepekatan 100 nM - 2 μM julat kepekatan. LOD didapati adalah 66.1 nM bagi penentuan DA. Dalam kajian elektrokimia, lengkuk amperometrik *i-t* telah digunakan untuk pengesanan bagi kepekatanrendah 4-nitrophenol (4-NP). GCE ubahsuaidengan nanokomposit rGO-Ag mempamerkan penurunan elektrokimia yang ketara terhadap 4-NP pada julat linear 1- 10 μM (R^2 = 0.9985) dengan had pengesanan 0.32 μM. Sebagai ringkasan, kerja-kerja ini telah berjaya mensintesis nanokomposit GO/rGO-Ag bagi sensor optik dan elektrokimia yang sangat sensitif.

ACKNOWLEDGEMENTS

Alhamdulillah thanks to Allah S.W.T. This thesis would not have been possible without Him.

First of all, i would like to express my deepest gratitude to my supervisor, Dr Huang Nay Ming whose ideas, suggestions and financial support helped me for the whole duration of research work and thesis writing up. It was a great experience to be working with you. I want to thank my colleagues, Azriena, Marlinda, Shahid Mehmood, Su Pei, John, Ban, Nurul and friends in the Low Dimensional Materials Research Centre for helping me throughout these years. Many thanks to Dr. Perumal Rameshkumar for the valuable advice given to me especially during the manuscript writing.

I would also like to thank the Department of Physics for providing me support and facilities, University Malaya PPP Grant (PG074-2013B), Ministry of Higher Education of University of Malaysia Research Grant, UMRG Programme (RP007C/13AFR), High Impact Research Grant (UM.C/625/1/HIR/MOHE/05), and Universiti Malaysia Kelantan for the SLAB/SLAI scholarship sponsored.

Last but no least, i would like to thank my family especially my wife Nasrun Hasenan, my sons An'ayyash and An'areesh and also my parents Aminah binti Mohd Nor and Mohamed Noor bin Salleh who give strength, support, and freedom to pursue my study. Thank you for your endless love. Thank you.

TABLE OF CONTENTS

LIST OF FIGURES

LIST OF TABLES

LIST OF SYMBOLS AND ABBREVIATIONS

4-NP	:	4-Nitrophenol
AFM	:	Atomic force microscope
AgNPs	:	Silver nanoparticles
CV	:	Cyclic voltammetry
CVD	:	Chemical vapor deposition
DA	:	Dopamine
FESEM	:	Field emission scanning electron microscopy
GCE	:	Glassy carbon electrode
GO	:	Graphene oxide
H_2O_2	:	Hydrogen peroxide
HOPG	:	Highly oriented pyrolitic graphite
HRTEM	:	High resolution transmission electron microscopy
IUPAC	:	International union of pure and applied chemistry
LOD	:	Limit of detection
LSV	:	Linear sweep voltammetry
rGO	:	Reduced Graphene Oxide
SERS	:	Surface enhanced raman spectroscopy
SiC	:	Silica carbide
SPR	:	Surface Plasmon Resonance
TEM	:	Transmission electron microscopy
UV-vis	:	Ultra violet - visible spectroscopy
XPS	:	X-ray photoelectron spectroscopy
XRD	:	X-ray diffraction

CHAPTER 1:
INTRODUCTION

The ability to manipulate objects and modify the scale dimensions has dramatically resulted in the development of current technology. These abilities can be applied in the industry that has high demand of manufacturing and producing compact industrial equipment. Hence, various studies have been conducted to generate, synthesis, and use the materials that are made of small size and dimensions. The idea to further explore into small dimension was triggered by the Physics Nobel Prize winner Richard P. Feynman in 1959. At the annual conference of the Association of the United States of Physics (APS) held in California Institute of Technology, a talk entitled "*There 's Plenty of Room at the Bottom*" was presented by Richard. It was strongly urged the scientific community to control, study, and modify the material with small dimension. It is expected that at these dimensions to have the ability to exploit the properties of nanoparticles that will bring various benefits related to human and environment. These are the earliest thoughts that were considered in the direction of "nanotechnology". The term nanotechnology has been used since the early 1974 and was introduced by Dr. Norio Taniguchi in his speech entitled "On the Basic Concept of Nano-Technology". Nano means infinitesimal and the word was derived from the Greek word *nanos* which means small. Presently, it has been used as a prefix in the list of standard physics unit which refers to one per billion (10^{-9}).

Nanotechnology is the science of hybrid that combines physics, chemistry, biology, and engineering in order to fashion, characterize, produce, and apply a device or system by simply controlling the shape and size on the nanometer scale. Undeniably, the nanomaterials show significant different properties as compared to the macroscopic materials. Furthermore, the arrangements of atoms are capable to alter the properties of the materials. For example, the tetrahedral lattice arrangement of carbon atoms will give

a diamond while the layered sheets arrangement of carbon atoms will produce graphite. The era of nanotechnology research is rapidly growing as a special ability in order to prevail in multiple disciplines. This growth can be achieved by an approval of funds that is worth RM 156 millions under the Tenth Malaysia Plan (RMK10) as well as the launch of the National Graphene Action Plan (NGAP) 2020, known as the "strategic and calculated venture on graphene" under the Eleventh Malaysia Plan (RMK11).

1.1 Graphene-silver nanocomposite

This thesis will focus on AgNPs decorated GO and rGO as the sensing application despite the fact that many reported sensors materials have shown to possess a very good sensing capability. These nanocomposites are used as the main materials to detect the analytes in various detection techniques.

1.2 Scope of Research

The focus presented in this thesis is based on the production of graphene oxide, graphene, and graphene silver nanocomposite conducted on various sensors applications with targeted properties especially the nanocomposites, which is operated via two techniques known as the microwave as well as the sonication processing. The major challenges driving through this doctoral work is to prepare graphene nanocomposites in producing a highly pristine graphene for sensors applications by using simple, easy, and cost-effective techniques. The difficulty of exfoliation from graphite as well as the rapid aggregation of the graphene layer caused by the strong van der Waals interaction has become the major drawbacks in allowing the graphene to be applied at their best performance. Herein, an effort has been placed in the processing and optimizing the silver metal amount in order to enhance the sensors performance.

1.3 Research Objectives

(1) To develop an easy, cost-effective, and less toxic method in synthesizing graphene nanocomposite to be used for sensor application. The target is to yield graphene, maximize its quality, and preserve its unique properties.

(2) To investigate and evaluate the properties of graphene nanocomposite as active material for sensors.

(3) To optimize the methodology parameter that affects the sensor sensitivity such as the incorporation conditions the silver metals. Extra care is necessary to be taken in order to achieve the best sensor performance.

(4) To understand the relationship between materials and sensor performance.

1.4 Outline of Thesis

Chapter 1 begins with the history on the discovery of graphene, the scopes of the research, and the objective of the thesis.

Chapter 2 discusses a comprehensive detail on graphene, which is then followed by its synthesizing and characterizing techniques. A brief discussion on the background, the working principles of the sensing technique, and the component for sensing applications are also presented.

Chapter 3 demonstrates the research methodology in preparing graphene oxide through the oxidation process of graphite as well as its characterization techniques. The instruments such as x-ray diffraction (XRD), Raman spectroscopy, ultra violet - visible spectroscopy (UV-vis), x-ray photoelectron spectroscopy (XPS), field emission scanning electron microscopy (FESEM), transmission electron microscopy (TEM), and electrochemical analysis were used in the study of characterization and properties.

Chapter 4 discusses the preparation, characterization, and sensors performance which are based on the synthesized nanocomposite:

In Chapter 4.1 the preparation, characterization of GO-Ag nanocomposite, and its optical sensing towards mercury ions are elaborated. Ag nanoparticle managed to uniformly decorate the GO layer and provide good surface plasmon resonance effect which contributed to the optical sensor by using horn sonicator. Furthermore, this technique is able to enhance the dispersion and yield the graphene nanocomposite.

Chapter 4.2 delves into the electrochemical determination of H_2O_2 by using amperometric technique. The assay was found to exhibit a good selectivity together with the common interference and become highly stable and reproducible for the repetitive experiments.

Chapter 4.3 reports the experimental setup for the synthesis and characterization of graphene oxide-silver (GO-Ag) nanocomposite for the SERS and optical sensor towards dopamine. The relationship between the present Ag nanoparticles with respect to the sensors performance was investigated and it was found that the Ag nanoparticles successfully helped to enhance the SERS properties.

Chapter 4.4 focuses on the development of reduced graphene oxide-silver (rGO-Ag) nanocomposite that will be applied in the electrochemical detection of 4-nitrophenol. The efficiency of the electrochemical sensor is further improved by incorporating Ag nanoparticles onto the rGO layer. The rGO-Ag nanocomposite is presented as an efficient electrode for electrochemical reaction.

The whole project that has been presented and discussed in this thesis is summarized in Chapter 5. With the achieved results, it can be concluded that an easy and simple way to synthesize graphene silver nanocomposite while preserving its sensing performance

managed to be explored. Finally, a possible future direction of this thesis is proposed at the end of the chapter.

CHAPTER 2:
LITERATURE REVIEW

2.1 Carbon Materials

Carbon is an interesting chemical element in this universe. It can be modified into a broad variety of architectures based on the macroscopic and nanoscopic scales. On top of that, carbon was claimed to be the most versatile elements in the periodic table due to its types of bonding (single, double, and triple bonds), including the bonding with different atoms. In the ground state which possesses the lowest energy of the electronic configuration, $1s^2 2s^2 2p^2$, the two core electrons at 1s will not react to form chemical bonding, while four valence electrons at 2*s* and 2*p* will react to form a bonding. There will be two unpaired 2p electrons which normally form only two bonds in the ground state. Apart from that, the chemical bond formation could result in the decrease of the system energy, which caused the carbon to maximize the number of bonds formed. The process of hybridization will take place in order to rearrange the configuration of the valence electrons, where by only 2*s* and 2*p* electrons are involved. One 2*s* electron will be promoted into an empty 2*p* orbital to form an excited state. In this excited state, the carbon is able to form four bonds which lead to the *sp*3 hybrid orbitals formation. Diamond is the typical molecule that satisfies this arrangement in various face-centered cubic crystals, namely diamond lattice. All the carbon atoms are present in the sp^3 hybridization and possess extreme mechanical properties due to the strong sp^3 covalent bonding between the atoms.

Another hybridization being considered is the interaction of three atomic orbitals among the four (one 2*s* orbital and two 2*p* orbitals), which causes the formation of three sp^2 hybrid orbitals filled with one electron. In the hybridization arrangement, the three sp^2 hybrid orbitals will form a bond with the three neighbors while the overlap of the orbitals will form π bonds between the carbon atoms, which correspond to the carbon-carbon double bond. Graphite is a three-dimensional crystal made of stacked layers

consisting of sp^2 hybridized carbon atoms. The structure shows the presence of strong covalent bonds while the π bonds provide weak interaction between the layers in the graphite structure. The stable bonding that occurs between carbon atoms under room temperatures and pressure is called graphite.

A single layer of graphite is also known as a 'Graphene'. It has been famous since it was discovered by Geim and Novoselov in 2004, in which they were rewarded with the 2010 Nobel Prize in Physics for 'groundbreaking experiments'. Since that moment, graphene has been intensively studied in order to come up with a number of ideas, including the electrical/electronic, mechanical, thermal, and medical properties. However, the vast research is not limited only to a certain particular field, but covers many areas such as chemistry, physics, engineering, materials science, and biology (Gogotsi, 2011, Wang et al., 2012, Novoselov et al., 2005, Guinea et al., 2009, Nair et al., 2008, He et al., 2010). The combination of a single layer of carbon atoms is arranged in a honeycomb like structure; however, the fact that graphene manufacturing is cost effective because the raw material comes from graphite has made graphene the ultimate 2 dimensional carbon molecules in the carbon family.

2.2 Historical Overview

In 1947, Philip Wallace had conducted a theoretical study on the electronic structure of graphite which provides a limited finding on graphene. A following study was conducted by Semenoff et al. (1984), in which they discovered that electricity has the ability to be transferred as charge carriers through the surface of graphene layer. The 'graphene' term was first mentioned in 1987 when Mouras et al. tried to describe the individual layer of carbon in the intercalation compounds formed in the graphite. Numerous attempts have been made in order to study the graphene layer, but the strong interactions with the surface that caused the charge to be transferred from the substrate to the single layer carbon has made it nearly impossible to be experimented.

In the year 2004, Geim and Novoselovof the University of Manchester were the first to isolate the elusive material and managed to successfully produce free-standing graphene flakes. The "Scotch-Tape method" that peels off the graphitic layers from the graphite layers by using a scotch-tape had become the fundamental of their research. This repeated action of peeling off is also known as "mechanical exfoliation". The remaining thin flakes of graphite were then transferred onto silicon dioxide which is coated with silicon substrate. A stable 2-D graphene layers with the thickness of a few atomic layers was successfully produced.

Apart from carbon, graphene which is the most explored nanotube material that is currently being studied regarding their application in the technology of electronic, mechanical, biomedical, photochemical, and environmental studies. It has become the most extensively studied material with more than 20,000 publications as shown in Figure 2.1 since it was officially famous in 2004, which makes graphene as one of the highly investigated compounds in materials science.

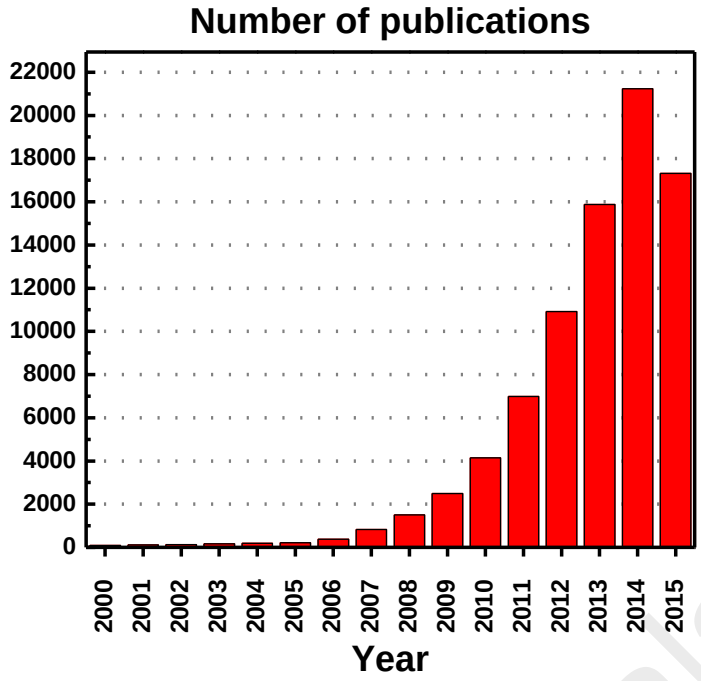

Figure 2.1: Publications on graphene from 2000 to September 2015. Data collected from ISI Web of Science (Search: Topic = Graphene). The end of 2015 expects over 22000.

2.3 Graphene

Graphene is known as 'two-dimensional planar sheet of sp^2 hybridized carbon atoms which are arranged into a honeycomb lattice with a carbon to carbon bond length of 0.142 nm'. It is the basic building block for graphitic family and can be wrapped into 0-D fullerenes, 1-D nanotubes or stacked into 3-D graphite as presented in Figure 2.2. According to the definition provided by IUPAC, graphene is 'a single atomic plane of graphite, which is sufficiently isolated from its environment to be considered free standing'.

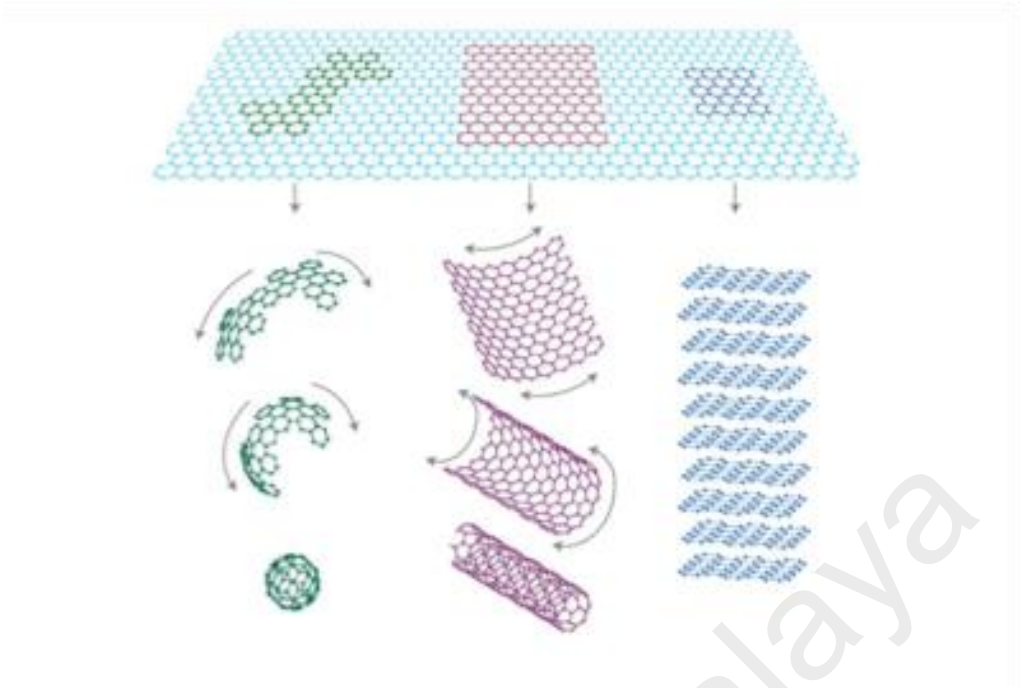

Figure 2.2: The basic of all graphitic form (source: Geim & Novoselov, 2007). Buckyball (a), nanotube (b) and graphene (c).

2.4 Synthesis of Graphene

2.4.1 Mechanical Exfoliation

In 2004, Geim and Novoselov from the University of Manchester have reported the first finding on the exfoliation of monolayer graphene from the graphite by transferring it onto a 300 nm silicon dioxide substrate (Novoselov et al., 2004). As shown in Figure 2.3, a graphene layer can be collected through mechanical exfoliation by peeling it off from highly oriented pyrolytic graphite (HOPG) by using Scotch tape. The thin layers of graphene are highly transparent to the bare eye, thus an optical microscope was chosen to visualize it due to the optical contrast between the graphene sheet and SiO_2 substrate. The thickness of few layers graphene was then measured using Atomic force microscopy (AFM). The quality of the prepared graphene using this technique is very high without any defects detected. However, the graphene prepared using this particular technique is not suitable for large-scale production and possess lack of controllability.

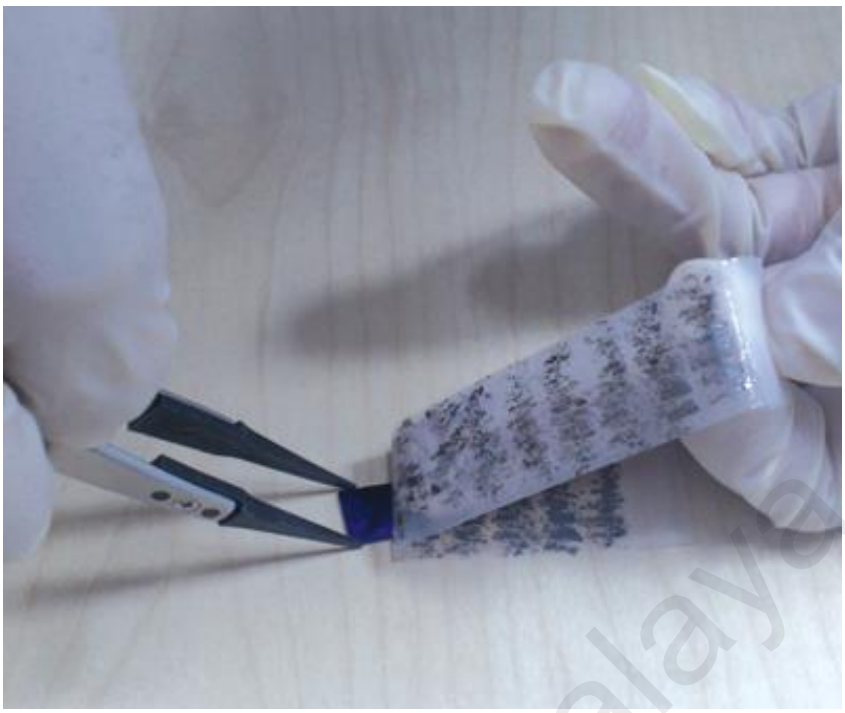

Figure 2.3: Scotch tape technique for peeling of monolayer and few-layer graphene. Source: (Van, 2012).

2.4.2 Epitaxial Growth

Epitaxial growth refers to the deposition of a crystalline layer on a crystalline substrate. The graphene is basically prepared by heating the silicon carbide (SiC) to high temperatures (> 1000 °C) and under low pressures (~10^{-6} torr). During the process, the silicon atoms will migrate from the surface by leaving behind rearranged carbon atoms which forms few layers graphene. A monolayer graphene on silicon carbide substrate was synthesized and introduced by A. J. Van Bommel group (Bommel et al., 1975). Since then, the epitaxial growth technique has become very popular among the researchers, for example, Hass et al. reported the growth mechanism and electronic properties of graphene layer on SiC (Hass et al., 2008). Apart from that, Juang et al. (2009) has reported some modifications on epitaxial growth by growing the epitaxial graphene on SiC substrate at 750 °C (low temperature). Meanwhile, Emtsev et al. (2009) prepared the epitaxial graphene on SiC substrate in argon atmosphere at

atmospheric pressure, which offers a very high potential for large-scale production and in-situ implementation on the fabrication of electronic devices. However, it must be noted that it is very hard to control the thickness of epitaxial graphene which is very crucial for electronic performance.

2.4.3 Chemical Vapor Deposition

Chemical vapor deposition (CVD) is a bottom-up technique which is applied in producing monolayer or few-layer graphene. The versatility of this technique has attracted the attention of many researchers because it is normally used to deposit diamond and carbon related material. Generally, the process is carried out with carbon sources such as methane (CH_4) diluted with hydrogen H_2 (Zhang et al., 2013, Celebi et al., 2012). The carbon source is decomposed through thermal process and a new carbon species that is produced will be adsorbed on the surface of a catalytic substrate such as copper (Bae et al., 2010), nickel (Kim et al., 2009), and cobalt (Blake et al., 2008) to form monolayer or few-layer graphene in an environment of high temperature with high vacuum.

In the past few years, researchers had been investigating the suitable process to synthesize monolayer and few-layer graphene with better quality under various parameters such as deposition time, pressure, type of substrate, substrate temperature, and gas composition. Ni and Co substrate possess the properties of intermediate and high carbon solubility which can form a solid solution of the segregated carbon atom at high temperature. The as produced carbon atoms from the substrate will then precipitate as a graphene layer during the cooling process (Reina et al., 2009). In 2008, Yu et al., reported that the thickness and quality of graphene layers can be controlled based on the cooling rate and the concentration of diffused carbon atoms onto the metal substrate (Yu et al., 2008). The advantage of this technique has been proven by Bae et al. (2010), in which the fabrication of 30 inches monolayer graphene on a roll of copper foil was

reported as shown in Figure 2.4. The process includes three steps: 1) the adhesion of polymer support (polyethylene terephthalate, PET) 2) the etching of copper, and 3) the transfer of graphene layers to the target substrate.

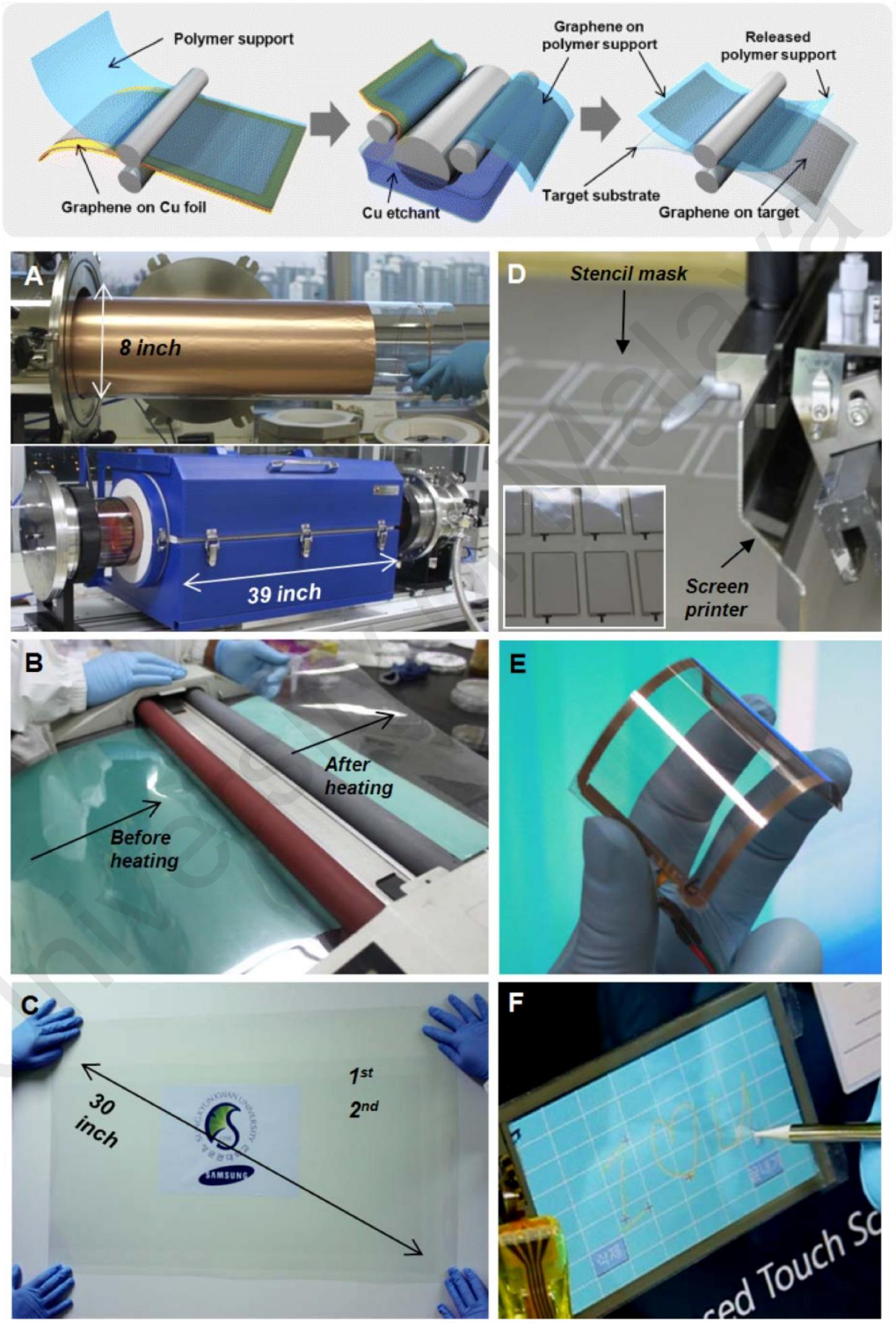

Figure 2.4: Schematic mechanism of the roll-based production of graphene films grown on a copper foil (Bae et al., 2010).

2.4.4 Reduction of Graphene Oxide

Graphitic oxide can be obtained through the oxidation of graphite flakes in the environment of strong acids and oxidizing agent. The chemical modification conducted through mechanical or thermal exfoliation on the graphite oxide basically produced graphene oxide, which is enriched with reactive oxygen functional groups on the basal plane with carboxyl-functionalized edges as shown in Figure 2.5 (Gao et al., 2009). The graphene oxide is very electrically insulated due to its disrupted sp^2 bonding interactions. The electrical conductivity properties can be repaired by restoring the π network through a rapid reaction known as reduction.

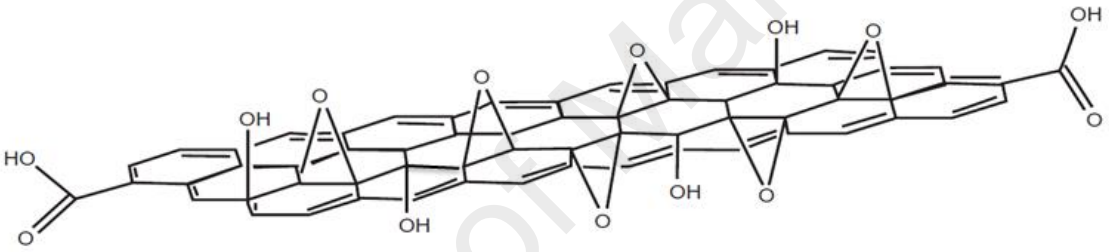

Figure 2.5: The chemical structure of graphene oxide enriched with hydroxyl and epoxide groups along with carboxyl-functionalized edges.

The final product is known by various names such as reduced graphene oxide (rGO), chemically reduced graphene oxide (CrGO), and graphene. However, "reduced graphene oxide" was chosen to be used in this thesis. However, the full reduction of oxygen functional groups has not yet been reported, which results in the restoration of the sp^2 network being modified. Hence, the location of rGO is far away to catch electrical conductivity of the pristine graphene. Several efforts have been made on strategizing the high level reduction of GO such as chemical reduction, thermal reduction, and electrochemical reduction.

2.4.4.1 Chemical Reduction

Stankovich and groups were the first to report on the reduction of colloidally dispersed GO using hydrazine monohydrate (Stankovich et al., 2007). It was chosen as reducing agent for aqueous dispersion of GO due to its strong reactivity with water. The whole idea is to intercalate the water molecules between the graphite sheets in order to increase the interlayer distance of graphite sheets for the purpose of weakening the van der Waals interaction between the graphite sheets. An electrostatic repulsion of the graphite layer will result in the exfoliation of GO caused by the low van der Waals interaction, which might produce a monolayer, bi-layer or few-layer graphene layer. The brown color of GO will turn to black and precipitate easily during the reaction, which can be explained by the less hydrophilic resulted by the loss of oxygen functional group.

There are several reducing agents which include sodium borohydride, $NaBH_4$ (Shin et al., 2009), hydrazine hydrate (Xu et al., 2014), and tanic acid (Zhang et al., 2012) that have been used to reduce the GO. Usually, the chemical process is conducted under ambient temperature or room temperature which makes it easier to handle, low in cost, and chemically stabilized. As reported by Shin et al. (2009), $NaBH_4$ shows a better reduction level compared to hydrazine; however, the rGO resistance shows much lower reduction level compared to the rGO prepared using hydrazine. In 2012, Zhang et al. have reported that rGO can be synthesized by one-pot preparative route using tanic acid, which was claimed to be a very cost effective and environmentally friendly water-based reduction of GO. Another effort or alternative that can be used for chemical reduction is by using green and natural reducing agent such as garlic (Izrini et al., 2015), vitamin C (Merino et al., 2010), and glucose (Zhu et al., 2010).

2.4.4.2 Thermal Reduction

Chemical reduction is considered as the most famous method in preparing rGO, but it is not the only capable method that can be applied. GO can be reduced better through heat treatment instead of chemical reductant due to its thermally unstable condition. A rapid thermal heating which is directly applied on the GO will create thermodynamically stable carbon oxide species, namely exfoliate and reduced graphene oxide which yield a very fine black powder (Zainy et al., 2012, Mcallister et al., 2007, Wu et al., 2009). The exfoliation of the stacked structure is resulted by the extrusion of CO or CO_2 gas that occur within the space between graphene oxide layers. The sudden generation of these gas at high temperature will create enormous pressure within the graphene oxide stacked sheets which also generates a pressure of 130 MPa at 1000 °C, which then separate the graphene sheets from each other (Mcallister et al., 2007). Even though this method is simple and promising in producing a large-scale of graphene, however, the final product achieved seems to have small lateral size and structural defects (Kudin et al., 2008, Schniepp et al., 2006). The electrical conductivity was 10^{-23} S cm^{-1} which is much smaller than pristine graphene despite all the defects (10^4 S cm^{-1}) (Cuong et al., 2010, Schniepp et al., 2006).

2.4.4.3 Electrochemical Reduction

Another effective method in reducing GO involves the electrochemical removal of oxygen functional group as reported by many researchers (Toh, et al., 2014, Kauppila, et al., 2013, Yang & Gunasekaran, 2013). This method is very attractive due to its flexibility, quick process, easy to handle, and non-toxic process which promotes the go green campaign by avoiding the use of toxic reductants (N_2H_4, $NaBH_4$). Typically, electrochemical reduction of GO can be conducted in two ways: 1) one step reduction approach and 2) two step reduction approach. In one-step approach, GO is directly reduced from an aqueous solution in the buffer electrolyte and deposited on the target

substrates such as ITO, glass, glassy carbon electrode and others. The electrochemical reduction process can be performed by using cyclic voltammetry (CV) (Ramesha & Sampath, 2009), linear sweep voltammetry (LSV) (Zhu et al., 2011), or at a constant voltage (Guo et al., 2009) in a standard three-electrode electrochemical cell. The reduction process is believed to take place when the GO layers are adjacent to a target electrode, yielding the graphene layer that is deposited directly onto the substrate surface (Chen et al., 2011). In 2010, An et al. applied the step-one approach on different conductive substrates by applying a voltage of 10 V in an aqueous of GO as shown in Figure 2.6.

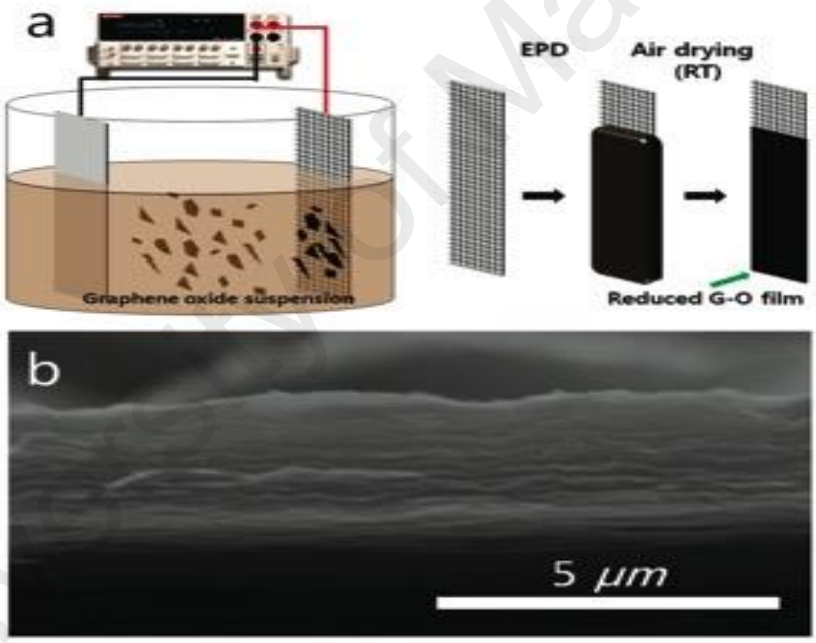

Figure 2.6: Schematic diagram of the electrochemical reduction process and cross-section image of FESEM image of reduced graphene oxide film (An et al., 2010).

In the two-step approach, GO is deposited onto the substrate and subsequently dried out to produce a GO-coated thin film. The coated substrate is then electrochemically reduced using a standard three-electrode electrochemical cell which contains a buffer solution or supporting electrolyte to produce rGO layer on the electrode substrate. As

reported by Eda et al. (2008), the GO is adhered to the substrate through van der Waals interactions. The pre-deposited GO film on various films is believed to undergo a controllable synthesis of electrochemical reduction graphene oxide in terms of shape, size, and thickness. Paredes, et al., (2008) reported that the desirable size and thickness of a film can be controlled according to the amount of GO deposited onto the substrate. However, the parameters such as uniformity, surface morphology, thickness, and area coverage are dependent on deposition techniques (Eda & Chhowalla, 2010).

2.5 Graphene Oxide: Synthesizing and Processing

A number of comprehensive papers on the preparation of graphene oxide and reduced graphene oxide have recently appeared. Generally, Brodie, Staudenmaier, and Hummers (1859) have reported the oxidation of graphite in so many levels. As discussed in their work, Brodie and Staudenmier applied a mixture of potassium chlorate ($KClO_3$) with nitric acid (HNO_3) (Brodie, 1859). In the following 40 years, Staudenmaeir improved Brodie's method by modifying the concentrated sulfuric acid (Staudenmaier, 1898). In 1958, Hummers and Offeman treated the graphite with potassium permanganate ($KMnO_4$) and sulfuric acid (H_2SO_4), which makes it relatively safe to oxidize the graphite. Since the discovery of graphene by Geim and Novoselov, GO has attracted a lot of attention among the researchers because it can be used as a precursor in producing a large-scale and very low-cost graphene. Up to date, the preparation of GO reported by Tour and coworkers has become the featured method (Marcano et al., 2010). In their work, the amount of potassium permanganate ($KMnO_4$) is increased and then mixed with phosphoric acid (H_3PO_4) that possesses the ratio of 9:1 (Figure 2.7). It was reported that the graphite in this method was oxidized at a higher level with more intact graphitic basal planes compared to Hummer's method. The carbon layer was enriched through oxygen functional groups which can expand the interlayer space of graphite planes from 0.34 to 0.8 nm.

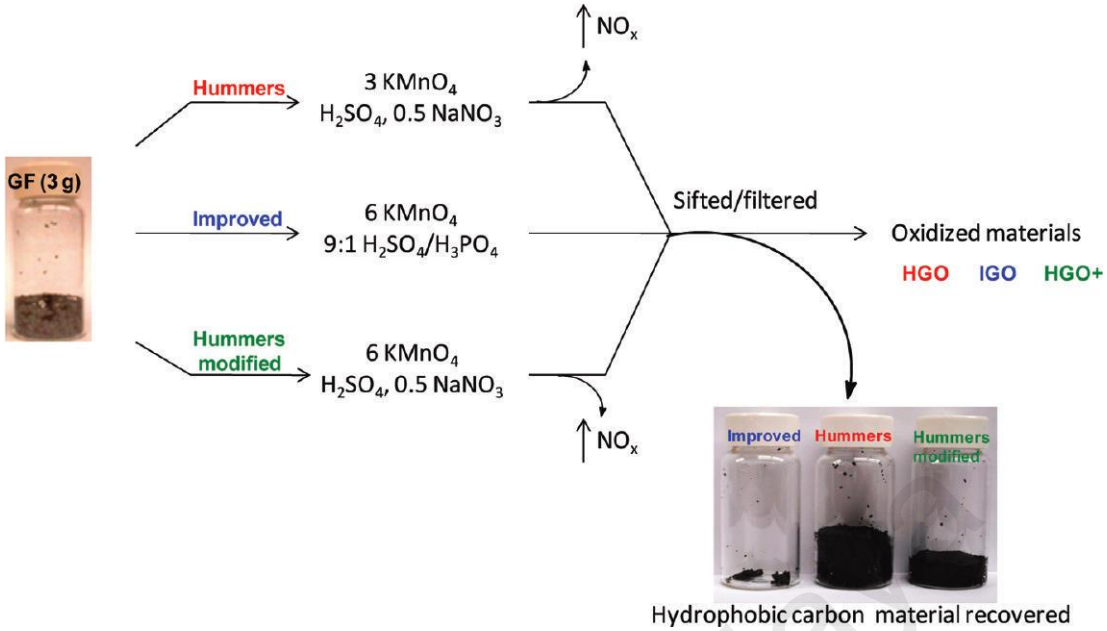

Figure 2.7: Preparation process of production GO. The small amount of recovered powder indicates the high efficiency of the improved synthesized method under-oxidized environment (Marcano et al., 2010).

The oxygenated functional groups of GO are highly hydrophilic which makes it possible to be exfoliated in many solvents and dispersed highly in water as shown in Figure 2.8. As reported by Li et al., (2008), the GO sheets are negatively charged and the electrostatic repulsion between the layers are able to form a stable suspension. The dispersions of GO in solvent can easily be done through stirring or sonication. The efficiency of dispersibilty of graphene oxide in solution to be further processed is highly dependent on the solvent as well as the surface functionalization during oxidation. Recently, it has been found that higher dispersibility is dependent on higher polarity of the surface. As reported by Si et al. (2008), the best ratio was found to be 1-4 mg mL^{-1}.

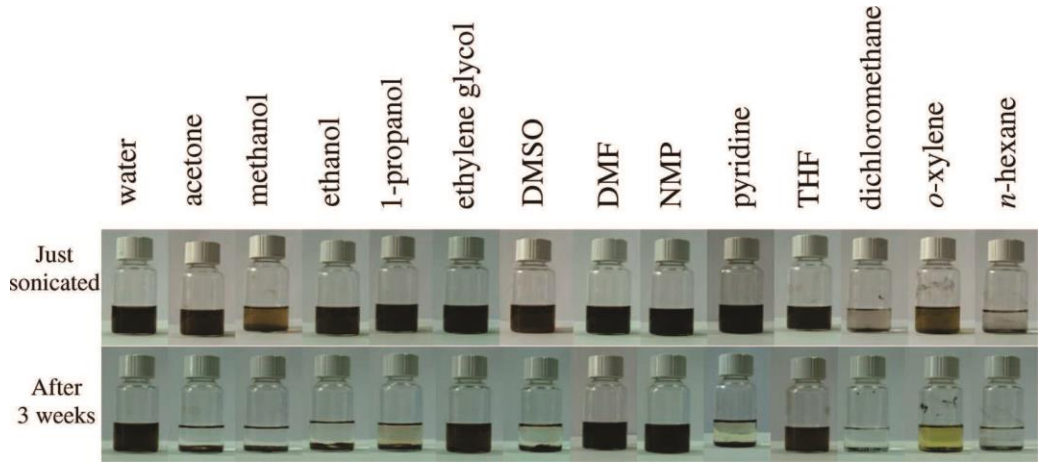

Figure 2.8: Photograph image of as-prepared graphite oxide in different 13 organic solvent via bath sonication immediately after sonication and 3 weeks after sonication. Source: (Paredes et al., 2008).

2.6 Graphene-based Inorganic Nanocomposite

The intergration of metal/metal oxide nanoparticles (NPs) into graphene matrix is considered as an important field of research in exploring their excellent properties and multi-disciplinary applications. The preparation of graphene with metal or metal oxide nanoparticles is based on research that was conducted the last few years. GO was used as a precursor which simultaneously acts as a substrate for the NPs embedded on it. After several papers published by Ruoff et al., graphene based composite successfully inspired the researchers to explore more about graphene composite including their applications. Most of the graphene NPs composites possess their own critical value, in which several components must fulfill some requirements in order to enhance their application value.

A variety of metal/metal oxides have been used in the synthesis of graphene nanoparticles nanocomposite, which include metal such as Ag (Tien et al., 2011), Au (Thavanathan et al., 2013), Pd (Wang et al., 2016), Pt (Kurt et al., 2016), Sn (Kim et al., 2016), Fe (Zhang et al., 2016), Cu (Sevim et al., 2016), and Co (Hatamie et al., 2016) as

well as metal oxide such as TiO_2 (Torres, et al., 2012), ZnO (Marlinda et al., 2012), Cu_2O (Zhang, et al., 2016), NiO (Jiang et al., 2013), Fe_2O_3 (Radhakrishnan et al., 2014), Fe_3O_4 (Teo, et al., 2012), SnO_2 (Nurzulaikha et al., 2015), MnO_2 (Yu et al., 2011), Al_2O_3 (Zheng et al., 2014) and Co_3O_4 (Shahid et al., 2015). Among all of the metal/metal oxide mentioned above, it was discovered that metal AgNPs have attracted large attention due to their wide applications and interesting properties that can be assigned to chemical sensing, electronics, catalysis, biosensing, and pharmaceuticals. Their excellent excitation of localized surface plasmon resonance (SPR) heavily depends on the size and shape which favour the use of AgNPs in optical sensor. AgNPs shows are considered to be low cytotoxicity towards human cells, thus it can absolutely be applied in the biomedical and pharmaceuticals fields.

2.7 Production of Graphene-based Nanocomposite

In-situ growth is one of the most popular method used in preparing graphene supporting nanoparticles. Usually, a bottom-up approach is applied in order to synthesize the metal nanoparticles, whereby metal ions are reduced to metal. Meanwhile, post graphenization technique is used to prepare graphene metal oxide nanocomposite. The salts containing metal ions have been used as precursors, in which it is mixed with graphene oxide and then converted to graphene metal oxide nanocomposite. For example, Ag+ ions were added into GO aqueous solution, followed by the addition of ammonia in order to produce Ag nanoparticles. The oxygenated groups on the surface of both GO and graphene are able to initiate the nucleation of silver nanoparticles. In addition, the graphene layer acts as a stabilizer of nanoparticles (Ikhsan et al., 2016). Furthermore, the nanocomposite was reduced by hydrazine, which formed a graphene decorated with Ag nanocomposite. However, in many cases, caping agent or polymer is applied in the procedure for the purpose of controlling the size,

shape, and morphology of both metal and metal oxide. It is crucial to note that these toxic materials are very harmful to the human body.

Normally, the nanocomposites are synthesized using chemical and physical methods, which are unfriendly and possess some problems such as poor stability and difficulty in reproducing AgNPs due to colloidal aggregation (Nickel et al., 2000). Therefore, a few considerable efforts to encounter this problem have been taken to synthesize AgNPs on silicate sol-gel (Rameshkumar et al., 2014), polymer (Cheng et al., 2011) and graphene sheets (Golsheikh et al., 2014). Among these, silver on the graphene sheets managed to show a better dispersion and void the aggregation caused by the large surface area and strong van der Waals interaction between the AgNPs and graphene layer.

2.7.1 Hydrothermal and Solvothermal Growth

Hydrothermal (aqueous) and solvothermal (non-aqueous) are very practical and versatile in synthesizing graphene nanocomposites. The procedure is carried out by mixing the precursor with graphene or graphene oxide in the solution, followed by hydrothermal or solvothermal reduction of the precursor at an elevated temperature in an autoclave. The formation of a variety of inorganic nanostructure materials takes place in the environment of high pressure of hydrothermal and solvothermal processing. It has been used to synthesize graphene-based nanocomposite of metal oxide such as ZnO (Marlinda et al., 2012), TiO_2 (Chang et al., 2012, How et al., 2014), CuO (Yusoff et al., 2013), Fe_3O_4 (Hu et al., 2014), and SnO_2 (Nurzulaikha et al., 2015), NiO (Jiang et al., 2013) as well as metal hydroxide such as MnOOH (Chen et al., 2010), $Co(OH)_2$ (Yao et al., 2013), $Ni(OH)_2$ (Min et al., 2014) and chalcogenides CdS (Gao et al., 2012), ZnS (Xue et al., 2011), CdTe (Lu et al., 2011), and MoS_2 (Ma et al., 2014). The advantage of this method involves its feasibility in producing high yield and nanostructure materials decorated graphene, namely nanoparticles, nanowires,

nanoflower, nanorods, and nanotubes with high crystallinity without the annealing and calcination treatment.

2.7.2 Electrochemical Deposition

Electrochemical is another popular alternative that can be applied to synthesize graphene nanocomposite. Metal, metal oxides, and metal alloy seem to be easily incorporated on the graphene layer through electrochemical method. This technique is very attractive because it is well known to be very fast, easy, and free from toxic. The metal nanoparticles or nanostructures can be formed by applying the voltage and current during electrochemical reduction from the precursor solution. Up to date, a lot of works have been reported on electrochemical fabrication of graphene-based nanocomposites such as Au (Fu et al., 2010), Pt (Yueming et al., 2009), Ag (Jin et al., 2015), Cu (Pavithra et al., 2014), ZnO (Hambali et al., 2014), NiO (Kim et al., 2013), and even CdSe (Kim et al., 2010).

As reported by Yin et al. (2010), the structure of ZnO is influenced by the conductivity of rGO, in which the particles nanostructure can be grown with low conductivity while the nanorods are collected when rGO possess high conductivity (Yin et al., 2010). Hence, it can be utilized to benefit the processing method and various applications. However, this technique relies on multi-step processing method, and Yu et al. (2011) reported the deposition of graphene incorporated with MnO_2 on textile substrate for capacitor performance by applying a small constant current 100 $\mu A/cm^2$ for 30-300 min deposition time in a mixed aqueous solution of 20 mM $Mn(NO_3)_2$ and 100 mM $NaNO_3$ as shown in Figure 2.9. The FESEM image presented in Figure 2.9B and 2.9C shows that MnO_2 nanoparticles are uniformly decorated on the surface of the textiles. Interestingly, this technique can similarly be applied to synthesize the nanocomposite of graphene Cu_2O and graphene ZrO_2 (Wu et al., 2011, Du et al., 2011).

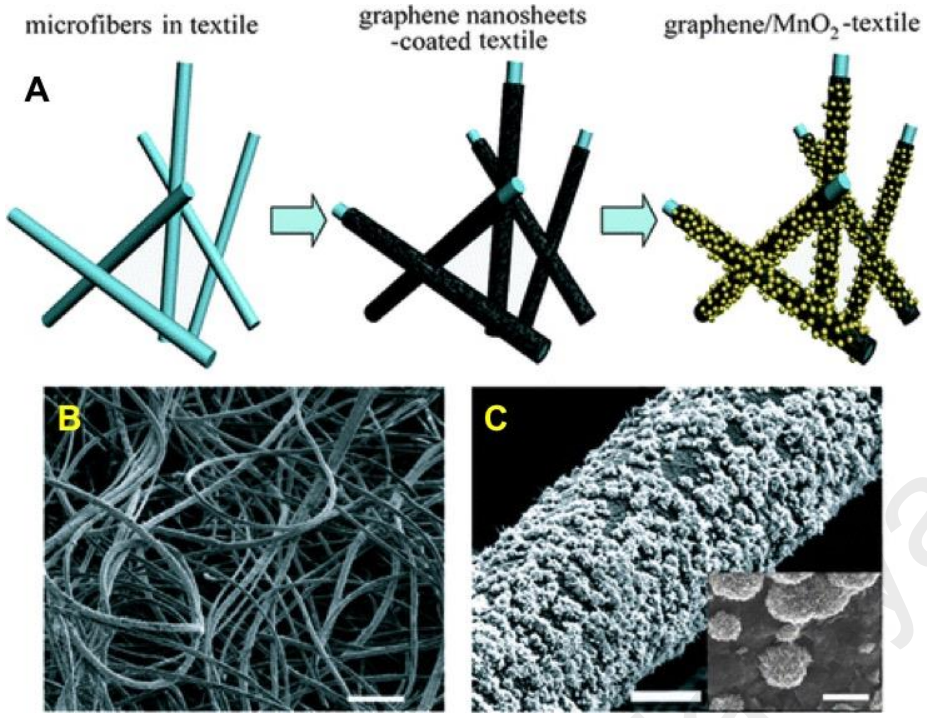

Figure 2.9: Schematic illustration of textile MnO_2-graphene nanocomposites. (b) SEM images of MnO_2 nanoparticles coated on textile after 60 min electrodeposition time and (c) SEM image of typical microfiber of textile decorated with mnO_2 nanoparticles. Inset shows, nanoflower structure of electrodeposited MnO_2 particles and interface-bond between nanoparticles and underneath graphene layer (Yu et al., 2011).

2.7.3 Physical Deposition/Mixing

Another flexible method that can be used to prepare graphene nanocomposite is by depositing the materials directly through a few physical techniques, namely physical mixing, spray-drying, and atomic layer deposition. The surface of graphene and/or nanomaterials is modified to ensure that it is bound together through covalent interaction or non-covalent interaction. For example, Zainy et al. reported the embedment of Ag nanoparticles onto graphene layer by grinding both $AgNO_3$ and graphene oxide together which is exposed to 1000 °C (Zainy et al., 2012). In another work by Hu et al. (2013), graphene composite is synthesized with $LiFePO_4$ NPs through the process of spray drying. The graphene modified with $LiFePO_4$ managed to significantly enhance the performance of lithium batteries. Meanwhile, high-*k* dielectric

metal such as Al_2O_3 were deposited on the graphene surface using the atomic layer method (Wang et al., 2008). Metal oxide was found to be formed on the edge or the defect site of graphene, while no deposition on the pristine graphene without defects was discovered.

2.8 Graphene oxide-Silver Nanocomposite

The report provided by Lea (1889) on the synthesis of a citrate-stabilized silver colloid has not only inspired the field of nanotechnology, but also triggered a massive interest in physics, chemistry, biology, and materials science. Silver (Ag) is the most extensively studied material (over the past 100 years) among all the nanomaterials, which makes it one of the famous nanomaterials used in the research of materials science. Nanosilver has been known to be very useful, cheaper than gold (Au), non-toxic, and environmental friendly. Thus it is frequently used in catalysis, pigments, photographics, wound treatment, conductive composites, and as a bio-agent. The ideal functional features include biocompatibility as well as unique ionic and electronic properties. Ag in all its forms is a metal with suitable surface plasmon resonance (SPR) band (380-450 nm) that is able to be used in sensor, photocatalytic reactions, and even in solar cells. Historically, some advancement milestones on synthesizing were certainly reported by Nie (Nie, 1997). Meanwhile, there are some works on optical properties that reported the use of the nanomaterial for antibacterial and medical application in the past 20 years (Kelly et al., 2003, Morones et al., 2005, Chen & Schluesener, 2008).

Over the past few years, the potential application has been widened towards sophisticated devices including smart surface coating, biomedical coating, photovoltaic, and device-sensor. It is crucial to maximize the specific surface area for some of these applications in order to achieve a maximum overall performance such as any sensor. However, the agglomeration and precipitation can be avoided by combining them with graphene oxide or graphene nanosheets, which may allow the chemical and physical

properties to be better modified. The modifications will not only cause the specific surface area to increase significantly, but the interparticle coupling effect may also change considerably (for example to aggregation, surface interactions, stability, and reproducibility). All of the above mentioned behaviors may drastically enhance the reaction/interaction between the surrounding environment and media, which makes more effective and novel for the system.

The synthesis of nanocomposites of graphene oxide or graphene silver nanoparticles may be achieved through various alternatives including chemical reduction, hydrothermal/solvothermal method, sol-gel methods, template assisted approaches, and electrochemical reactions. In 2013, Tang et al. prepared graphene oxide-silver by reducing $AgNO_3$ with sodium citrate in the presence of GO suspension. The different amounts of AgNPs deposited on the GO sheets was controlled by the ratio of AgNPs to GO (0.65, 1, and 2), which is measured based on the complexometric titration technique. The nanocomposites were reported to exhibit excellent aqueous dispersion with spherical of AgNPs, and the size is dependent on the ratio of AgNPs to GO as shown in Figure 2.10. Driven by their green method, Ikhsan et al. (2015) reported the same environmentally benign technique by using garlic as a reducing agent under bright sunlight irradiation. A small AgNPs can be grown through a simple processing on the GO sheets with nearly uniform shape and size without branced nanostructures (Izrini et al., 2015).

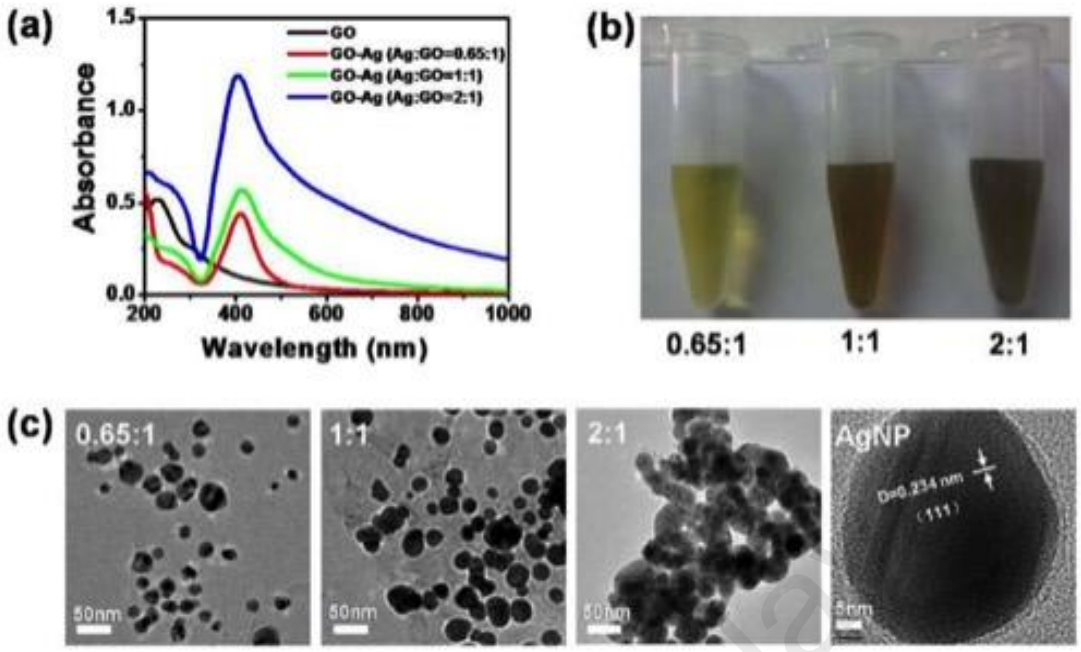

Figure 2.10: UV-Vis characterization of GO-Ag nanocomposites with different AgNPs to GO ratios (a), photograph of aqueous GO-Ag nanocomposites (b) and TEM images of GO-Ag nanocomposite with different ratio. The right one is a HRTEM of single AgNP on the GO layer (Tang et al., 2013).

Meanwhile, Kumar et al. (2013) modified the surface of graphene oxide by using hydrophilic N-(trimethoxysilylpropyl) ethylenediamine triacetic acid sodium salt (TETA) with a simple modification as presented in Figure 2.11. The functionalized graphene oxide (FGO) was prepared through a simple stirring under room temperature without adding any extra chemicals. In their report, the NaOH was used to reduce the silver nanoparticle as well as control the size of nanoparticle by adjusting the pH of the solutions, while the FGO serves as substrate, stabilizer, and reducing agent.

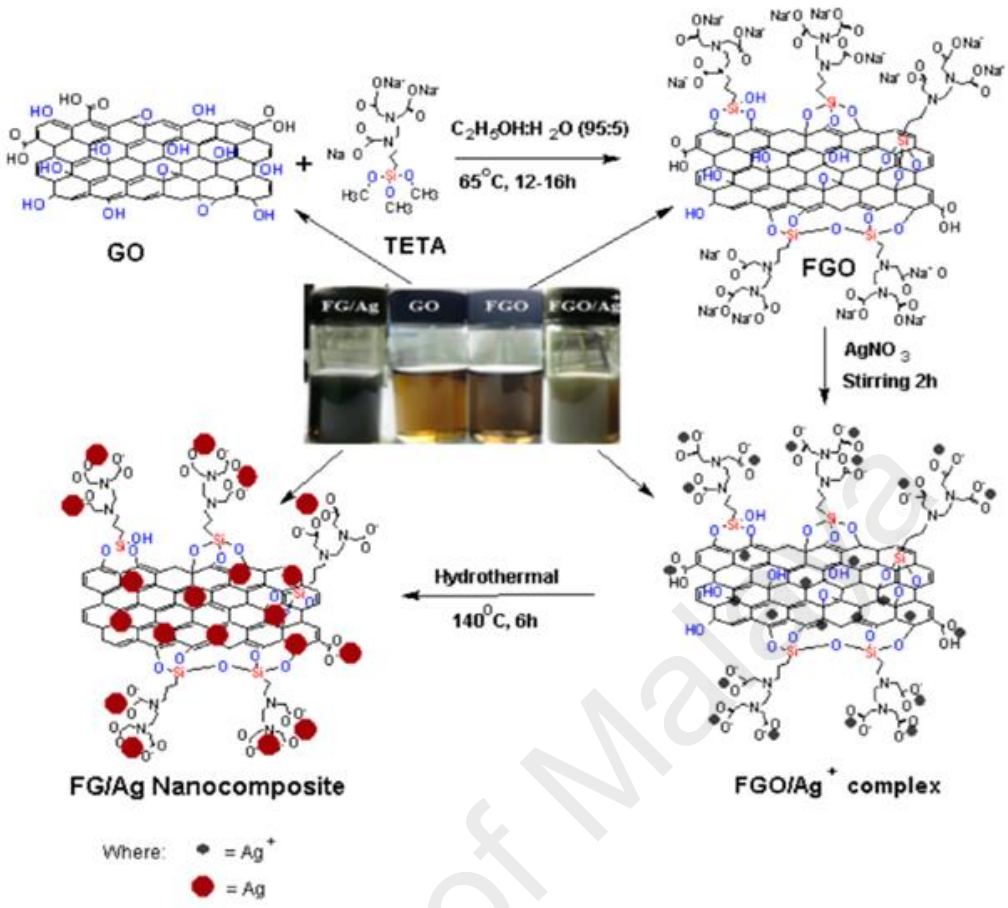

Figure 2.11: The preparation of FGO/Ag nanocomposites by reacting GO with TETA at room temperature (Vijay Kumar et al., 2013).

2.9 Graphene-based nanocomposite: Principle and Methods of Application Evaluation

High conductivity, a very large surface area, light weight, and cheaper graphene provide a very large platform for various applications on graphene based nanocomposite. The combination of graphene and nanomaterials is not only expected to enhance the properties of graphene and nananocrystals, but a good side effect was also shown through the interaction between the materials. Irrefutably, the graphene-based nanocomposites show a better performance in sensing and other related applications.

2.9.1 Sensing

2.9.1.1 Optical Sensor

Sensor is a device that detects or determines a physical parameter and then converts it into signal, which is recorded by an instrument or observer (El-Safty & Shenashen, 2012). One of the recently famous sensors used is based on the optical properties. An optical method has played a dominant role in analytical sciences in a wide field of research including material science, biotechnology, bio-chemistry, and medical chemistry. The non-invasive, non-destructive, and multi-monitoring analytes was once used to determine the chemical and biochemical substances qualitatively and quantitatively based on the interactions of analytes. Colorimetry and photometry measurement of the analyzed sample were tested by using chemical reagents or their own optical properties for the optical identifications. This technique offers higher potential for the rapid and selective measurements with different specificity and sensitivity.

Graphene nanocomposite is considered as a very good secondary sensor to enhance that fabricated by noble metal such as Au, Ag, and Pt nanoparticles that are widely used in the optical sensor. In addition, graphene layer acts as both conductive channels and secondary sensor for the active material in the optical sensor. Graphene-silver nanocomposite has become a very attractive material for the optical sensor because it works as secondary material to enhance the almalgam formation when reacted with mercury ions. In addition, the graphene layer can be used as a supporting substrate to reduce the aggregation of Ag nanoparticles as reported by Kamali et al. (2015) and Golsheikh et al. (2014).

2.9.1.2 Electrochemical sensor

Electrochemical technique employs the technique of electronic and analytical method which being combined together. The measurement of electrical products such as

current, potential, charge, and the relationship towards chemical parameter are typically known in electrochemistry. The mechanism takes place between the electrode and solution interface, in which the electrode has the potential to drive the electron transfer reaction to record the resulting current. The chemical species are forced to undergo the reduction and oxidation process by gaining and losing an electron, respectively. This technique promises high sensitivity and selectivity in determining the electroactive species with just a small volume of samples (5-100 μL) and a very low limit of detection up to nanomolar scale can be achieved.

Pristine graphene exhibits extremely large specific surface area, conducting behavior, and availability for functionalized surface which are highly unique for the electrochemical applications. In the past few years, many works on graphene electrochemical sensor have been reported in sensing dopamine, glucose, ascorbic acid, H_2O_2, DNA, and 4-nitrophenol. However, it was found to possess low electron mobility due to the electronic double-layer regime. One of the efforts to counter this drawback is by integrating extra high conductive materials to enhance the electron transfer. In addition, the electronic behavior of graphene will improve the electrochemical reaction. Until today, electrode active materials have been applied to achieve higher sensitivity with better formation of electrochemical species such as metal nanoparticles (Au, Ag, Pt, Pd, Cu), metal oxide (ZnO, TiO_2, CuO, Fe_2O_3, Fe_3O_4, SnO), polymers (chitosan, polyaniline, polypyrole, nafion), carbon nanotubes, clay, and zeolite to be incorporated with graphene layer in the application of electrochemical sensor.

Firstly, Wang and et al. (2009) reported that graphene was used as the electrode modifier in detecting DA, which managed to initiate the development of electrochemical sensor using graphene-based composite materials with metal, metal oxides, doping, and polymer. In 2013, Lu et al. used the strategy of hybridizing the rGO

and AgNPs as hybrid-based electrochemical actuators. The rGO and AgNPs are simultaneously reduced by hydrazine while AgNPs is successfully deposited and effectively inherent in the rGO network as presented in Figure 2.12. It was claimed that the presence of AgNPs can increase the stability of electrochemical sensor and provide a typical behavior of an electrochemical capacitor, which indicates a better electrochemical performance and measurement.

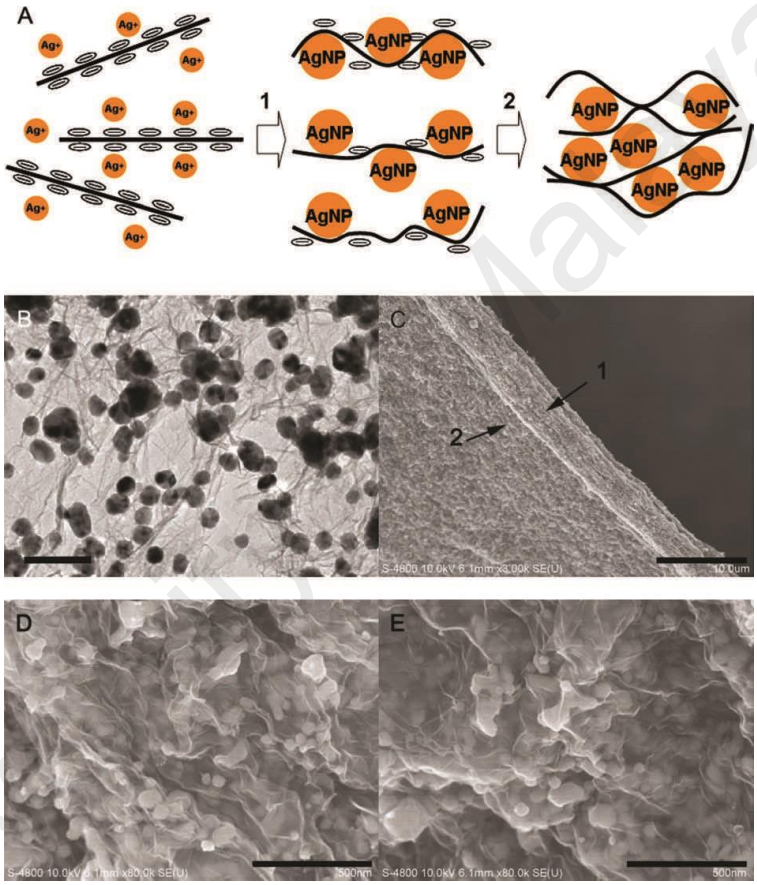

Figure 2.12: A) Illustration of the formation of the AgNPs on the GO layer and rGO/Ag composite. B) TEM image of rGO/Ag C) SEM image of membrane. D and E) high-resolution SEM images of the cross section viewed from labeled 1 and 2 respectively with the scale bar 500 nm (Lu et al., 2013).

Shahid et al. (2015) reported a reduced graphene oxide that decorated with cobalt oxide nanocube with platinum nanoparticles (rGO-Co_3O_4@Pt) for the electrochemical detection of nitric oxide (NO). As can be seen in Figure 2.13 d, the Pt NPs are densely decorated on Co_3O_4 nanocube while the nanocube is strongly anchored onto the rGO

matrix. The nanocomposite modified GC electrode managed to enhance the catalytic peak current by shifting the oxidation overpotential of *in situ* generated NO towards the less positive potential. The amperometric *i-t* curve detection of NO shows a better performance with the lowest detection limit of 1.73 μM. In addition, the nanocomposite displays good selectivity towards NO in the presence of a 100-fold higher concentration of other physiologically analytes (Shahid et al., 2015).

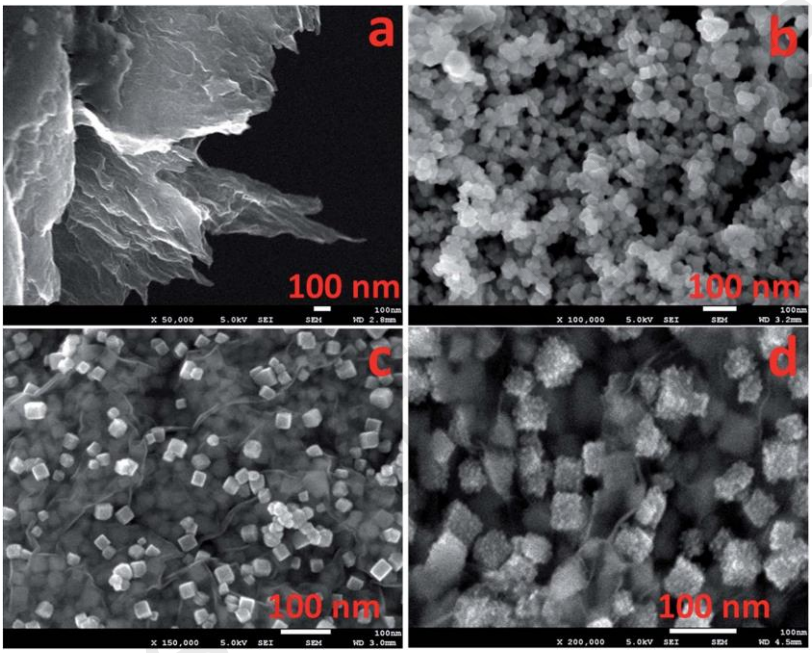

Figure 2.13: The images of (a) layers of reduced graphene oxide (b) Co_3O_4 nanocubes without the rGO layer (c) Co_3O_4 nanocubes on the rGO layer and (d) rGO-Co_3O_4@Pt nanocomposite (Shahid et al., 2015).

In this thesis, graphene silver nanocomposite was utilized to define the performance such as the electrochemical properties and the multi-usefulness of nanocomposite as an electrode material to be used for the next generation.

2.9.1.3 Surface Enhanced Raman Spectroscopy (SERS)

Surface Enhanced Raman Spectroscopy (SERS) is a technique that is applied to study the Raman signals from Raman-active analytes molecules which are adsorbed or interacted onto metal surfaces. The SERS primarily observed the analytes adsorbed onto

the active surface metals (Au, Ag, and Cu) through the excitation wavelength in the region of visible or near infrared (NIR). The phenomenon behind this process is caused by the electromagnetic enhancement mechanism that resulted by the roughness of the material surface. An interesting methodology oxidation-reduction on electrode surfaces, vapour deposition onto substrate, and metal deposition through lithography is able to decorate the surface with smaller particles or aggregates of particles which could contribute to the roughness features. The resonance oscillations of the free electrons being produced will enhance the electromagnetic field at the particle's roughness with the incident light, which is known as localized surface plasmon resonance (LPSR).

2.9.2 Other Applications

Graphene-based nanocomposites have also been studied on antibacterial applications and radical scavenging. The nanocomposites were reported to demonstrate an excellent antibacterial towards Escherichia coli and Pseudomonous aeruginosa. Silver or gold has been known well to be acting as a natural antibacterial agent. Apart from that, the presence of graphene layer supports and stabilizes NPs on its surface while also keeping them dispersed very well, thus enhancing the active surface of the NPs. The degree of the efficiency depends on the size and nanostructure of NPs on the surface of graphene layer. On top of that, the graphene itself plays an important role as antibacterial. In addition, graphene-based nanocomposite were reported to occur on the antioxidant or radical scavenging applications (Qiu et al., 2014). In 2016, Kurt et al. prepared a graphene decorated with platinum (Pt) and Palladium (Pd) nanoparticles through the chemical oxidation-reduction method for the purpose of antioxidant activity. The nanocomposite of graphene-metal was found to possess better free radical scavenging activity compared to noble metal NPs.

CHAPTER 3:
EXPERIMENTAL SECTION

3.1 Materials

The chemicals and materials used in this work are summarized in Table 3.1.

Table 3.1: List of chemical and materials

Chemicals	Formula	Purity (%)	Supplier
Graphite	C	90%	Ashbury Inc.
Kalium permanganate	$KMnO_4$	99.9%	Merck
Sulfuric acid	H_2SO_4	95-98%	R&M Chemicals
Ortho-Phosphoric acid	H_3PO_4	85%	R&M Chemicals
Hydrochloric acid	HCl	37%	R&M Chemicals
Hydrogen peroxide	H_2O_2	30%	SYSTERM
Ammonia solution	NH_3	25%	Sigma-Aldrich
Silver nitrate	$AgNO_3$	99.7%	Bendosen
Dopamine	$C_8H_{11}NO_2$	99.0%	Merck
Mercury(II) chloride	Hg	99.5	Sigma-Aldrich
4-Nitrophenol	$C_6H_5NO_3$	98%	R & M Chemicals
Pottasium Hexacyanoferrate II	$K_4Fe(CN)_6.3H_2O$	98.5%	SYSTERM
***di*-Sodium hydrogen Phosphate (anhydrous)**	Na_2HPO_4	99.0%	SYSTERM
Sodium dihydrogen Phosphate (anhydrous)	NaH_2PO_4	99.0%	SYSTERM

3.2 Procedure for the Preparation of Graphene Oxide (GO)

Graphene oxide (GO) was prepared from natural graphite by using the simplified Hummer's method. In the procedure, about 3 g of graphite flakes was mixed with H_2SO_4:H_3PO_4 (320:80 mL) and $KMnO_4$ (18 g). The mixture was stirred for 3 days to achieve the maximum oxidation of graphite. The H_2O_2 solution was added to stop the oxidation of graphite after the color is changed from dark purplish green to dark brown. The high oxidation level of graphite can be observed by the bright yellow color of the

solution. The collected product was washed thrice with 1 M of aqueous HCl, and repeatedly washed with deionized water until a pH of 5 was reached. The washing process was carried out using centrifugation with the centrifugation force of 10000 g. The thickening of the end product of graphene oxide was detected and is believed to be the result of graphite oxide experienced exfoliation during the washing process.

3.3 Visual and Spectrophotometric Determination of Mercury (II) Using Silver Nanoparticles Modified With Graphene Oxide

3.3.1 Synthesis of GO-Ag nanocomposite

GO-Ag nanocomposite was synthesized as follows: First, silver-ammonia complex solution was prepared by slowly adding 100 µL of ammonia (25 wt.%) into 10 ml of 10 mM $AgNO_3$ solution, and the mixture was vigorously stirred. Next, the stirred solution was mixed with 5 mL of aqueous GO solution (0.5 mg/mL) and the mixture produced was ultrasonicated for 5 min. The ultrasonic horn (Misonix Sonicator S-4000, USA, 20 kHz) was irradiated at 60% amplitude for 5 min, with a 3 s pulse and 5 s relaxation cycle. A yellowish brown color solution of GO-Ag nanocomposite was obtained and the product was centrifuged with the centrifugation force of 10000 g and washed with deionized water for three times. The nanocomposite was prepared with lower concentration of ammonia solution (1 wt.% and 10 wt.%) to achieve an optimized synthesis.

Meanwhile, for the SERS experiment, Silver-ammonia $[Ag(NH_3)_2OH]$ complex solution was prepared by slowly adding 80 µL ammonia (25 wt%) into 10 mL silver nitrate solution (20 mM) while stirring it at the same time, and a clear solution managed to be observed. The $[Ag(NH_3)_2OH]$ solution was then mixed with 0.5 mg/mL of aqueous GO solution (volume ratio of GO:$[Ag(NH_3)_2OH]$is 3:1) and sonicated for 5 min to ensure the homogeneity before being exposed to microwave irradiation for 30 s. Finally, the product was centrifuged at a centrifugation force of 10000 g and washed

with deionized water for three times. The mechanisms of the preparation are shown in the Figure 3.1.

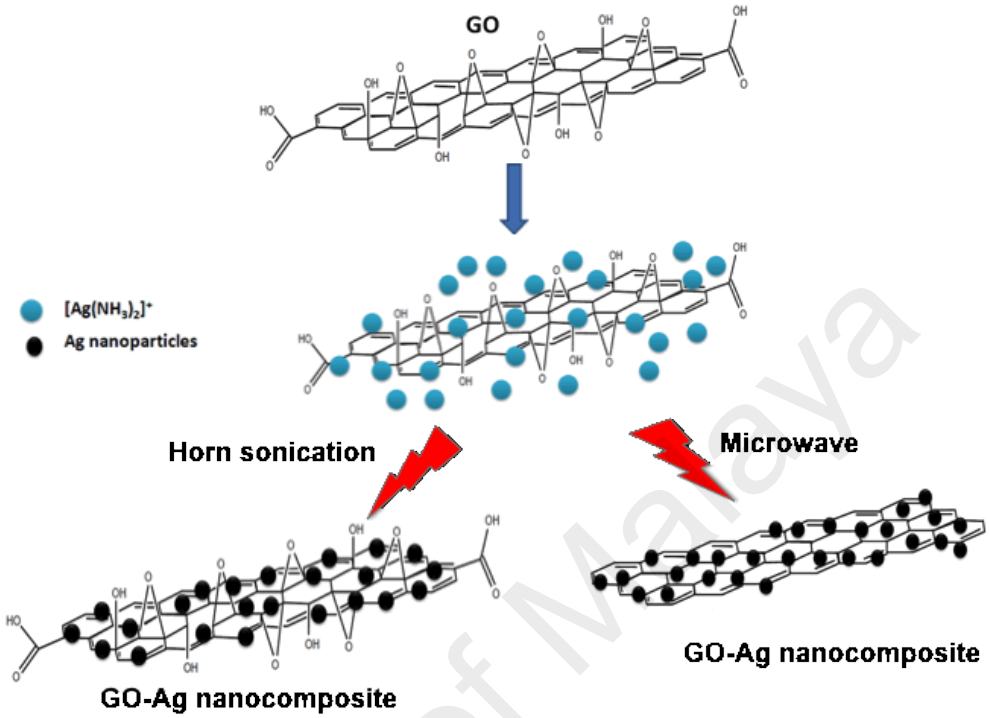

Figure 3.1: Schematic diagram of mechanism preparation of GO-Ag by using a Silver-ammonia complex.

3.3.2 Optical Sensing of Hg(II) Ions

The optical determination of Hg (II) was performed in aqueous solution of GO-Ag nanocomposite using Thermo Scientific Evolution 300 UV-vis absorption spectrophotometer. A 5 µL of freshly prepared aqueous solution of Hg(II) were added to 2 mL of GO-Ag nanocomposite solution which is shaken well and subjected to 2 minutes resting time. The changes of GO-Ag absorbance band due to the addition of different concentration of Hg(II) were monitored by recording the absorption spectra. For colorimetric detection, an optimum level of higher concentration of different metal ions was separately added into the GO-Ag nanocomposite solution, which is then

shaken well and allowed to rest. Finally, the color changes managed to be observed with bare eyes.

3.3.3 Electrochemical Measurements

All the electrochemical studies were carried out using PAR-VersaSTAT-3 Electrochemical Workstation (www.princetonappliedresearch.com). The electrochemical experiments were conducted in a three–electrode electrochemical cell system at room temperature. The GO-Ag nanocomposite modified glassy carbon electrode (GCE) was used as the working electrode. A platinum wire and silver/silver chloride (Ag/AgCl) electrode were respectively used as counter and reference electrodes (**Figure 3.2**). The GCE was polished with 0.05 micron alumina slurry and then cleaned with continuous potential cycling between +1 and –1 V in 0.1 M H_2SO_4. The modified electrode was fabricated by drop casting of 5 μL of aqueous GO-Ag nanocomposite solution on GCE surface and allowed to dry at room temperature for an hour. A 0.1 M phosphate buffer (pH 7.2) was used as supporting electrolyte in the electrochemical experiments and all the potentials are quoted against Ag/AgCl reference electrode unless mentioned otherwise.

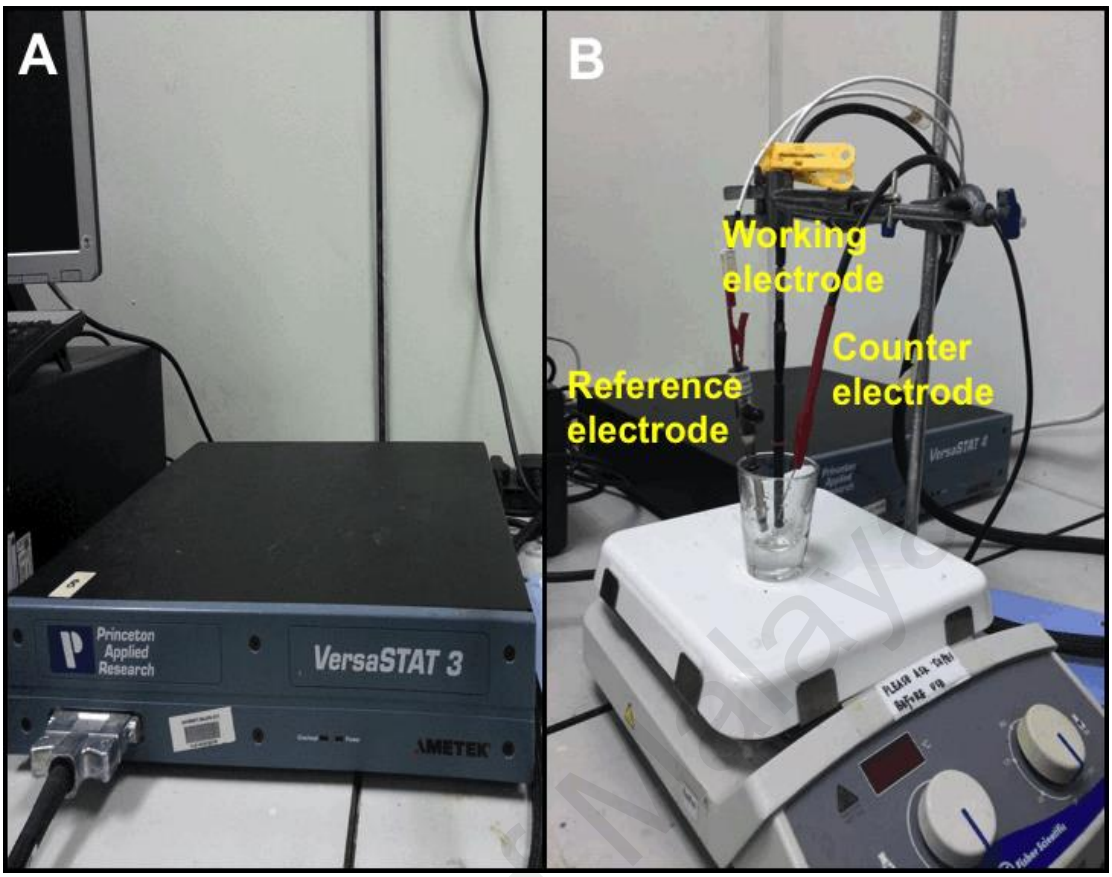

Figure 3.2: (A) Potentiostat (PAR-Versastat 3 Applied Research Princeton, USA) and (B) electrochemical setup.

3.4 Microwave assisted synthesis of graphene oxide-silver nanocomposite and its applications in SERS and spectrophotometric determination of dopamine

3.4.1 SERS Detection

1 µL of GO-Ag nanocomposite was drop-casted onto a clean glass plate, followed by a known concentration of dopamine aqueous solution being drop-casted onto the GO-Ag layer. The coated glass plate was allowed to dry at room temperature for 3 h. The SERS spectra were then recorded using Raman spectroscopy.

3.4.2 Optical sensing of dopamine

Optical detection of dopamine was performed in aqueous solution of GO-Ag nanocomposite using Evolution^{TM} 600 UV-vis absorption spectrophotometer. A 10 µL of 20 µM of freshly prepared aqueous solution of dopamine was added to 2 mL of GO-

Ag nanocomposite solution, which was then shook well and allowed to rest at the constant of 2 min. The changes of GO-Ag absorption band resulted by the addition of different concentrations of dopamine were monitored by recording the absorption spectra.

3.5 Microwave synthesis of reduced graphene oxide decorated with silver nanoparticles for electrochemical detection of 4-nitrophenol

3.5.1 Synthesis of rGO-Ag nanocomposite

Briefly, 80 µL ammonia (25 wt%) was slowly added into 10 mL of silver nitrate solution (20 mM). The mixture was vigorously stirred until a clear solution observed, thus indicating the formation of complex $[Ag(NH_3)_2OH]$. The solution was then mixed with 0.5 mg/mL of aqueous GO solution (volume ratio GO:$[Ag(NH_3)_2OH]$= 3:1) and sonicated for 5 min to ensure the homogeneity of the mixture. The reaction mixture was then exposed to microwave irradiation with the times being set differently (30 s, 1 min, and 3 min). The final product was centrifuged at a centrifugal force of 10000 g and washed with deionized water for three times. The nanocomposites prepared at different irradiation times are represented as rGO-Ag (30 s), rGO-Ag (1 min), and rGO-Ag (3 min).

3.5.2 Preparation of modified electrode for electrochemical sensing of 4-nitrophenol

The glassy carbon electrode (GCE) with diameter of 3 mm was cleaned by polishing it three times by using 0.05 µm alumina powder and washed with distilled water, which was followed by air drying it at room temperature. 5 µL of rGO-Ag nanocomposite was dropped on the surface of GCE electrode and allowed to dry at room temperature. The electrochemical experiments were conducted by using PAR-VersaSTAT-3 Electrochemical Workstation (www.princetonappliedresearch.com). A 0.1 M phosphate buffer (pH 6) was used as supporting electrolyte in the conventional three-electrode cell with Platinum (Pt) wire, while the silver/silver chloride (Ag/AgCl) were used as the

counter and reference electrodes, respectively. Meanwhile, the electrolyte solution was purged with nitrogen gas for 30 min before each experiment was carried out.

3.6 Characterization techniques

The samples were characterized through different methods for the purpose of studying and understanding the crystal structures, optical properties, morphology, elemental compositions, and their applications.

3.6.1 X-ray Diffraction (XRD)

The crystallographic information of the sample in this work was determined using XRD machine, Siemens D5000 with monochromatic Cu Kα radiation (λ = 1.5406 Å) at a scan rate of 0.02° s^{-1} operated at 40 kV and 40 mA scanning from 5°-80°. PAN analytical X'pert Highscore software was used to analyzed the atomic structure.

3.6.2 X-ray Photoelectron Spectroscopy (XPS)

X-ray photoelectron spectroscopy (XPS) measurement was conducted on powders samples by using synchrotron radiation from beamline no 3.2 at the Synchrotron light Research Institute, Thailand. The X-ray is used as the light source to excite the electrons in the inner core-level orbital. The energy from free photoelectrons will provide the information of the material, which includes the elemental composition, chemical stoichiometry, chemical state, and electronic state of the samples.

3.6.3 Raman Spectroscopy

A spectroscopic technique based on inelastic scattering of monochromatic light from the laser source when interacting with the sample can be carried out by using Raman spectroscopy. Photons from the laser light will hit the sample surface and undergo absorption, reflection, or scattering. These reemitted photons will portray the properties of vibrational, rotational, and frequency transition of the samples through Raman spectrum. In this study, Raman spectra were obtained using Raman inVia 2000 system

green laser emitting at 514 nm. The scan region for the purpose of measurements was carried out from 100-3000 cm^{-1}.

3.6.4 Ultraviolet-visible Spectroscopy (UV-vis)

The optical properties of the samples were characterized by using Avaspec UV-vis spectrometer. Furthermore, an optical sensor can also be executed by studying the shift in the wavelength of the absorbance peak.

3.6.5 Electron Microscopy

Field emission scanning electron microscopy, FESEM (Hitachi, SU 8000) was used to examine the surface morphology of the samples, while the transmission electron microscopy, TEM (Hitachi, HT-7700) and high resolution TEM (JEOL JEM-2100 F) were used to study the morphology, structure, shape, and size of the samples. Energy dispersive X-ray spectroscopy (EDX) was used to identify the elemental composition in the samples. The IMT i-solution full image analysis software was used to measure the size distribution of nanoparticles.

3.7 Electrochemical characterization and sensing measurements

3.7.1 Cyclic voltammetry

Cyclic voltammetry was carried out to study the qualitative information of redox potentials on electroactive species such as thermodynamics of redox process, kinetics reactions of heteregenous electron movement, and adsorption process. Figure 3.3 shows the routine record and report on the characteristics of the CV being at the peak height (Ip) as well as the potential at which the peak occurs (Ep). A typical CV curve at the electrochemical process was recorded by applying a voltammetric potential, and the current that was monitored provides the rise of unique profile as shown in the figure.

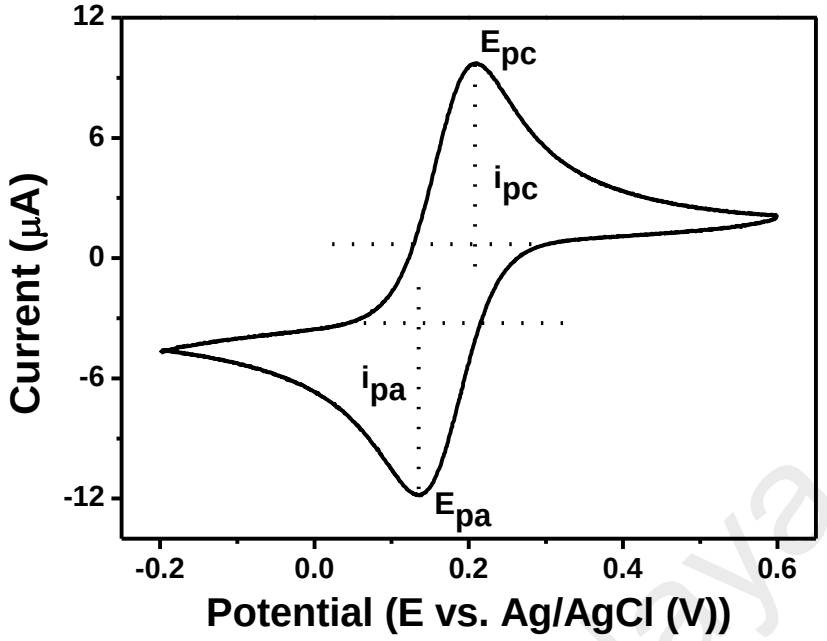

Figure 3.3: Typical cyclic voltammogram of a reversible reaction. i_{pc} and i_{pa} correspond to the peak cathodic and anodic current respectively.

3.7.2 Electrochemical Impedance Spectroscopy (EIS)

The interfacial charge transfer process is characterized based on the response function of alternating current (ac) generated versus the alternating voltage (av) in the EIS system. The EIS was carried out with the frequency range from 0.01 Hz and 10000 Hz with an AC amplitude of 10 mV.

CHAPTER 4:
RESULTS AND DISCUSSIONS

4.1 Visual and spectrophotometric determination of mercury(II) using silver nanoparticles modified with graphene oxide

4.1.1 Introduction

In recent years, there has been a considerable interest on the synthesis of silver (Ag) nanoparticles (NPs) because of their various applications and unique properties in catalysis (Jana et al., 1999), chemical sensing (Wu & Meng, 2005), antibacterial (Agnihotri et al., 2014), pharmaceutical (Jain et al., 2009), and biosensing (Frederix et al., 2003). A variety of chemical and physical methods have been proposed to prepare unsupported Ag NPs and however, these NPs were hard to reproducible and had poor stability due to colloidal aggregation (Nickel et al., 2000). To overcome such issues, alternative efforts have been made to prepare Ag NPs on support materials particularly on graphene/graphene oxide (GO) nanosheets (Li & Liu, 2010, Kochmann et al., 2012).

A large surface area of GO nanosheet and strong Van der Waals force between GO and Ag NPs can significantly reduce nanoparticles aggregation and with the interfacial interactions will ensure the stability and reproducibility of Ag NPs (Zhao et al., 2010). Recent studies reported that graphene oxide-silver (GO-Ag) nanocomposites can be synthesized through *in situ* reduction of Ag salts on GO nanosheet or decoration of GO with pre-synthesized Ag NPs (Zhou et al., 2009, Liu et al., 2011, Liu et al., 2011). GO, a two dimensional carbon material, can be easily mixed with Ag salt to obtain scalable quantity of nanocomposites *via* a chemical reduction (Paredes et al., 2008). The chemical method also suffers from the use of toxic and hazardous reducing agents like hydrazine, $NaBH_4$, and formaldehyde, to reduce both GO and Ag^+ which are exposing risks to the environmental and health (Tian et al., 2012). To avoid these problems, the GO-Ag nanocomposite is prepared by horn sonication method without using any hazardous chemicals and this method is attractive due to its ability to produce variety of

nanostructures including metals (Tripathy et al., 2013, Darroudi et al., 2012) and metal oxides (Zak et al., 2013, Geng et al., 2011).

Heavy metals play important roles in living systems and they are potential environmental pollutants even at ppm level concentration. Among them, mercury (Hg) is of great concern because of its deleterious effects to human health and environment and it exists as metallic, inorganic, and organic forms (Amini et al., 2008). Mercuric ions (Hg (II)), the most stable form of inorganic mercury, present mostly in surface water due to its high water solubility and it can cause serious health problems in human mainly in brain, nervous system, kidneys, and endocrine system (Clarkson et al., 2003). Therefore, it is critical to be able to detect and measure the level of Hg (II) with high sensitivity and selectivity in the presence of other heavy metal ions. Therefore, the determination of Hg (II) ions using a cost effective method with rapid response is highly recommended and the optical assay is highly attractive due to the easy determination of metal ions by using spectroscopic instrumentation technique. Ultra-sensitive determination of Hg (II) has been already reported using different spectrophotometric assays (Chen et al., 2015, Abdelhamid & Wu, 2015). Previously, Ag NPs based optical assays have been successfully employed for a simple and cost effective determination of Hg(II) in aqueous medium (Farhadi et al., 2012, Rameshkumar et al., 2014).

A GO-Ag nanocomposite was prepared by using a ultrasonic irradiation and its applicability was studied for the selective optical determination of Hg(II). A decrease in absorption intensity with color change in GO-Ag nanocomposite was observed with Hg(II) addition. A good selectivity was also observed toward the determination of Hg(II) in the presence of other relevant heavy metal ions.

4.1.2 Results and Discussion

4.1.2.1 Absorption and HRTEM studies of GO-Ag nanocomposite

The formation of Ag NPs was primarily confirmed with the UV-vis absorption spectrum as shown in the Figure 4.1. The appearance of a peak at 227 nm was contributed to the π-π* transition of aromatic C—C bonds and a shoulder peak at ~300 nm corresponds to n-π* transitions of C=O bonds present in GO (Figure 4.1a) (Izrini et al., 2015). After ultrasonic irradiation on the mixture of the $[Ag(NH_3)_2]^+$ and GO solution, a new peak appeared at 400 nm indicating the formation surface plasmon resonance (SPR) absorption band of the Ag NPs (Figure 4.1b-d) (Rameshkumar et al., 2014). The effect of change in concentration of ammonia solution on the formation of the GO-Ag nanocomposite was studied.

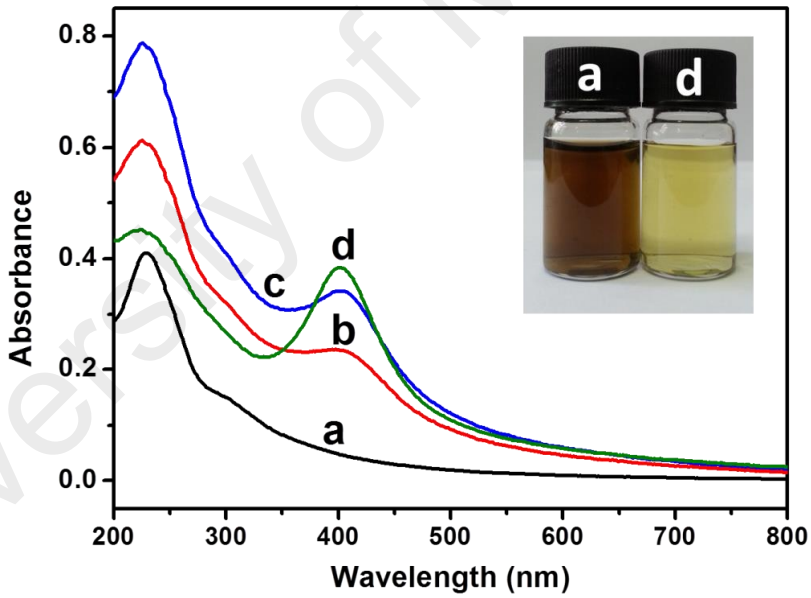

Figure 4.1: UV-visible absorption spectra of GO solution (a) GO-Ag nanocomposite (b-d) (b: 1 %, c: 10 % and 25 % ammonia). Inset: Photograph of GO-Ag nanocomposite solutions.

Three different percentage solutions of ammonia (1%, 10%, and 25%) were used in the synthesis and the usage of 25% ammonia facilitated a better formation of Ag NPs. This can be understood by the appearance of intense SPR peak of Ag NPs present in the

GO-Agnanocomposite with 25% ammonia. The increase of pH of the synthesis solution assisted the complete formation of Ag NPs during ultrasonic irradiation process. The single SPR absorption feature of Ag NPs indicates that the particles may probably have spherical shape with different sizes (Rameshkumar et al., 2014). The appearance absorption peaks at 227 and 300 nm remain with less intensity after the formation GO-Ag nanocomposite and it suggests that the partial reduction of GO might occur during ultrasonic synthesis.

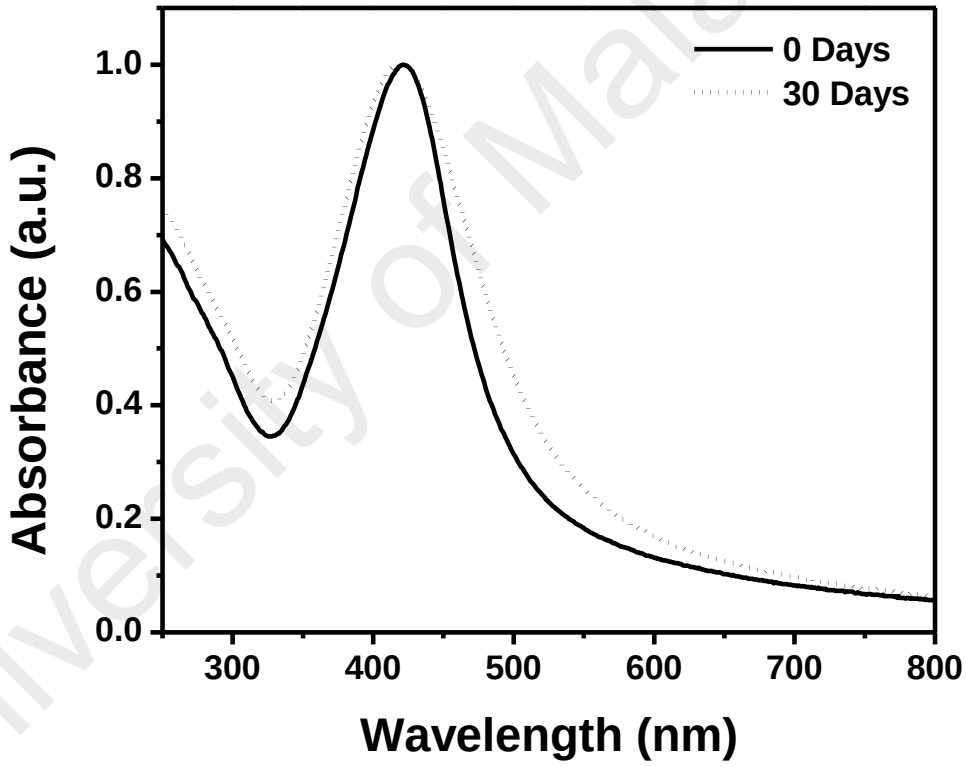

Figure 4.2: UV-Vis absorption spectra of GO-Ag nanocomposite for 0 day and after 30 days.

Inset of Figure 4.1 displays the color change of GO during the formation of GO-Ag nanocomposite and the appearance of yellowish brown color confirmed the formation of Ag NPs on GO sheet. As shown in the Figure 4.2, the stability of the Ag NPs was

checked by monitoring its SPR band on different days and the NPs showed good stability more than a month without changing its SPR band position and intensity. TEM analysis was performed to study the morphology of the GO-Ag nanocomposite. Figure 4.3 displays the TEM images with different magnifications recorded for GO-Ag nanocomposite. It can be seen that the successful deposition of poly-dispersed spherical Ag NPs on GO sheets (Figure 4.3A and B). The spherical shape of Ag NPs relies on the single SPR absorption feature and the average particle size was found to be 12±2.8 nm by taking account of 500 particles for particle size analysis (Figure 4.3C and D). The spherical shape, SPR absorption feature and particle size are correlates with the work reported by Agnihotri et al., in 2014.

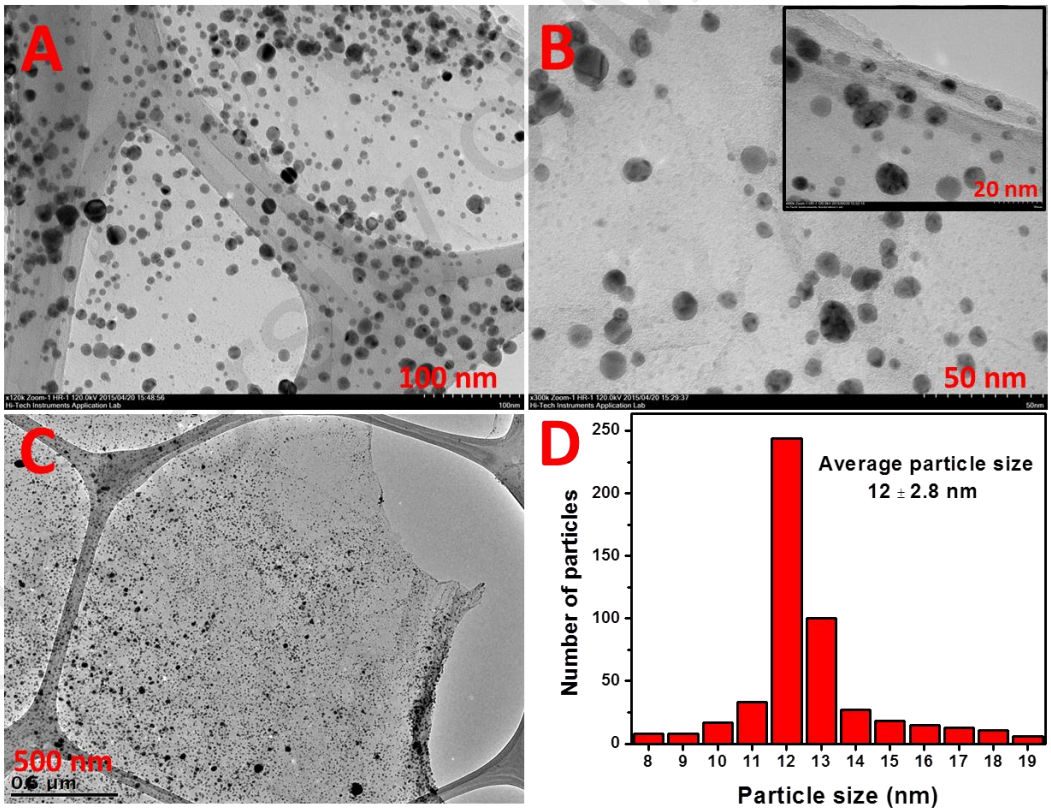

Figure 4.3: TEM images of GO-Ag nanocomposite with different magnifications (A-C) and particle size histogram (D).

4.1.2.2 XRD and Raman studies of GO-Ag nanocomposite

The crystallinity of GO-Ag nanocomposite material was studied by the XRD analysis. From the XRD pattern, it can be seen that the characteristic GO peak centered at 10.0^{o} corresponds to the (0 0 1) reflection of GO (Figure 4.4a) (Radhakrishnan et al., 2014). After the ultrasonic irradiation on the GO-Ag nanocomposite, the peak at 10.0^{o} shifted to 13^{o} and a broad peak appeared at around 31.5^{o} which suggests the reduction of GO after 5 min (Figure 4.4(b-d)). Further, the diffraction peaks appeared at 38.1°, 44.1°, 64.2° and 77.2° correspond to the (111), (200), (2 2 0) and (3 1 1) crystal planes of face-centered cubic (fcc) Ag (Figure 4.4(b-d)). The 2θ values of Ag diffraction match with the standard database values (JCPDS card no. 89-3722). The intensity of Ag diffraction peaks increased with increasing the concentration ammonia in the synthesis of GO-Ag nanocomposite. These results confirm the complete formation of Ag NPs on GO with higher concentration of ammonia under ultrasonic irradiation.

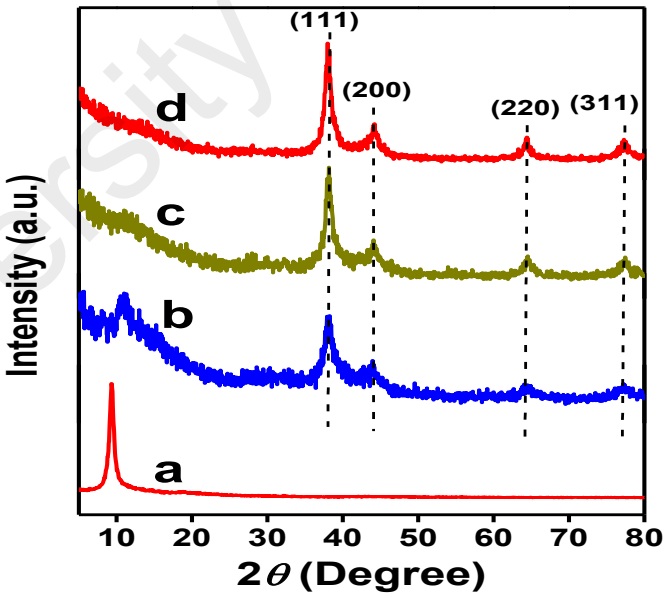

Figure 4.4: XRD patterns of GO (a) GO-Ag nanocomposite (b-d) (b: 1%, c: 10% and d: 25% ammonia).

Raman spectroscopy has been accepted as a versatile and purely optical technique to characterize graphitic or graphitic composite materials. Figure 4.5 shows the two characteristic Raman peaks of GO, namely D and G bands, for GO sheet, GO-Ag1, GO-Ag10 and GO-Ag25. The D band is assigned to the breathing mode of A_{1g} symmetry involving phonons near the K zone boundary, whereas the G band is assigned to the E_{2g} mode of sp^2-bonded carbon atoms (Ferrari & Robertson, 2000). The D and G bands of GO appeared at 1350 cm^{-1} and 1597 cm^{-1}, respectively with the intensity ratio, I_D/I_G, of 0.95. The I_D/I_G ratio of GO-Ag nanocomposite increases with increasing the concentration of ammonia, indicating the increased π-conjugation in aromatics carbons after the ultrasonication treatment. In addition, the Raman spectra of GO-Ag nanocomposite shows that the G band has shifted to lower wavenumbers, which attributed to the reduction in GO during preparation process (Lambert et al., 2009). The Raman results indicated that GO might partially be reduced during the synthesis of GO-Ag nanocomposite.

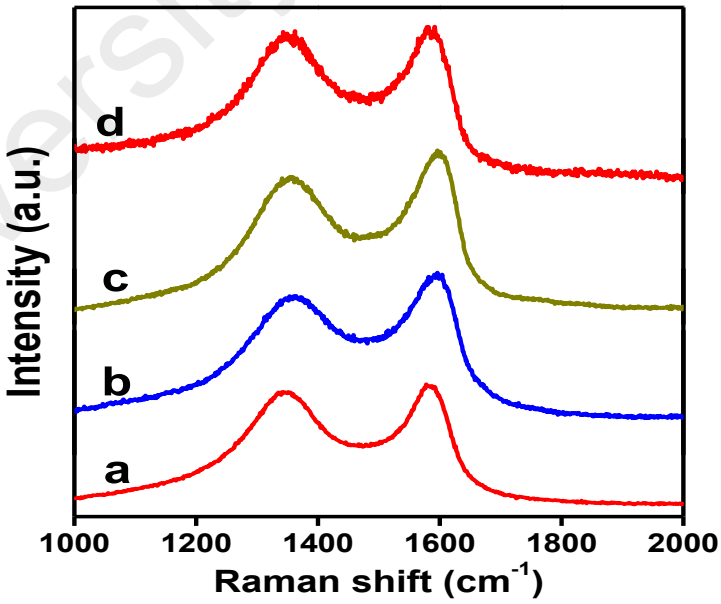

Figure 4.5: Raman spectra of GO (a) and GO-Ag nanocomposite (b-d) (b: 1%, c: 10% and d: 25% ammonia).

4.1.2.3 Spectral and colorimetric determination of Hg(II) ions

The GO-Ag nanocomposite material was tested for the optical determination of Hg(II). Because of the formation of intense SPR absorption band of Ag NPs it would be easy to monitor the changes in the SPR band during the determination of Hg(II). Figure 4.6A shows the SPR absorption spectral changes observed for Ag-GO (d) nanocomposite upon addition of 5 µM Hg(II). A significant decrease in the absorption intensity with a blue shift on the SPR band of the Ag NPs was clearly observed upon increasing the concentration of Hg(II). The blue shift and significant decrease in the absorption peak intensity was due to the redox interaction between the Hg(II) and Ag NPs (Rameshkumar, Manivannan, & Ramaraj, 2013). Since the redox potential of Hg(II)/Hg(0) (+0.85 V) couple is higher than Ag(I)/Ag(0) (+0.8 V) couple, Hg(II) can oxidize the metallic Ag atoms and hence Hg atoms and Ag^{+} ions are produced (Rameshkumar et al., 2013).

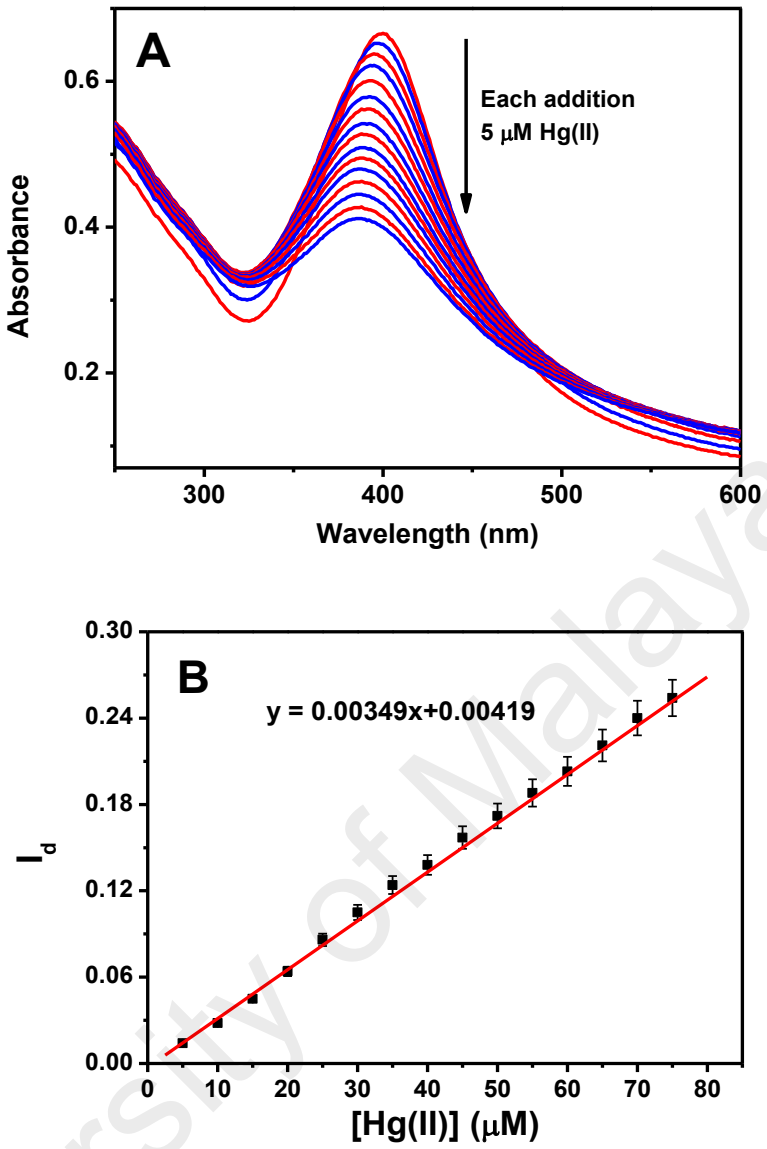

Figure 4.6: SPR absorption spectral changes of GO-Ag nanocomposite upon each addition of 5 μM Hg(II) (A) and the plot of concentration versus difference in absorption intensity (B).

The blue shift in the SPR band can be attributed to the adsorption of Hg onto GO-Ag surface and thereby formed Ag amalgam (Rameshkumar et al., 2013). The plot of absorption intensity difference (I_d) against the Hg(II) concentration showed a linear relationship (R^2 = 0.997) in the Hg(II) concentration range of 5-75 μM (Figure 4.6B). The results were reproducible with three repeated measurements and the limit of detection was calculated as 0.59 μM toward the determination of Hg(II).

The color changes of GO-Ag nanocomposite solution were monitored after the individual addition of 100 µM Hg(II) and 500 µM other environmentally relevant heavy metal ions such as K^+, Mn^{2+} , Fe^{2+} , Ni^{2+}, Cd^{2+}, Cu^{2+}, Pb^{2+} and Zn^{2+} (Figure 4.7). It was noticed that only with the addition of Hg(II) GO-Ag turned colourless whereas, the nanocomposite exhibited its original color even after the addition of 5-fold higher concentration of other metal ions. The SPR spectral changes of Ag NPs were individually measured after the addition of different metal ions and shown as bar diagram in Figure 4.7.

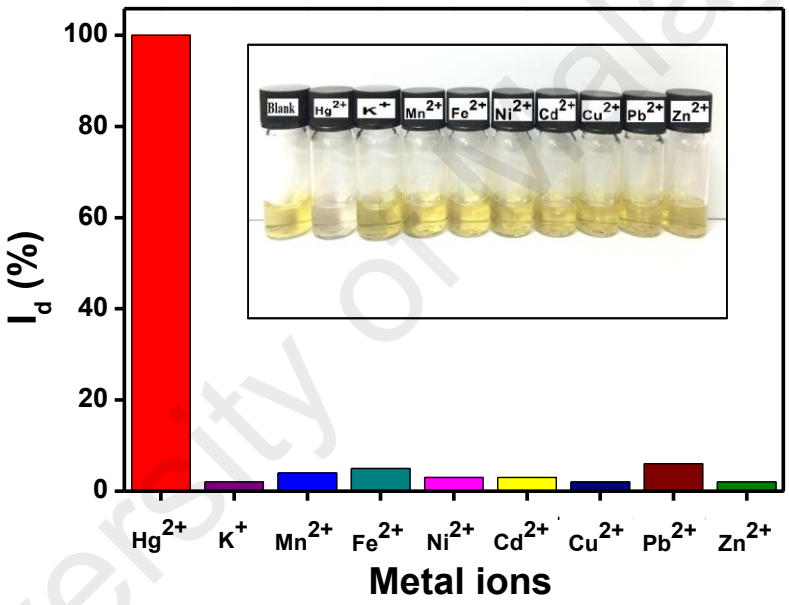

Figure 4.7: Absorption intensity changes observed for GO-Ag nanocomposite solution with the addition of 100 µM Hg(II) and 500 µM other heavy metal ions individually. Inset: photograph of GO-Ag nanocomposite solution after the addition of different metal ions.

A large absorption intensity difference was observed with Hg(II) and no significant changes were noticed with other metal ions. This suggests that the Hg(II) completely quenched the SPR band of Ag NPs by redox interaction. Selectivity of the present assay toward the determination of Hg(II) was also checked by introducing all the interested

metal ions together into the same GO-Ag (d) nanocomposite solution. The spectral changes were monitored after the addition of each 500 μM of other metal ions one by one into the same nanocomposite solution and no significant change was observed in the SPR band (Figure 4.8A(a)). Only after the addition of Hg(II) (100 μM) in the same solution, the SPR band intensity enormously decreased with a significant blue shift in the wavelength (Figure 4.8A(b)). A small decrement in the SPR band intensity observed with other metal ions may be due to the significant dilution caused by the addition of all metal ions together. These results concluded that the GO-Ag nanocomposite is highly selective toward the determination of Hg(II) in the presence of other common toxic metal ions. TEM image of GO-Ag nanocomposite after the addition of Hg(II) was collected and it showed the morphological change of Ag NPs due to the oxidative etching process (Figure 4.8B) (Rameshkumar et al., 2014).

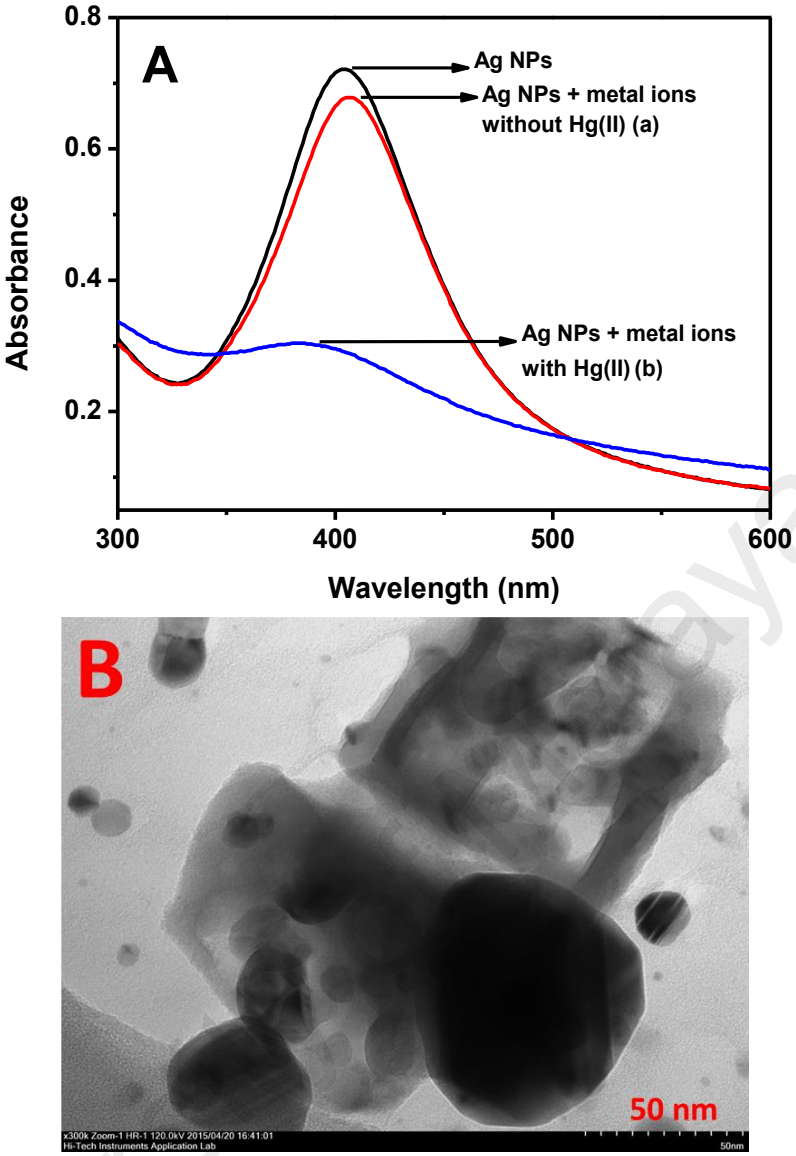

Figure 4.8: SPR spectral changes observed for GO-Ag nanocomposite with the addition of metal ions together (each 500 µM) in the absence (a) and presence (b) of 100 µM Hg(II) (A). TEM image (B) after the addition of Hg(II).

The Ag NPs surfaces were oxidized by the interaction of Hg(II) and probably Ag amalgam occurs. The formation of Ag amalgam was confirmed by XPS analysis. Figure 4.9A shows the XPS spectrum of Hg 4f recorded after the addition of Hg(II) into GO-Ag nanocomposite. The XPS peaks observed at 99.3 and 103.3 eV are assigned to the Hg $4f_{7/2}$ and Hg $4f_{5/2}$ peaks, respectively for metallic Hg. This result reveals the formation Hg(0) during the redox reaction and hence confirming the possibility of

occurring amalgamation with Ag. The survey of XPS analysis of GO-Ag nanocomposite with Hg(II) is shown in Figure 4.9B.

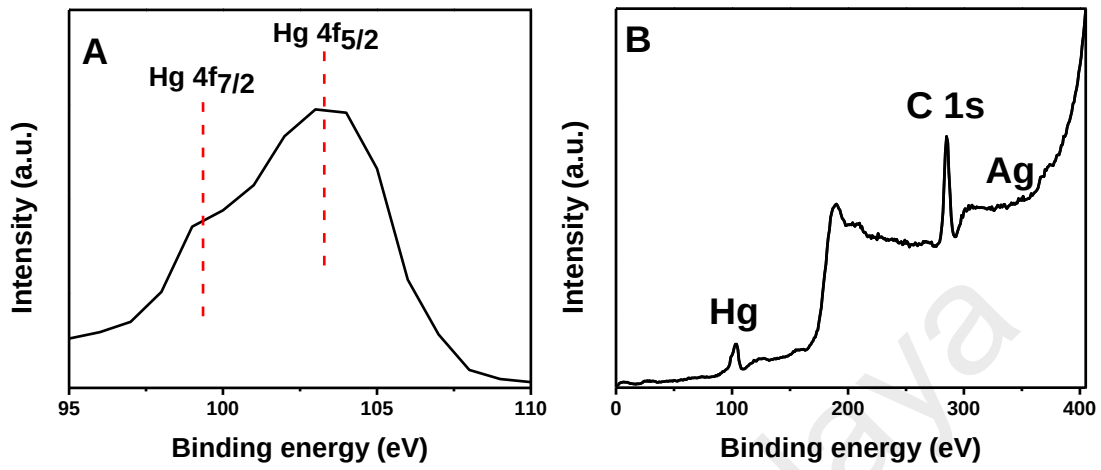

Figure 4.9: XPS spectrum of Hg 4f (A) that recorded for GO-Ag nanocomposite after the addition of Hg(II) and XPS survey spectrum of GO-Ag nanocomposite after the addition of Hg(II) (B).

Table 4.1 summarizes the comparison of analytical performance of the present assay with some of the reported optical assays toward the determination of Hg(II). The Ag NPs were successfully formed on GO sheet by using ultrasonication method. No other reducing agents and surfactants were used for the growth of Ag NPs and the nanocomposite was stable for more than two months. The Ag NPs based low-cost nanocomposite assay displayed an appreciable detection limit with good selectivity towards the optical determination of mercuric ions. The functional groups present in the GO prevented the agglomeration/aggregation of Ag NPs and hence, the surface area of Ag NPs could be fully available for the interaction of mercury ions.

Table 4.1: Comparison of the as-reported assays with the GO-Ag nanocomposite for the optical determination of Hg(II).

Material	Method	Limit of detection (µM)	Selectivity	Reference
Green synthesized Ag NPs	UV-visible	2.2	Selective	(Farhadi et al., 2012)
TPDT[a]–Ag NPs	UV-visible	5.0	Selective	(Rameshkumar et al., 2014)
TPDT–SiO_2/Ag NPs	UV-visible	5.0	Selective	(Rameshkumar et al., 2013)
NSEA[b]–Ag NPs	UV-visible	10.0	Selective	(Anbazhagan et al. 2014)
MA[c]–DTC[d]–Au NPs	UV-visible	0.045	Non-selective	(Mehta & Kailasa, 2015)
TPDT–Au NRs[e]	UV-visible	0.5	Selective	(Jayabal et al., 2014)
Protein–Au NPs	UV-visible	0.2	Non-selective	(Guo et al., 2011)
L-Tyrosine-Au NPs	UV-visible	0.053	Non-selective	(Annadhasan et al., 2014)
L-Tyrosine-Ag NPs	UV-visible	0.016	Non-selective	(Annadhasan et al., 2014)
GO-Ag nanocomposite	UV-visible	0.59	Selective	Present work

[a]*N*–[3–(trimethoxysilyl) propyl] diethylenetriamine, [b]N–steroylethanolamine, [c]Malonamide,[d] Dithiocarbamate, [e]Nanorods.

4.1.3 Conclusions

We successfully synthesized GO-Ag nanocomposite by using ultrasonic irradiation and studied the optical determination of Hg(II). The nanocomposite was successfully characterized by UV-visible absorption spectra, XRD, TEM and Raman analyses. During the optical determination of Hg(II), the SPR band quenching accompanied with color change of GO-Ag nanocomposite was observed. The nanocomposite exhibited an excellent selectivity toward the determination of Hg(II) in the presence of other common heavy metal ions and the LOD was calculated as 0.59 μM for Hg(II) determination. The present study adds further credit to the Ag NPs based nanocomposite assay for the spectrophotometric determination of Hg(II).

4.2 A glassy carbon electrode modified with graphene oxide and silver nanoparticles for amperometric determination of hydrogen peroxide

4.2.1 Introduction

Hydrogen peroxide (H_2O_2) is considered to be an essential mediator in food, pharmaceutical, clinical, environmental analyses and it is a by product in many oxidase catalyzed reactions (Bartlett et al., 1998). Several analytical techniques have been employed for the determination of H_2O_2 including spectrophotometry (Matsubara et al., 1992), chemiluminescence (Hanaoka et al., 2001), and electrochemistry (Yongxins et al., 2013, Li et al., 2005). Among these techniques, electrochemical method has been extensively applied for the determination of H_2O_2 due to its low cost instrumentation, easy operation, an easy transportability of instrument, sensitivity and fast response. Nanostructures of metals (Shihong et al., 2013, Liu et al., 2013) and metal oxides (Jiang et al., 2014, Jia et al., 2009) based electrochemical assays have been widely employed for the determination of H_2O_2.Many research groups reported that silver nanoparticles (AgNPs) modified electrode exhibited electrocatalytic activity for the reduction of H_2O_2 (Welch et al., 2005, Cui et al., 2008, Yingwei et al., 2012, Rameshkumar et al., 2014).

Moreover, it is appreciable to develop an enzyme–free H_2O_2 sensor because of the high cost of enzyme and complicated immobilization process.

A graphene oxide-silver (GO-Ag) nanocomposite was synthesized using a ultrasonic irradiation method and its applicability was studied for the electrochemical determination of H_2O_2 using the corresponding glassy carbon (GC) modified electrode. GO has received a great deal of attention because of its easy preparation on a large-scale and its unique properties (Zhang et al., 2011). GO is an oxygenated, hydrophilic layered carbon material that can be readily functionalized by chemical reaction. It provides a high surface area with large number of functional groups for the stabilization of AgNPs (Izrini et al., 2015). The GO-Ag nanocomposite showed a good catalytic response on the reduction of H_2O_2 and produced a detection limit of 28.3 μM by using amperometric i-t curve toward the determination of H_2O_2.The nanocomposite assay is stable and selective toward H_2O_2 determination among the common physiological interferents such as dopamine, ascorbic acid, uric acid and glucose.

4.2.2 Results and discussion

4.2.2.1 Electrochemical behavior of $[Fe(CN)_6]^{3-/4-}$ couple at GO-Ag nanocomposite modified electrode

Electrochemical impedance spectroscopy (EIS) study is used to gain information about the interfacial properties of surface-modified electrodes and $[Fe(CN)_6]^{3-/4-}$ redox couple was used as a probe to investigate the conducting behavior of the GO-Ag nanocomposite modified electrode surface as well as for testing the kinetic barrier of the electrode/solution interface (Maduraiveeran & Ramaraj, 2007). The Nyquist diagram represents the plot of imaginary versus real part of the complex impedance. Figure 4.10 displayed the Nyquist plots of GCE, GCE/GO and GCE/GO-Ag nanocomposite electrodes for 2.5 mM $[Fe(CN)_6]^{3-/4-}$ in 0.1 M KCl. Bare GCE showed a semicircle-like plot with large charge transfer resistance value (R_{ct}) (Figure 4.10A(a)). The Nyquist plot

of GO modified electrode seems to be semicircle with large diameter which indicates a large increase of resistance due to the hindrance of electron-transfer kinetics caused by the non-conducting behavior of GO at the modified electrode surface (Figure 4.10A(b)). The R_{ct} value of GCE for $[Fe(CN)_6]^{3-/4-}$ redox couple was highly decreased after the modification with GO-Ag nanocomposite due to the deposition of highly conductive AgNPs on GO sheet (Figure 4.10A(c)).

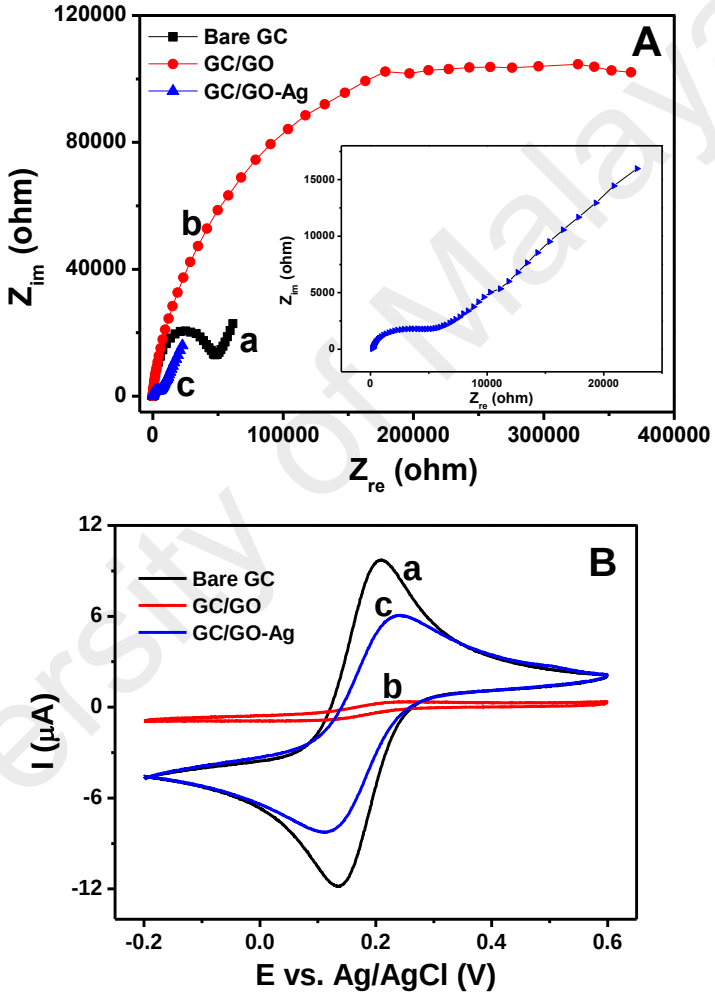

Figure 4.10: A) Nyquist plots obtained for 2.5 mM of $K_3[Fe(CN)_6]$ in 0.1 M KCl at bare GCE (a), GCE/GO (b) and GCE/GO-Ag nanocomposite (c) electrodes. Inset shows the expanded view of "c".B) Cyclic voltammograms recorded for 2.5 mM of $K_3[Fe(CN)_6]$ at bare GCE (a), GCE/GO (b) and GCE/GO-Ag nanocomposite (c) electrodes in 0.1 M KCl with a scan rate of 50 mV s^{-1}.

Moreover, the linear portion of the Nyquist plot indicated that the electrochemical reaction may be facilitated by the diffusion controlled process. Bode-phase plots of the modified electrodes were collected in the frequency range of 0.01–10000 Hz (Figure 4.11A) and a low charge-transfer resistance was observed for GO-Ag nanocomposite modified electrode when compared to the other electrodes. Bode impedance plot of GO-Ag nanocomposite modified electrode showed a lesser log Z value at a low frequency range of 1-100 Hz in logarithm when compared to the other modified electrodes (Figure 4.11B).

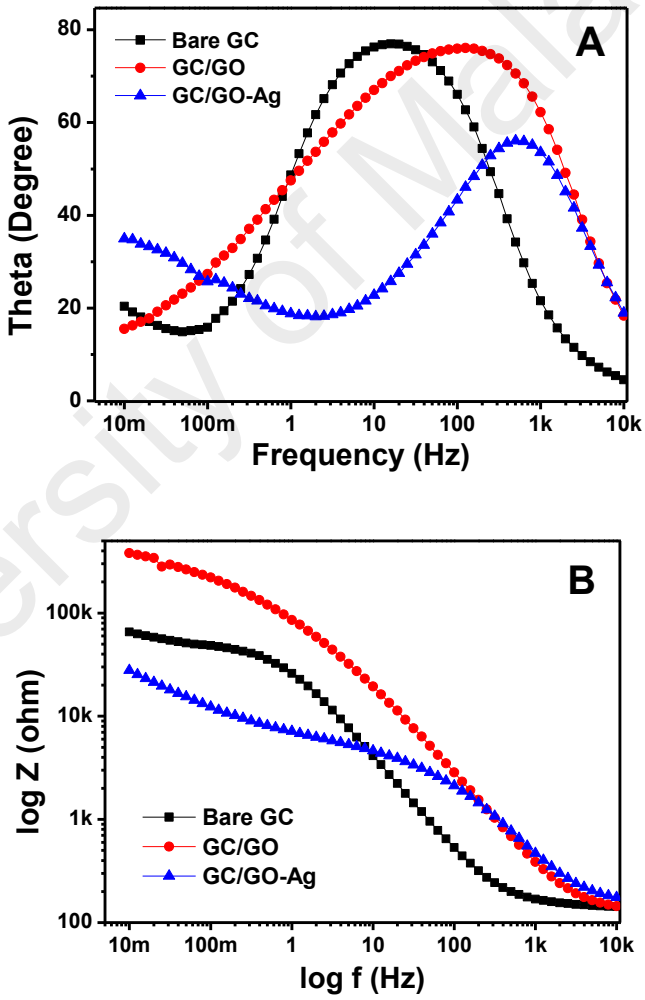

Figure 4.11: Bode phase plots (A) and Bode impedance plots (log Z *vs.* log f) (B) obtained for bare GCE, GCE/GO and GCE/GO-Ag nanocomposite electrodes for 1 mM $K_3[Fe(CN)_6]$ in 0.1 M KCl.

The cyclic voltammetric responses that observed for $[Fe(CN)_6]^{3-/4-}$ redox analyte at the bare GCE, GCE/GO and GCE/GO-Ag nanocomposite modified electrodes are shown in Figure 4.10B. As known, bare GCE displayed a reversible electrochemical response for the redox reaction of $[Fe(CN)_6]^{3-/4-}$ couple with a peak-to-peak separation of 71 mV (Figure 4.10B(a)). The GC/GO modified electrode displayed a reversible voltammetric signal very low peak currents and large peak-to-peak separation when compared to bare GCE (Figure 4.10B(b)). This observation reveals the kinetic hindrance of GO modified electrode on the electron transfer process.

The redox current response with reversibility was enormously enhanced by the modification of GO-Ag nanocomposite when compared to GO modified electrode (Figure 4.10B(c)). The current enhancement of GO-Ag nanocomposite modified electrode is attributed to the conducting behavior of AgNPs present at the electrode surface and the AgNPs deposited on the GO surface acted as a new electrode which makes a good electrical contact with the GCE surface. The EIS and cyclic voltammetric studies suggested that the present GO-Ag nanocomposite modified electrode can be used for suitable electrocatalytic applications.

4.2.2.2 Electrocatalytic reduction of H_2O_2

The electrocatalytic reduction of H_2O_2 was studied at GO-Ag nanocomposite modified GC electrode. The cyclic voltammetric responses for the reduction of 1 mM H_2O_2 at the bare GCE, GO and GO–Ag nanocomposite modified electrodes in 0.1 M phosphate buffer (pH 7.2) are displayed in Figure 4.12A. Interestingly, the GO–Ag nanocomposite modified electrode showed a catalytic peak current at the peak potential of –0.5 V for the reduction of H_2O_2 (Figure 4.12A(c)) and no voltammetric response was observed at bare GCE (Figure 4.12A(a)) as well as for GCE/GO (Figure 4.12A(b)) electrode. The nanocomposite modified electrode did not show any peak current in the absence of H_2O_2 (Figure 4.12A(d)). The presence of AgNPs at the GO-Ag

nanocomposite modified electrode favors the electron transfer to H_2O_2 during the electrocatalytic reduction. AgNPs provide larger surface area for the specific interaction of H_2O_2 and thereby enhanced the electron-transfer kinetics during the electrocatalytic reduction of H_2O_2.

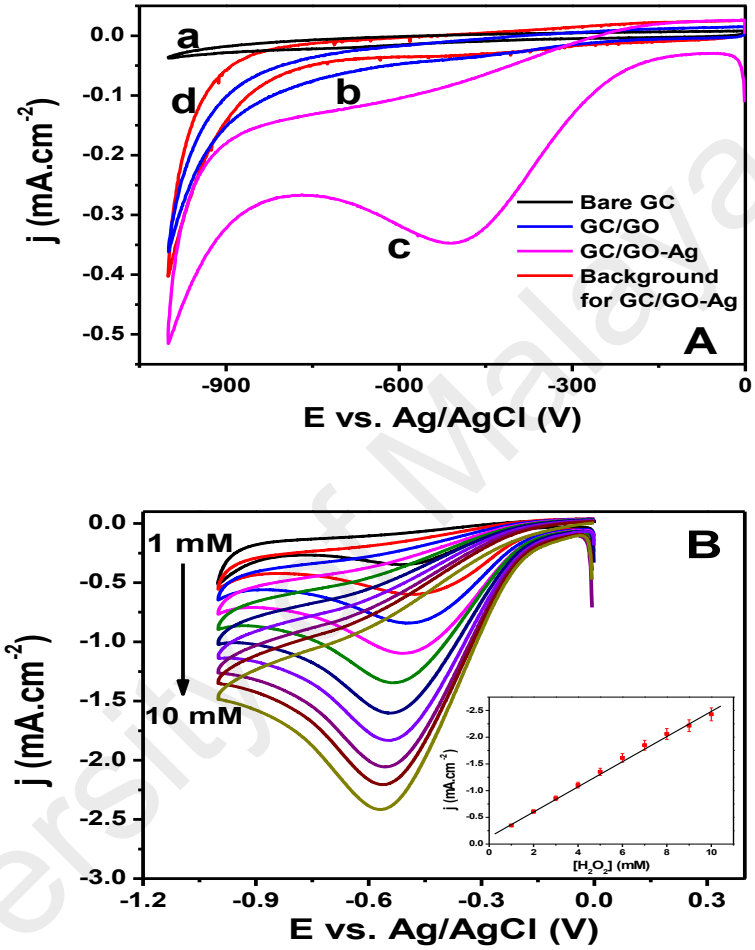

Figure 4.12: A) Cyclic voltammograms recorded for 1 mM H_2O_2 at bare GCE (a), GCE/GO (b) and GCE/GO-Ag nanocomposite (c) electrodes in 0.1 M phosphate buffer (pH 7.2) at a scan rate of 50 mV s^{-1}. (d) Cyclic voltammogram recorded at GCE/GO-Ag nanocomposite modified electrode in the absence H_2O_2. B) Cyclic voltammograms recorded for successive additions of H_2O_2 (1-10 mM) in 0.1 M phosphate buffer (pH 7.2) at GCE/GO-Ag nanocomposite modified electrode with a scan rate of 50 mV s^{-1}. Inset shows the plot of peak current versus the concentration of H_2O_2.

The loading of GO-Ag nanocomposite on GCE was optimized by making the sample with different dilutions (Figure 4.13). The bulk nanocomposite showed a poor catalytic response toward the electrocatalytic reduction of H_2O_2 due to the kinetic hindrance exerted by the large amount of GO.

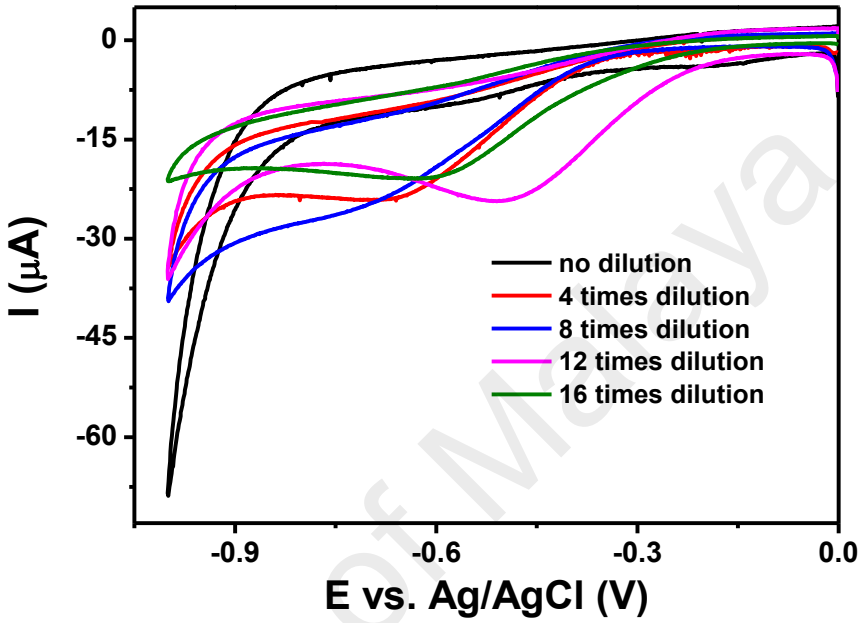

Figure 4.13: Cyclic voltammograms for 1 mM H_2O_2 at GC/GO-Ag nanocomposite modified electrode with different loading of GO-Ag nanocomposite in 0.1 M phosphate buffer (pH 7.2). Scan rate was 50 mV s^{-1}.

Under optimized loading, the nanocomposite showed better catalytic reduction peak current with a significant shift in the overpotential. The result was reproducible and repeatable with different electrodes and successive experiments. The peak current increased with increasing the concentration of H_2O_2 (Figure 4.12B) and the plot of peak current versus concentration showed a linear relation (Figure 4.12B(inset)). Effect of varying scan rate on the catalytic reduction current of H_2O_2 was also studied for GO–Ag nanocomposite modified electrode (Figure 4.14). Increasing scan rate resulted in increased catalytic peak current of H_2O_2 reduction and a linear relationship observed between the peak currents and square roots of scan rates (Figure 4.14 (inset)). This

concludes that the reduction of H_2O_2 at the GO-Ag nanocomposite modified electrode is controlled by diffusion process (Rameshkumar et al., 2014).

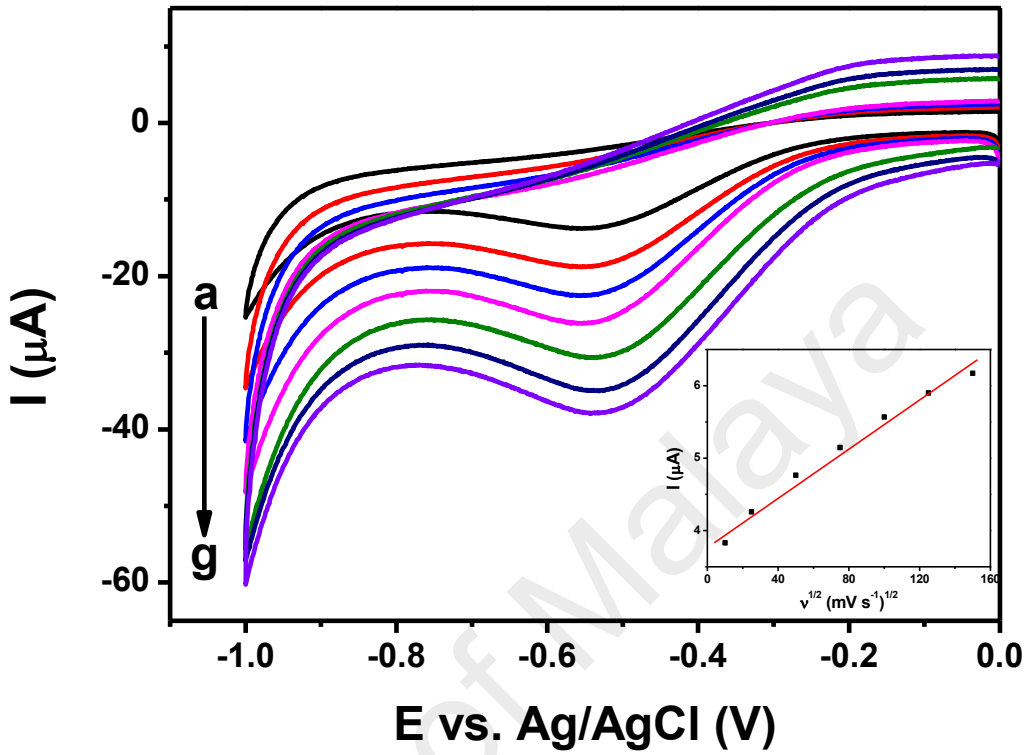

Figure 4.14: Cyclic voltammograms for 1 mM H_2O_2 at GC/GO-Ag nanocomposite modified electrode in 0.1 M phosphate buffer (pH 7.2) with various scan rates (a: 10, b: 25, c: 50, d: 75, e: 100, f: 125 and g: 150 mV s^{-1}). Inset represents the plot of peak current versus square root of scan rate.

4.2.2.3 Enzymeless electrochemical determination of H_2O_2

An electrochemical assay was prepared based on GO-Ag nanocomposite for enzymeless determination of H_2O_2. The amperometric i-t curve responses were recorded at the GO-Ag nanocomposite modified electrode for the successive additions of H_2O_2 with a concentration range of 100 µM-15 mM at a regular time interval of 60 s in N_2 saturated and homogeneously stirred solution of 0.1 M phosphate buffer (Figure 4.15).

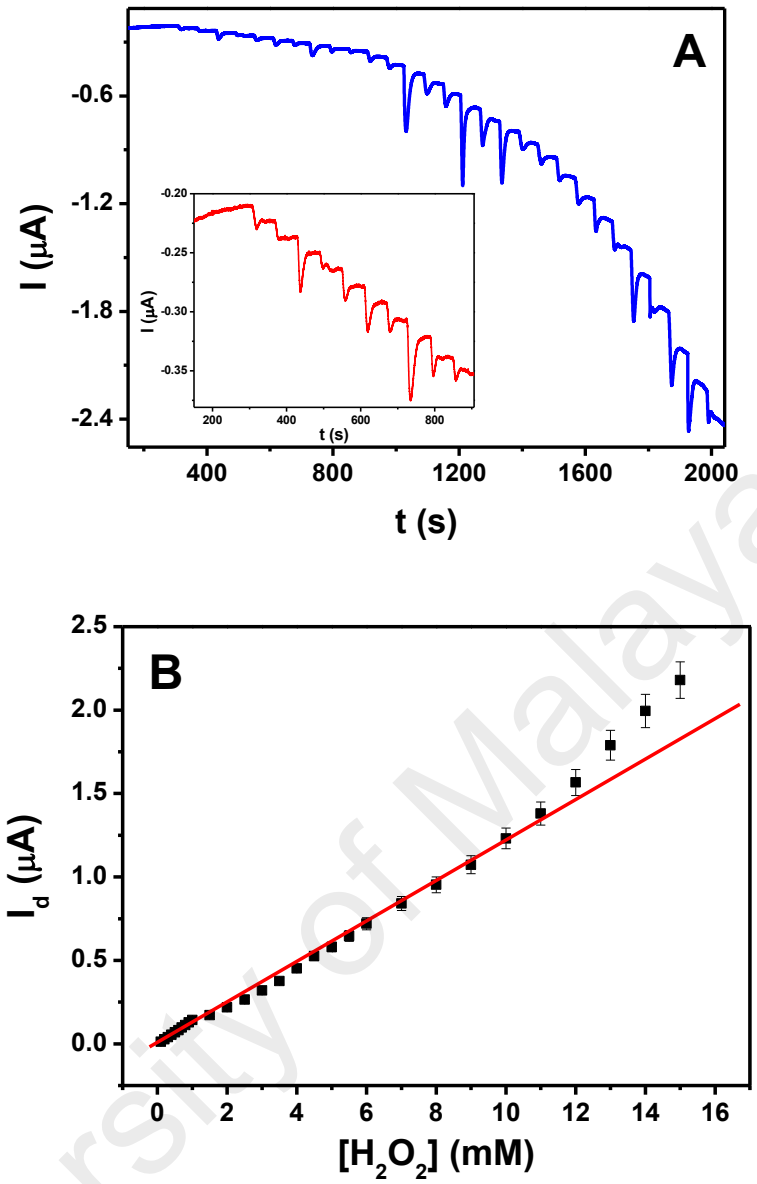

Figure 4.15: A) Amperometric i-t curve responses at GCE/GO-Ag nanocomposite modified electrode for successive additions of H_2O_2 (100 µM-15 mM) in homogeneously stirred solution of 0.1 M phosphate buffer (pH 7.2) at a regular time interval of 60 s. Applied potential was -0.3 V vs. Ag/AgCl. Inset shows the expanded view of current response for each 100 µM addition of H_2O_2. B) Plot of current difference versus the concentration of H_2O_2.

The applied potential used (-0.3 V) for amperometry was lower than peak potential (-0.5 V) to avoid or decrease the interferences caused by the electroactive species present in the solution (Yingwei et al., 2012). Enhancement in the current response was

observed for the successive injection of different concentrations of H_2O_2 (100 µM-15 mM) and the plot of current difference (I_p) versus concentrations showed a linear line (Figure 4.15B).

Table 4.2: Comparison of some of the reported silver-based nanostructures based electrochemical assays for the determination of H_2O_2

Material[a]	Detection potential (V)	Detection limit (µM)	Linear range (µM)	Interferents studied[b]	Reference
GCE/PVP-AgNWs	–0·3 V vs. Ag/AgCl	2.3	20–3620	–	(Yang et al., 2012)
Silver nanowire array	−0.2 V vs. SCE	29.2	100–3100	AA, OA, SO, PO, EtOH, glucose, UA	(Kurowska et al., 2013)
GCE/AgNPs	−0.85V vs. SCE	10.0	25–500, 500–5500	AA, glucose, UA, sucrose	(Raoof et al., 2012)
GCE/Au@Ag@C	−0.55 V vs. Ag/AgCl	8.32	75–4750	glucose, DA, UA, AA	(Yancai et al., 2015)
GCE/CNTs–AgNPs	−0.45 V vs. Ag/AgCl	1.6	50–9000	–	(Shi et al., 2011)
Porous Au–Pt NPs	+0.1V vs. Ag/AgCl	50.0	300–10000	AA, AP	(Lee et al., 2011)
Ag NPs-PVA/Pt	−0.5V vs. SCE	10.0	45–6000	–	(Guascito et al., 2008)
Nanorough Ag	−0.3 V vs. SCE	6.0	10–22500	AA, UA, SO_4^{2-}, CO_3^{2-}, Fe^{3+}, ClO_3^-, Cl^-	(Lian et al., 2009)
GCE/GO-Ag nanocomposite	−0.3 V vs. Ag/AgCl	28.3	100-11000	DA, AA, UA, glucose	Present work

[a]PVP = Polyvinylpyrrolidone, AgNWs = Silver nanowires,CNTs = Carbon nanotubes, PVA = polyvinyl alcohol,[b] OA = Oxalic acid, SO = Sodium oxalate, PO = Potassium oxalate, AP = Acetaminophen.

The nanocomposite modified electrode showed a linear range of 100 μM–11 mM with correlation coefficient, R^2 = 0.988 (y = 0.1218x+0.0019) toward the determination of H_2O_2. The current responses were reproducible for the repeated measurements. The sensitivity of the modified electrode was found as 0.1218±0.0025 μA/mM and the LOD was calculated to be 28.3 μM. Table 4.2 shows the comparison of analytical performance of the present assay with some of the reported metal nanostructure based assays toward the electrochemical determination of H_2O_2.

4.2.2.4 Interference study

Selectivity of the GO-Ag nanocomposite assay toward the determination of H_2O_2 was investigated by introducing common physiological interferents in the same homogeneouly stirred phosphate buffer containing H_2O_2 and the change in current response was noticed. Figure 4.16 displays a continuously recorded amperometric i–t curve response for the successive additions of H_2O_2 and interferents in 0.1 M phosphate buffer (pH 7.2) with a regular interval of 60 s.

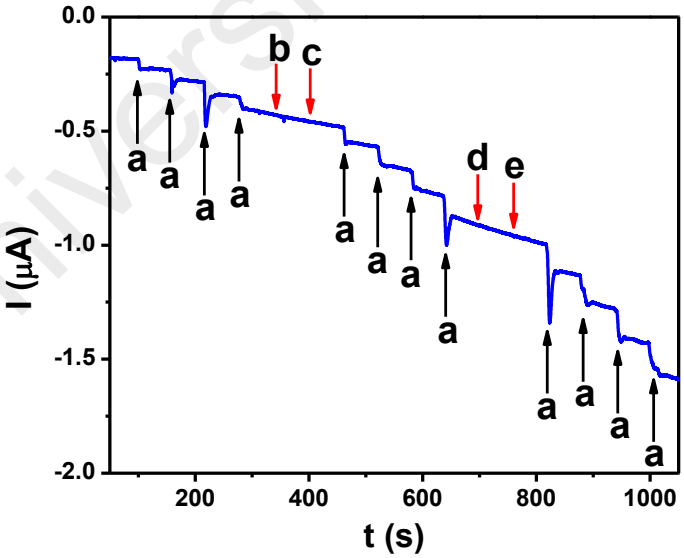

Figure 4.16: Amperometric i–t curve responses obtained at GCE/GO-Agnanocomposite modified electrode for the successive addition of 1 mM H_2O_2(a) and each 5 mM of DA (b), AA (c), UA (d) and glucose (e) in phosphate buffer (pH 7.2) at a regular time interval of 60 s. Applied potential was -0.3 V vs. Ag/AgCl.

The current response of the interferents DA and AA was studied by injecting them one by one after the few successive additions of 1 mM H_2O_2 in the same stirred phosphate buffer. However, the addition of interferent molecules did not produce any current response even with 5-fold higher concentration. Again the injection of H_2O_2 in the same solution displayed almost same magnitude of current response for the reduction of H_2O_2. After the few successive additions of H_2O_2, the more interferents such as uric acid and glucose were added one by one in the continuously recorded i-t curve and the addition of these interferents did not show any enhancement in the current response. However, the addition of 1 mM H_2O_2 to the same solution again resulted in a clear and fast response. These results indicated that the present assay exhibits a good selectivity and sensitivity towards the determination of H_2O_2 even in the presence of 5-fold excess of common physiological interferents.

The square wave voltammetric (SWV) technique was also employed for the determination of H_2O_2 by using GO-Ag nanocomposite modified GCE. The SWV responses observed for the successive addition of 100 µM H_2O_2 are shown in Figure 4.17A. The peak current corresponding to the reduction of H_2O_2 at the modified electrode increased with respect to the concentration of H_2O_2 and the plot of peak current versus concentration displayed a linear relation (Figure 4.17B). The observation of split in the SWV peaks may be due to the pre-adsorption of H_2O_2 molecules at the nanocomposite modified electrode (Lyon & Stevenson, 2006).

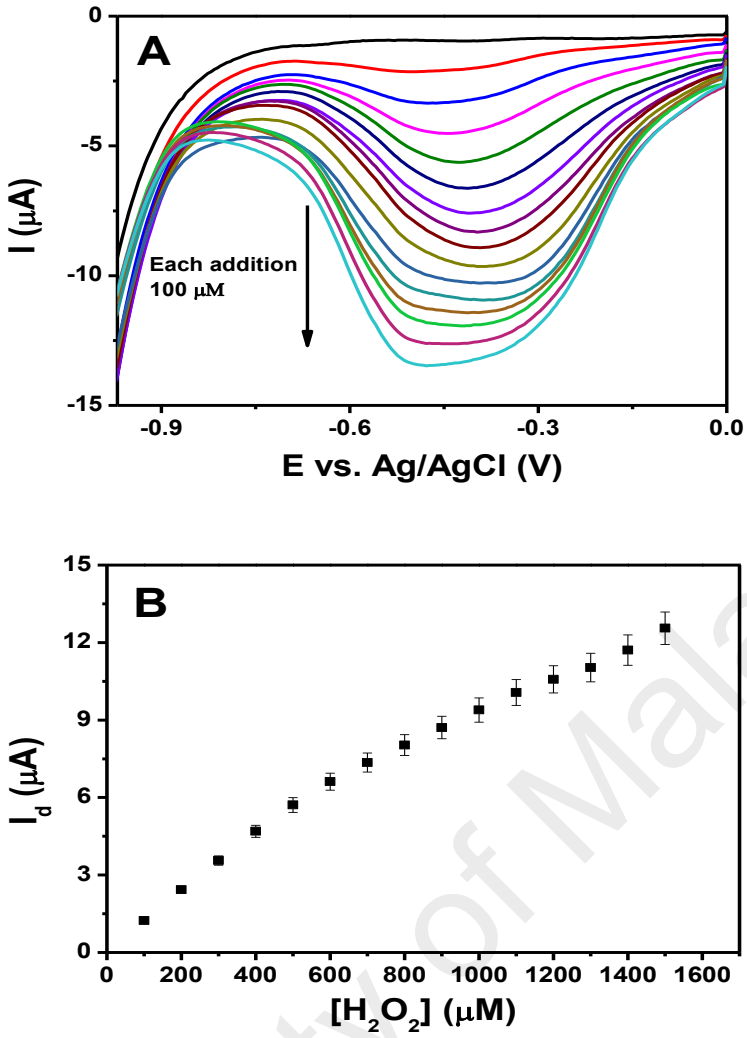

Figure 4.17: A) SWV responses obtained at GC/GO-Ag nanocomposite modified electrode for the successive additions of each 100 μM H_2O_2 in 0.1 M PBS (pH 7.2). B) Plot of difference in current versus concentration of H_2O_2.

4.2.3 Conclusion

We successfully fabricated an assay for the electrochemical determination of H_2O_2 by using GO-Ag nanocomposite. The GO-Ag nanocomposite modified GCE showed an excellent electrocatalytic performance on H_2O_2 reduction. The amperometric i-t curve displayed a linear range of 100 μM–11 mM (R^2 = 0.988) with the LOD of 28.3 μM toward the determination of H_2O_2. The nanocomposite assay exhibited a good selectivity among the common interferents such as DA, AA, UA and glucose. The

electrochemical assay was stable and the current responseswere reproducible for the repetitive measurements.

4.3 Microwave assisted synthesis of graphene oxide-silver nanocomposite and its applications in SERS and spectrophotometric determination of dopamine

4.3.1 Introduction

In recent years, graphene oxide (GO) has been gaining a lot of interest worldwide due to its excellent properties, which makes it possible to be assigned in various applications (Stankovich et al., 2007, Lightcap et al., 2010). GO which is known as two-dimensional carbon-layered structure that possesses a large theoretical specific surface area which contains oxygen-containing groups, carboxyl, hydroxyl, epoxide, and carbonyl groups (Stankovich et al., 2007). The presence of these functional groups in GO has caused it to be easily dispersed in water and colloidally stable in solvents. Thus, the improvement of many aspects such as its biocompatibility (Karuppiah et al., 2014), absorbance capacity (Yang et al., 2011), and nanoscale substrate in preparing reduced graphene oxide-based nanocomposite materials (Kumar et al., 2013) were observed.

In addition, GO has also become very popular due to its bulk scalability and cost effectiveness in preparing graphene. Among all of the studies being carried out on GO, silver nanoparticles (AgNPs) decorated graphene nanocomposites have been the main focus among the researchers, which is believed to be the attribute of their multifunctional abilities and enhanced performance in a wide range of applications such as sensing and catalysis (Kamali et al., 2015, Golsheikh et al., 2014, Rameshkumar et al., 2014). The usage of AgNPs is appreciated in nanocomposite synthesis because it is low in cost, while the synthesis of AgNPs can be easily monitored according to their typical surface plasmon resonance (SPR) absorption feature (Lingxin et al., 2013).

Until today, several techniques have been adopted to prepare AgNPs-decorated GO such as hydrothermal (Shen et al., 2011), ultrasonication (Das et al., 2011), and gamma-

ray irradiation (Wang et al., 2013). However, these methods are not feasible as they require sophisticated skills and expertise. Therefore, nowadays, microwave irradiation has been widely used in the synthesis of nanoparticles and composite materials due to its homogenous heating procedure and the reaction rate which can be easily speed up only by controlling the orders of magnitude compared to the conventional heating process (Huang et al., 2011).

Neurotransmitters are considered crucial in both the central and peripheral nervous systems due to their functions to deliver the coding of information in the form of nerve impulse from the brain (Albert et al., 2009). Dopamine (DA) is an important monoamine neurotransmitter that is produced from phenylalanine. Inside the brain, substantia nigra and the ventral tegmental area is a small factory that produces DA. An abnormal DA level in the brain could lead to some diseases such as euphoria as well as pleasurable and rewarding feelings (Pandikumar et al., 2014). It is important to note that the symptom of stress, fatigue, low motivation and depression are caused by the low level of DA in human body.

Meanwhile, schizophrenia and social anxiety are basically the result of excessive amounts of DA in the human body systems. Disordered DA in the frontal lobes may contribute to attention deficit disorder and damage the neurocognitive functions such as memory, attention, and critical thinking. The measurement of DA is also recommended to be conducted as the marker level for monitoring Parkinson's disease (Pandikumar et al., 2014). Hence, the development of a sensor for the determination of DA is crucial to diagnose disease. Apart from being the cheapest and flexible technique, optical sensors provides a lot of advantages including non-invasiveness, low toxicity, and multianalyte detection compared to other sensing techniques (Nagl & Wolfbeis, 2007). On the other hand, surface enhanced Raman scattering (SERS) is a promising technique to be applied

for biological diagnosis, chemical detection, and biomedical application. Raman scattering is enhanced when the molecules are adsorbed or approached to a noble metal surface (Qin et al., 2015). This property is typically useful in detecting, sensing, or imaging the biological samples such as DNA, proteins, cells, and tissues.

In this study, the microwave irradiation assisted synthesis of GO-Ag nanocomposite and its applications in SERS and spectrophotometric determination of DA are reported. A uniform distribution of spherical AgNPs with an average size of 19 nm was observed on the GO sheet, which produced excellent surface plasmon resonance (SPR) properties of AgNPs. The nanocomposite showed the presence of good SERS activity on DA substrate. Spectrophotometric determination of DA was also performed on the nanocomposite and the limit of detection of DA was observed and recorded at 66.1 nM.

4.3.2 Results and Discussion

4.3.2.1 Characterization of GO-Ag nanocomposite

The UV-visible absorption spectra of GO and GO-Ag nanocomposite are shown in Figure 4.18. As revealed by the spectrum, two characteristic peaks of GO were observed at 227 and 299 nm, which were then assigned to the $\pi \rightarrow \pi^*$ transition of aromatic C-C bond and the $n \rightarrow \pi^*$ transition of C=O group, respectively (Noor et al. , 2016). Finally, a distinct peak was obviously observed at 403 nm after the mixture of $[Ag(NH_3)_2]^+$ and GO solution is being treated for microwave irradiation. It is safe to conclude that this peak corresponds to the SPR effect of AgNPs (Abdel et al., 2012).

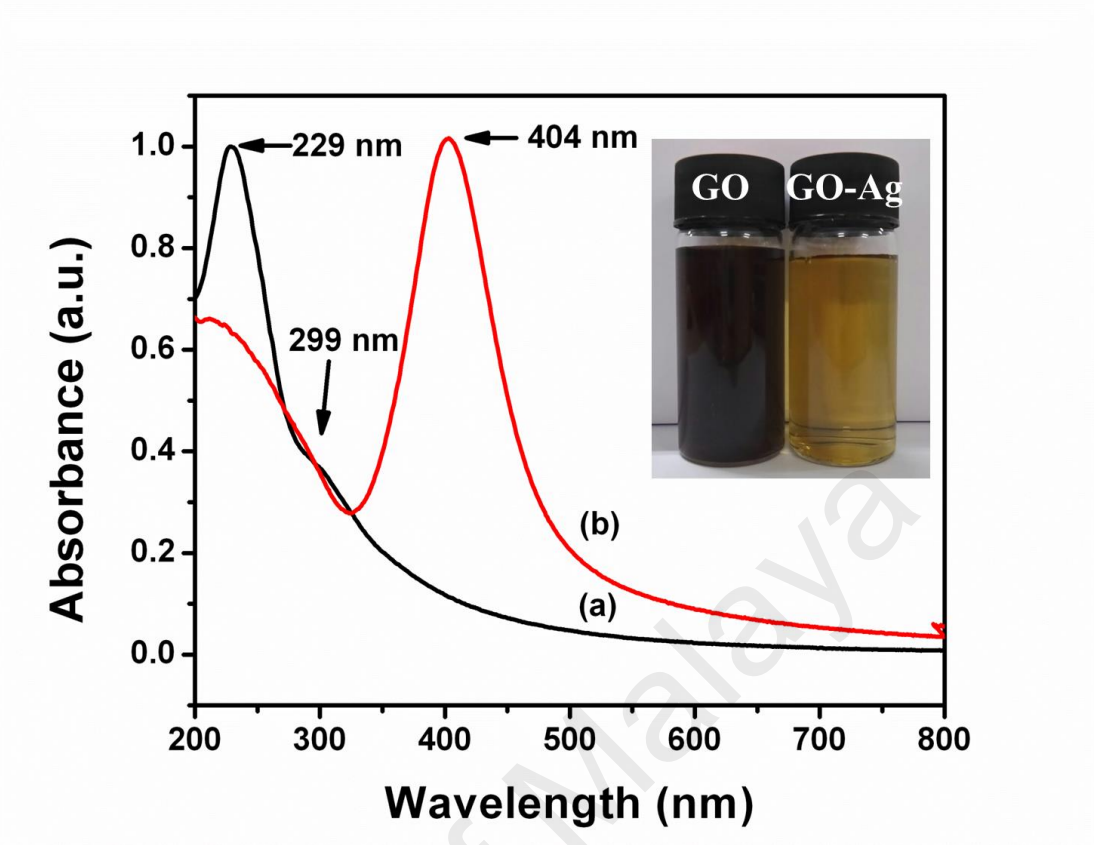

Figure 4.18: UV-visible absorption spectra of GO (a) and GO-Ag nanocomposite (b). Inset: Photograph of GO and GO-Ag nanocomposite solutions.

In addition, the existence of absorbance peak at 220 nm and SPR peak suggest that GO was not reduced for microwave irradiation time of 30 s. Instead, an absorption peak was observed clearly at 402 nm after 30 s of microwave irradiation which leads to the formation of spherical AgNPs. A schematic illustration for the formation of GO-Ag nanocomposite that carried out by using microwave irradiation is shown in Figure 4.19.

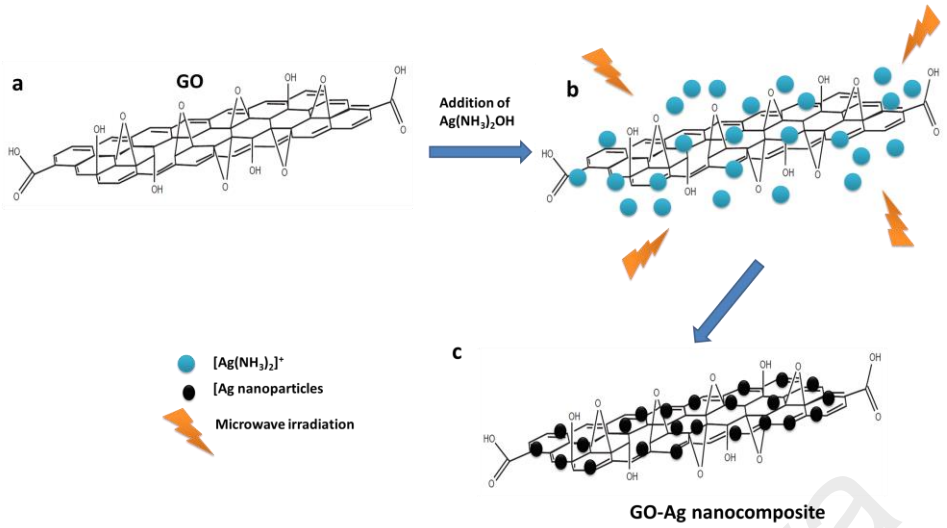

Figure 4.19: Schematic illustration for the synthesis of GO-Ag nanocomposite under microwave irradiation.

GO layer is commonly known to be negatively charged due to the ionisation of carboxyl and hydroxyl groups as shown in Figure 4.19 (a) (Li et al., 2008). As can be observed in Figure 4.19 (b), the positively charged silver complexes $[Ag(NH_3)_2]^+$is absorbed on the GO layers through electrostatic attraction. With the treatment of microwave irradiation presented in Figure 4.19 (c), the aqueous mixture experiences continuous heating through the accumulated microwave energy, which leads to the production of highly reactive H and OH radicals resulted by the pyrolysis process of water molecules (Pol et al., 2002). The generated H radicals act as reducing agent for the adsorbed $[Ag(NH_3)_2]^+$ions in order to form AgNPS through microwave irradiation.

Figure 4.20 shows the XRD patterns of both GO and GO-Ag nanocomposite. Pristine GO portrays its well-known peak at 10.0^o that is assigned to a *d*-spacing of 0.82 nm, which is best attributed to the C-plane of (0 0 1) diffraction (Zainy et al., 2012). The XRD pattern of GO-Ag is possible to be well indexed to JCPDS 89-3722, which correspond to the (111), (200), (220), and (311) planar crystallographic of the face-centered cubic (fcc) silver nanoparticles. Apart from that, the C-plane of (001) peak of

GO produces a less prominent peak after completing the microwave irradiation, which is believed to be resulted by the growth of AgNPs on the surface of GO nanosheets that prevents the restacking of GO layers (Teo et al., 2012, Xie et al., 2012).

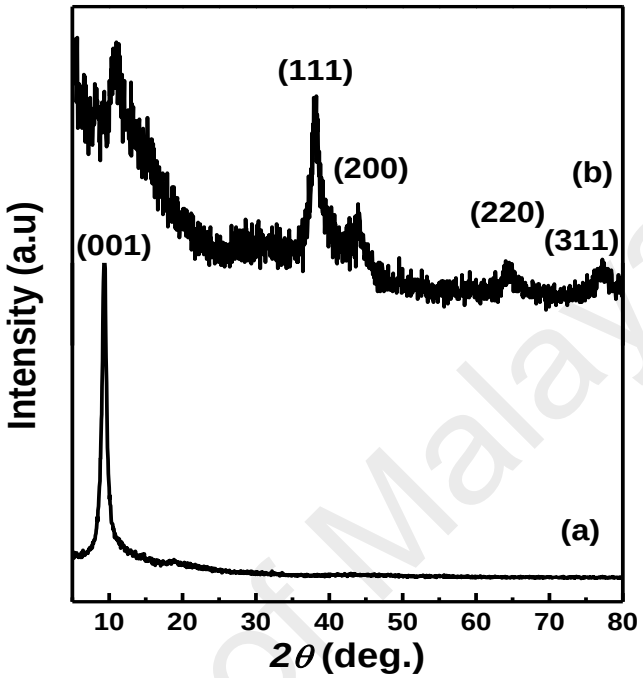

Figure 4.20: XRD patterns of GO (a) and GO-Ag nanocomposite (b).

Figure 4.21 shows the Raman spectra of GO and GO-Ag nanocomposite with different irradiation times. Both GO and GO-Ag nanocomposites produce two characteristic peaks, which are labeled as D and G bands of GO. The D band corresponds to the defect detected in the layer caused by the vibration of sp^3-bonded carbon atoms, whereas the G band is ascribed to the E_{2g} mode of sp^2-bonded carbon atoms (Zhu et al., 2010). Meanwhile, the intensity peaks of the D and G bands were enhanced in the presence of AgNPs due to the surface enhanced Raman scattering effect from AgNPs.

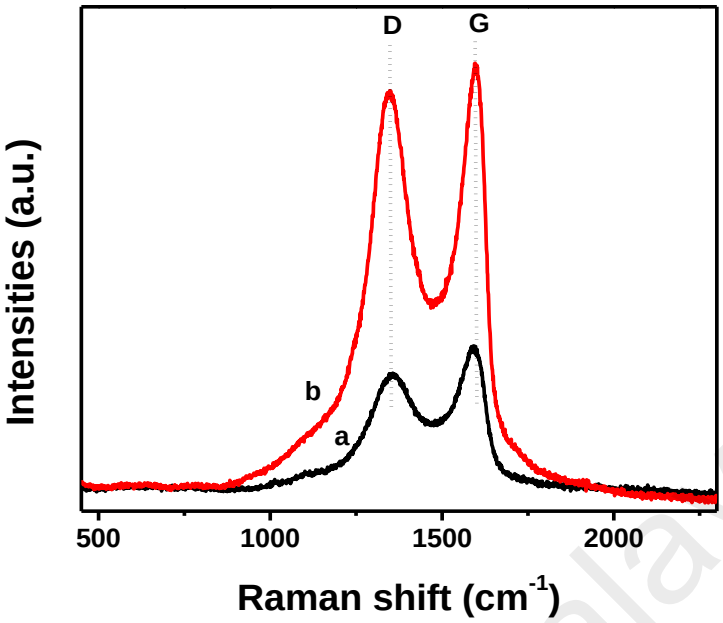

Figure 4.21: Raman spectra of GO (a) and GO-Ag nanocomposite (b).

The morphology of the GO-Ag nanocomposite was studied and investigated by using TEM analysis. Figure 4.22A and Figure 4.22B display the TEM images with different recorded magnifications of GO-Ag nanocomposite. On top of that, the successful deposition of spherical AgNPs on GO sheetsis also presented in Figure 4.22A. The spherical shape of AgNPs that corroborates on the single SPR absorption band in the UV-vis spectrum as well as the average particle size was calculated to be at 19±5.8 nm by selecting 300 particles in the particle size analysis. Figure 4.22B shows a HRTEM image of single AgNPs embedded on the GO sheet. The measured lattice fringe of 0.23 and 0.20 nm correspond well to the (1 1 1) and (2 0 0) planes of Ag nanocrystal, respectively (JCPDS no. 89-3722). It can be concluded that this observation supports the formation nanocrystal of Ag in the XRD pattern.

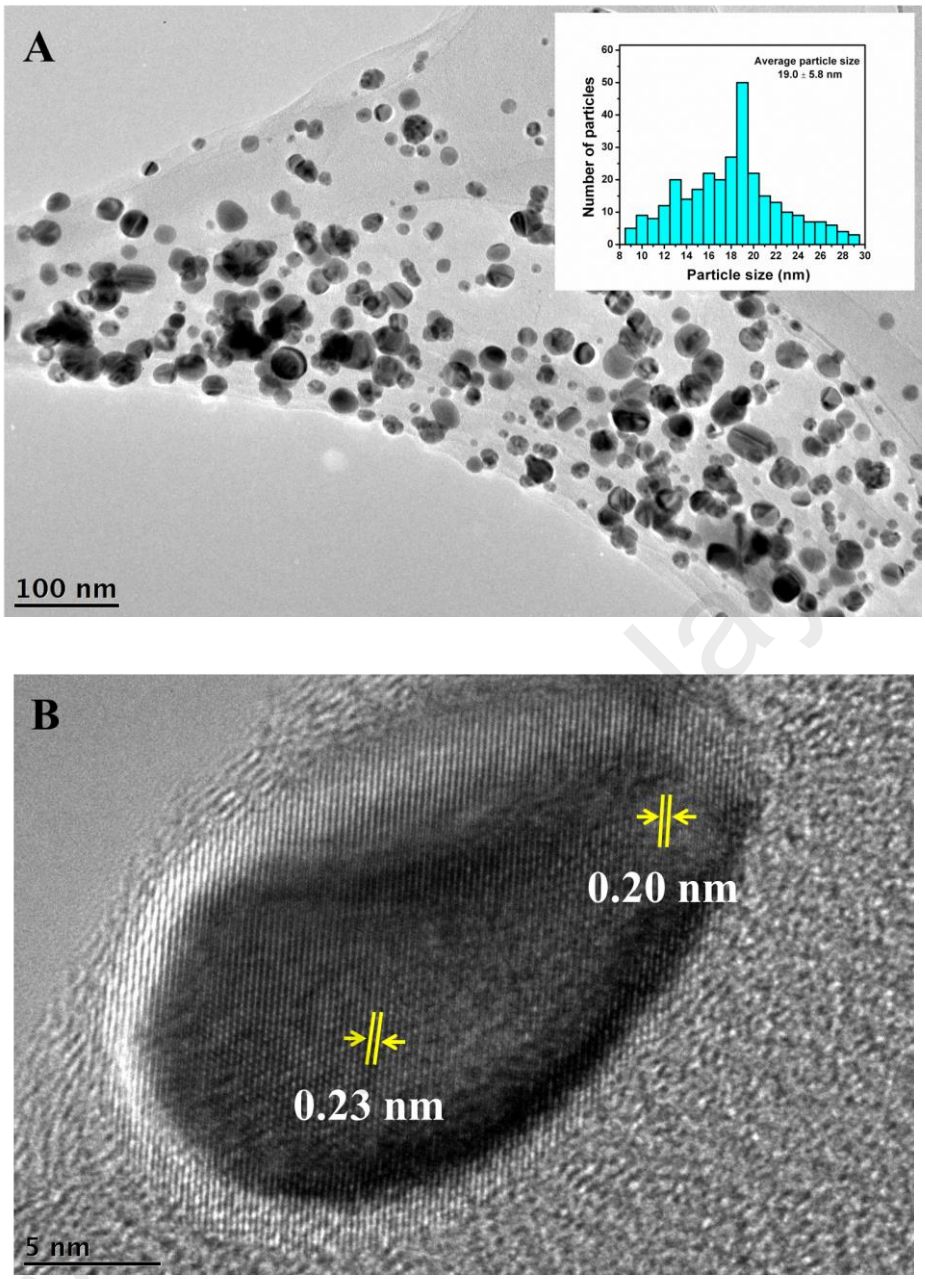

Figure 4.22: TEM images of GO-Ag nanocomposite recorded with the low (a) and high (b) magnifications. (Inset: Particle size histogram).

4.3.2.2 SERS Activity of GO-Ag Nanocomposite

DA was used as a model Raman probe to evaluate the SERS activity which is carried out on GO-Ag nanocomposite. Figure 4.23A (a) shows the Raman spectrum of pure solid dopamine powder with the most prominent peaks recorded at 747, 793, 960, and 1287 cm^{-1}. Figure 4.23A (b and c) displays the SERS spectra for 1 x 10^{-3} M DA with

both the GO and GO-Ag nanocomposite acting as SERS substrates. As shown in Figure 4.23A (b), a tiny apparent Raman peaks of DA was detected on the surface of GO alone. In comparison to the spectrum of DA, the SERS spectrum obtained on GO-Ag nanocomposite shows a distinct frequency shifts on a few observable changes in the band intensity as can presented in Figure 4.23A (c). Figure 4.23B shows the SERS spectra of GO-Ag nanocomposite with different concentrations of DA (1×10^{-6} to 1×10^{-3} M). The main peak of DA at 747 and 793 cm^{-1} are distinguishable up to 1×10^{-6} M, which strongly suggests that DA can be detected with GO-Ag nanocomposite at a concentration as low as 1×10^{-6} M.

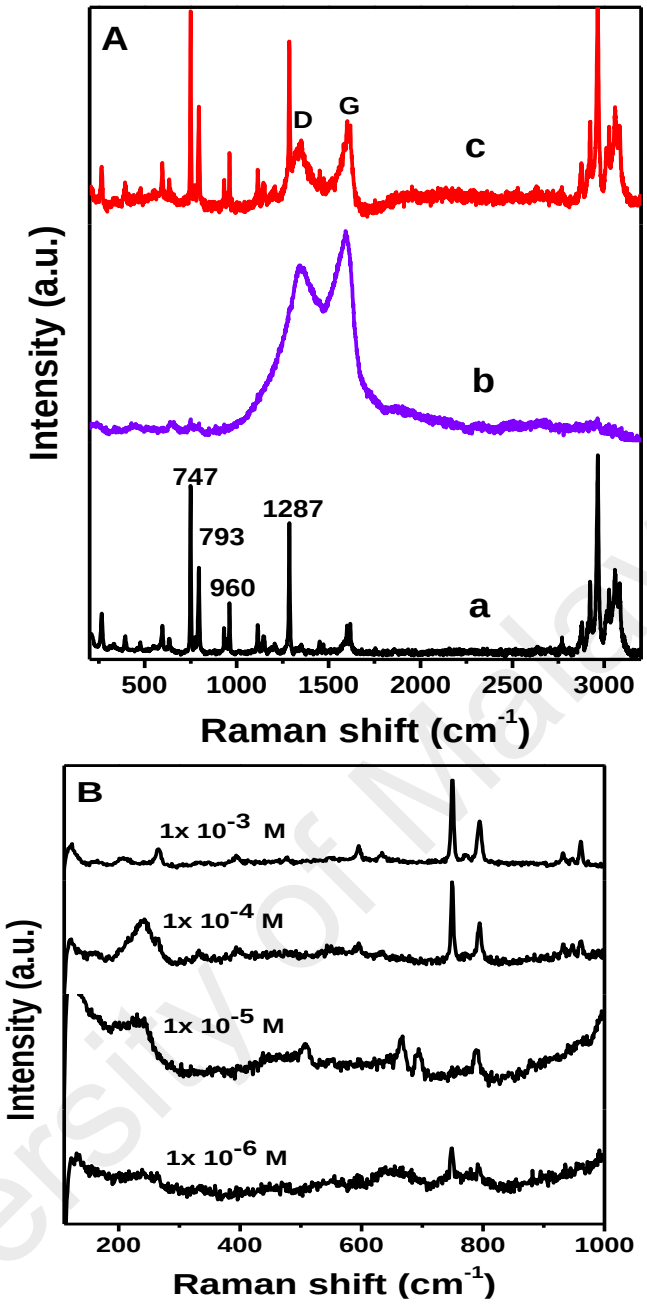

Figure 4.23: A) Raman spectrum of DA (a), SERS spectra of DA and GO (b) and GO-Ag nanocomposite (c). B) SERS spectra of DA with different concentrations on GO-Ag nanocomposite.

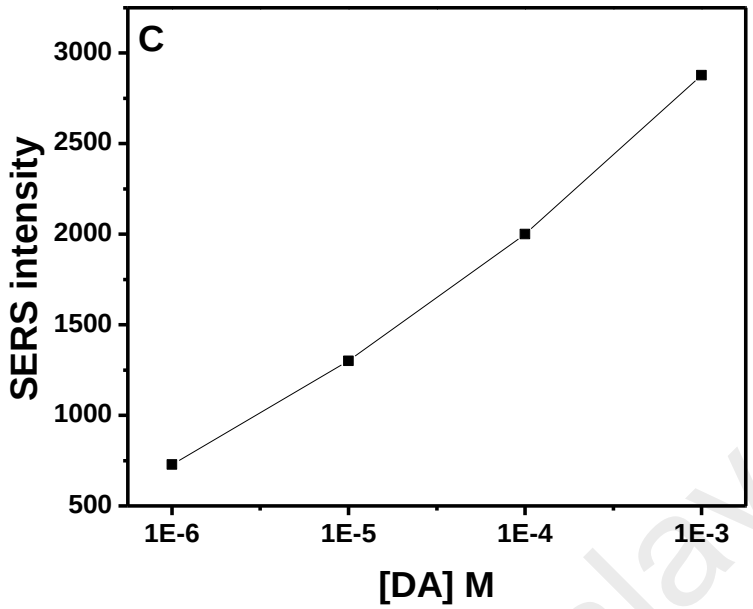

Figure 4.24: The plots of SERS intensity of DA at 800 cm^{-1} versus the concentration of DA.

4.3.2.3 Optical determination of dopamine

The UV-vis spectral changes were recorded during the successive additions of DA into the GO-Ag nanocomposite in order to study the efficiency of GO-Ag for the spectrophotometric determination of DA. As presented in Figure 4.25A, the SPR band intensity of GO-Ag nanocomposite is significantly increased with an observable occurrence of red shift when the concentration of DA is also increased. The GO layer stabilized the AgNPs and facilitated the adsorption of DA on the surface of AgNPs.

As shown in Figure 4.25B, the maximum absorption intensity of GO-Ag nanocomposite being observed on each addition of DA was plotted against the concentration of DA. As depicted in the same figure, the calibration curve which is subjected to the concentration of DA shows a straight line. Meanwhile, the limit of detection of spectrophotometric was calculated and recorded at 66.0 nM. Table 4.3 shows the comparison of analytical performance of the present assay with some of the

reported metal nanostructure-based assays occurred during the spectrophotometry determination of DA.

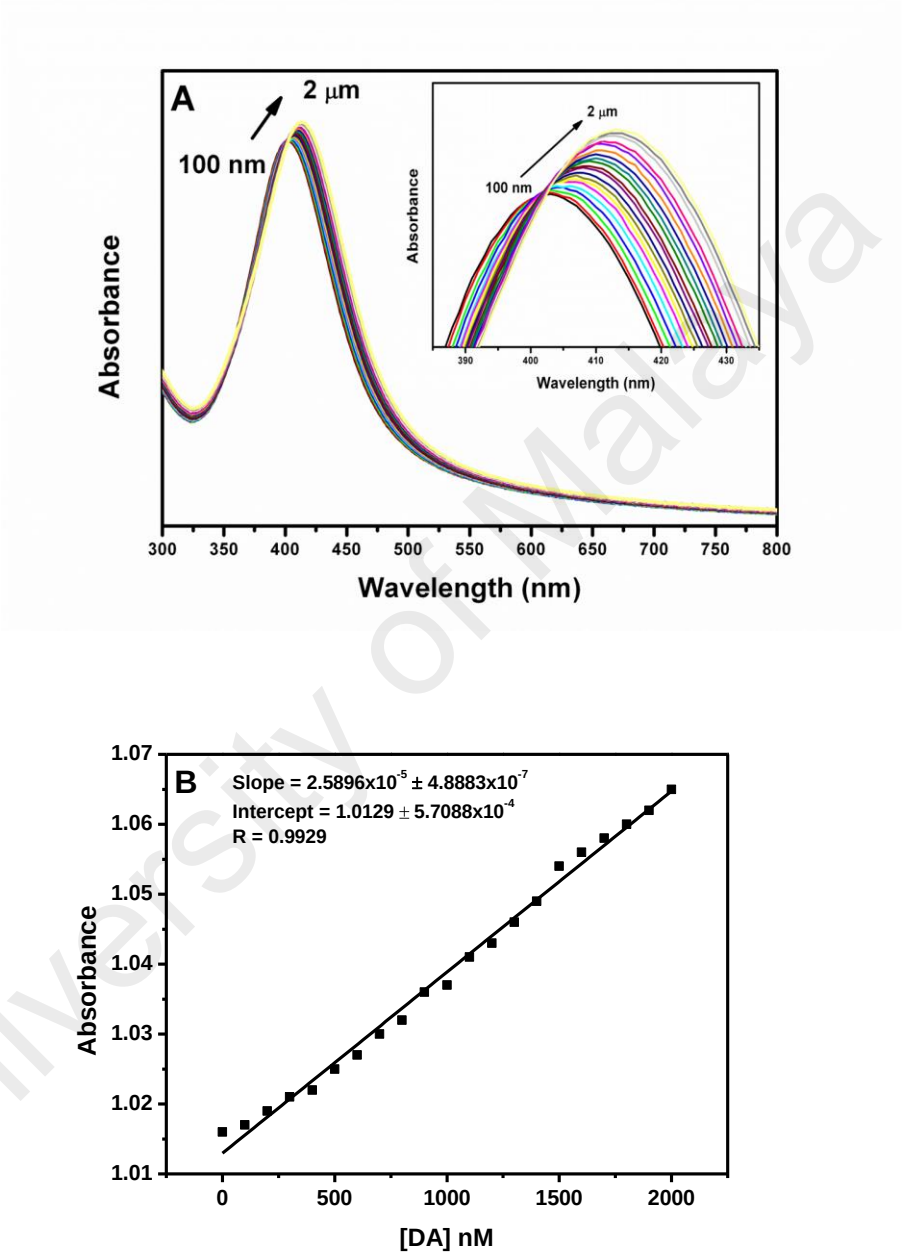

Figure 4.25: SPR absorption spectral changes of GO-Ag nanocomposite upon each addition of 5μM DA (A) and calibration plot of concentration versus difference in absorption intensity (B). Inset: Expanded view of red-shifted absorption intensity.

Table 4.3: A comparison of some of the reported sensors for DA detection via various methodologies.

Sensing material	**Analytical technique**	**LOD**	**Reference**
Luminol-Ag(III) complex	Electrophoresis	0.069 μM	(Xu et al., 2012)
AgNPs composite	Electrochemical	0.5 nM	(Evtugyn et al., 2011)
AgNPs/rGO	Electrochemical	5.4 μM	(Kaur et al., 2013)
Rod-shape CuO NPs	Electrochemical	0.055 μM	(Reddy et al., 2012)
GE/Au/GE/CFE	Electrochemical	0.59 μM	(Du et al., 2013)
G/HDT/Au/SAMs	Electrochemical	90 μM	(Raoof et al., 2010)
$Ag_{core}Au_{shell}$ NPs	Optical	0.1 μM	(Bu & Lee, 2012)
Chitosan-gold	SERS	1 mM	(Lim & Kang, 2013)
AuNPs	Optical	30 nM	(Yuanfu et al., 2010)
GO-Ag composite	Optical	66.0 nM	This work
GO-Ag composite	SERS	1.0 μM	This work

AgNPs = silver nanoparticle AuNPs = gold nanoparticle GE = graphene CFE = carbon fibre electrode G = gold HDT = 1,6-Hexanedithiol SAMs = self-assembled monolayers

A plausible explanation for the large red shift is related to the changes in the morphology of AgNPs that caused by the addition of DA. Figure 4.26A shows the aggregation of AgNPs that occurred after adding the DA into the GO-Ag nanocomposite solution.

According to the Mie theory, any changes being made in the refractive index of the local environment of metal nanoparticles surface can possibly cause some adjustment in the intensity as well as the position of the SPR absorption band. The increase in the refractive index of the surrounding medium often causes a red shift in the SPR absorption band of AgNPs. On top of that, the SPR is mainly dependent on the free electron density of metal NPs which is affected by the charge transfer that occurs during the bonding of metal NPs and adsorbed molecules. It is worth to note that the red-shifted of the SPR band is caused by the electron transfer from the AgNPs to DA molecule (Bu & Lee, 2012, Ghosh & Pal, 2007).

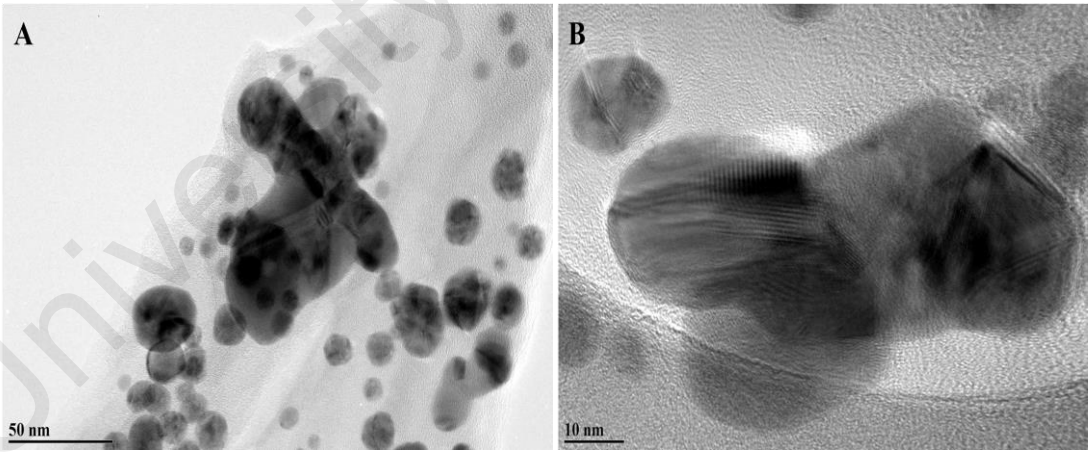

Figure 4.26: TEM image of GO-Ag nanocomposite after the addition of DA.

4.3.3 Conclusion

GO-Ag nanocomposite was successfully prepared by using microwave irradiation while the spectrophotometric and SERS determination of dopamine (DA) were

evaluated. The nanocomposite was characterized based on UV-visible absorption spectra, XRD, Raman, and TEM analyses. A uniform distribution of 19 nm AgNPs on the GO sheet showed the presence of an excellent SERS activity, and DA at concentration as low as 1 x 10^{-6} M managed to be detected. The red-shifted in the absorbance peak was observed and the LOD was calculated to be 66.0 nM during the spectrophotometric determination of DA. The present study adds further credit to AgNPs nanocomposite by demonstrating a potential application in SERS as well as spectrophotometric determination of DA.

4.4 Microwave synthesis of reduced graphene oxide decorated with silver nanoparticles for electrochemical detection of 4-nitrophenol

4.4.1 Introduction

Graphene, a monolayer of sp^2 carbon atoms densely packed into a honeycomb structure has a unique nanostructure with extraordinary properties and has become an attractive nanoscale building block for the new materials (Zhu et al., 2010). Thus, it offers potential applications in various advanced technology such as sensors, supercapacitors and catalysis (Luo et al. 2015, Yang & Gunasekaran, 2013, Chang & Wu, 2013). Because of its characteristics including high electrical conductivity, possess a large surface-to-volume ratio and chemical tolerance; make it predominantly employed as a matrix for composite.

On top of this, insertion of nanoparticles (NPs) into a graphene matrix has been the focus of research for the exploration of their properties and applications (Chang & Wu, 2013). Among these, silver metal nanoparticles (AgNPs) decorated graphene nanocomposites have been the main focus among researchers because of their multifunctional abilities (Kumar et al., 2013, Lima et al., 2014). This is due to its absorption feature arising from the surface Plasmon resonance (SPR) effect in which AgNPs decorated graphene are the most frequently researched nanocomposite which are

reflected in their enhanced performance in a wide range of applications including catalysis, electronics and sensors (Chen et al., 2013, Golsheikh et al., 2014, Rameshkumar et al., 2014, Zangeneh Kamali et al., 2015).

A variety of chemical and physical techniques has been employed to prepare AgNPs, however a poor stability and hard to reproducible due to colloidal aggregation become the major drawback. To overcome these issues, a graphene was chosen as a support material for growing the AgNPs. A large surface area of graphene nanosheets and strong Van der Waals force between the graphene layer and AgNPs reduces the nanoparticles aggregation. Besides, the interfacial interactions strengthen the stability and reproducibility of AgNPs. In recent years, studies reported that the AgNPs decorated graphene nanocomposites synthesized through *in situ* reduction of Ag^{+} ions on graphene oxide (GO) surface or decoration of GO with pre-synthesized synthesized AgNPs (Liu et al., 2010, Golsheikh et al., 2014). Such strategies involve multiple steps hence make the procedure very complex. In addition, the process normally require a toxic and hazardous reducing and/or stabilizing agents like hydrazine, $NaBH_4$, formaldehyde which are exposing risks to the health and environment (Tian et al., 2012).

Until today, several techniques have been adopted to prepare Ag NPs-decorated graphene oxide such as, hydrothermal (Shen et al., 2011) and ultrasonication (Das et al., 2011). However, these methods are not feasible as they require strong skills and expertise in this field. In this paper, we demonstrate a one-step, cost effective and easy synthesis of rGO uniformly decorated with AgNPs using the microwave assisted method as an alternative approach as it does not involve any toxic reducing or stabilizing agents.

Nitroaromatic compounds are extensively used in the manufacturing of pharmaceutical product, pesticides, fungicides and dyes which are considered to be highly toxic even at a very low concentration, hence responsible for various health problems in human beings and damage to the environment (Yin et al., 2012, Madhu et al., 2014, Santhiago et al., 2014). Due to its carcinogenic, mutagenic and embryonic toxicants, 4-nitrophenol needs to be monitored by a reliable technique which gives an efficient analytical procedures. Several methods have been reported such as spectrophotometry, capillary electrophoresis and liquid chromatography in determining of 4-NP. However, electrochemical sensing has attracted attention because of its excellent sensitivity, a rapid response, easy to operate and inexpensive (Madhu et al., 2014, Tang et al., 2013). On the other hand, the nitro compounds could be electrochemically reduced in the presence of aromatic or heterocyclic compounds that permits the sensing of 4-NP (Zeng et al., 2014, Liu et al., 2009, Ikhsan et al., 2016).

An electrochemical sensing platform made of the rGO-Ag nanocomposite was developed for the detection of 4-NP. The nanocomposite was prepared by using microwave irradiation in the absence of reducing agents. The rGO-Ag (3 min) nanocomposite modified glassy carbon electrode was used for the amperometric detection of 4-NP at a working potential of -0.52 V and the limit of 4-NP detection was found to be 0.32 μM. It showed good selectivity to 4-NP in the presence of intereferent molecules and could be successfully applied for the determination of 4-NP in real water samples.

4.4.2 Results and Discussion

4.4.2.1 Characterization of the rGO-Ag nanocomposite

The formation of AgNPs was primarily confirmed by using UV-Vis absorption spectroscopy. The UV-visible absorption spectra of GO and rGO-Ag (30 s, 1 min and 3 min) nanocomposites are shown in Figure 4.27. As revealed by the spectrum, two

characteristic peaks of GO were observed at 227 and 299 nm, which were assigned to the $\pi \rightarrow \pi^*$ transition of aromatic C-C bond and the $n \rightarrow \pi^*$ transition of C=O group, respectively (Figure 4.27 (a)). A distinct peak was obviously detected at 402 nm for the rGO-Ag (30 s, 1 min and 3 min) nanocomposites (Figure 4.27 (b-d)). This peak corresponds to the surface plasmon resonance (SPR) absorption feature of the AgNPs (Abdel et al., 2012). In addition, the disappearance of the absorbance peak at 227 nm and existence of SPR peak suggested that after 3 min of the microwave irradiation, the reduction of GO to rGO and Ag^+ ions to AgNPs were occurred simultaneously. The intensity of the SPR band of the rGO-Ag nanocomposite increased with the increasing of microwave irradiation time. A very sharp and narrow absorption band was observed after 3 min of irradiation, indicated the complete formation of spherical AgNPs.

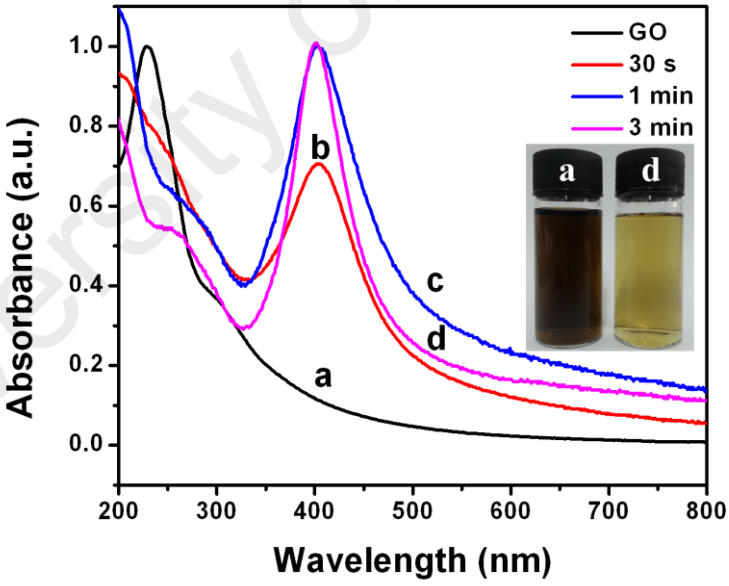

Figure 4.27: UV-vis absorption spectra of GO (a) and rGO-Ag nanocomposites (b: 30 s, c: 1 min and d: 3 min). Inset shows the photograph of aqueous solutions of GO and rGO-Ag (3 min).

The morphology of the AgNPs decorated on the rGO sheet was characterized using TEM studies. Figure 4.28 shows the TEM image at different magnifications (A-C) of the rGO-Ag (3 min) nanocomposite and its particle size distribution (D). A well-distributed poly-dispersed spherical AgNPs were formed on rGO sheet after the 3 min of microwave irradiation.

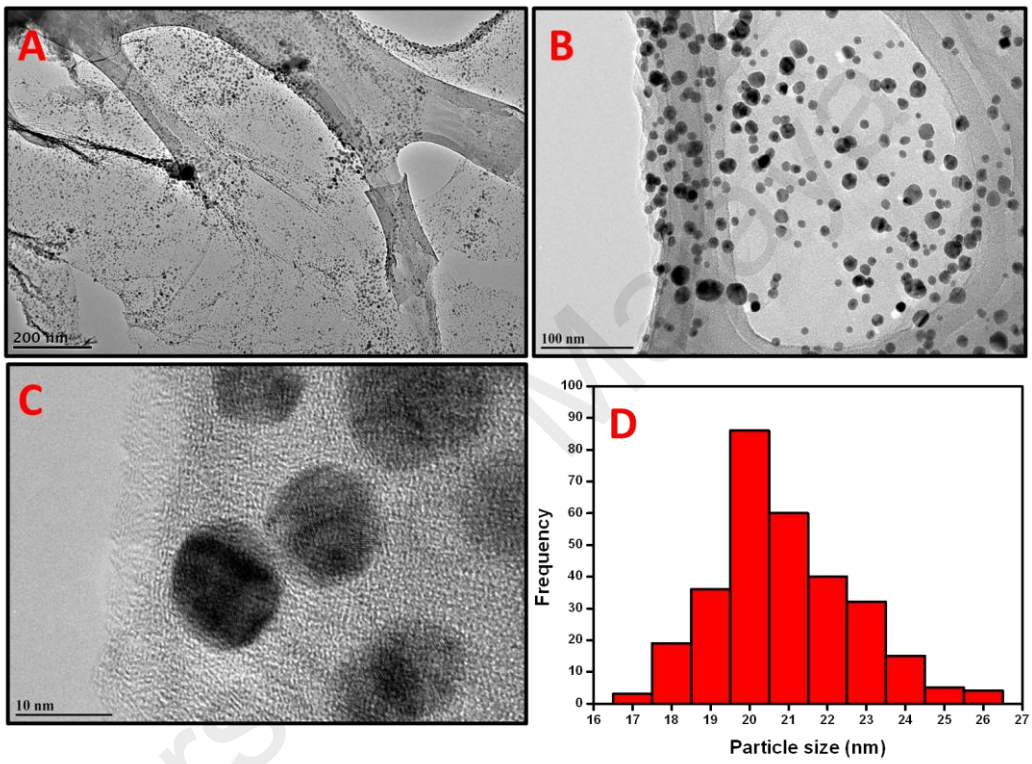

Figure 4.28: TEM images (A-C) and particle size histogram (D) of rGO-Ag (3 min) nanocomposite.

The average particle size was calculated to be 20 nm by taking account of 100 particles for the particle size measurement. In retrospect, the spherical shape of AgNPs relies on the single SPR absorption feature in the UV-vis spectrum. The TEM images of rGO-Ag nanocomposite prepared at 30 s and 1 min of irradiation times also showed the spherical AgNPs (Figure 4.29).

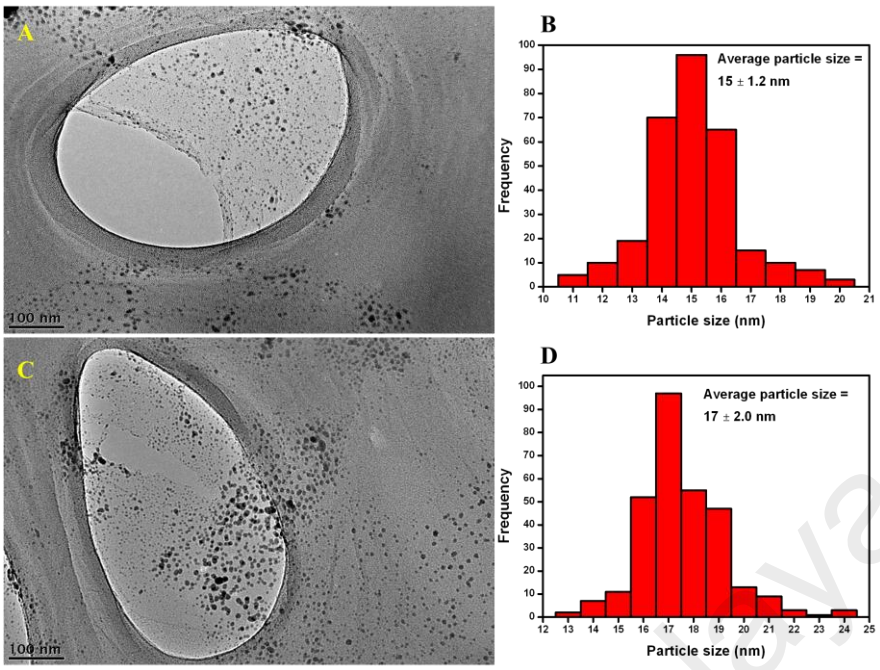

Figure 4.29: TEM images (A and C) and particle distribution histograms of rGO-Ag nanocomposites (B and D) prepared at 30 s (A and B) and 1 min (C and D).

Figure 4.30 displays the XRD patterns of GO and rGO-Ag (30 s, 1 min and 3 min) nanocomposites. It was seen that the characteristic peak of GO centered at 10.0^{o}, which was assigned to the (0 0 1) reflection of GO. After treatment with the microwave irradiation, the peak at 10.0^{o} shifted to 13^{o} suggested the reduction of GO (Zainy et al., 2012). The diffraction peaks observed at 38.1, 44.1 64.2 and 77.2° correspond to the (1 1 1), (2 0 0), (2 2 0) and (3 1 1) crystal planes of face-centered cubic (fcc) Ag NPs, respectively. The 2θ values matched with the standard database of JCPDS card no. 89-3722 (Agnihotri et al., 2014). The intensity of AgNPs diffraction peaks increased with the increasing time of microwave irradiation in the synthesis of rGO-Ag nanocomposite. These results confirmed the complete simultaneous formation of AgNPs and rGO under microwave irradiation.

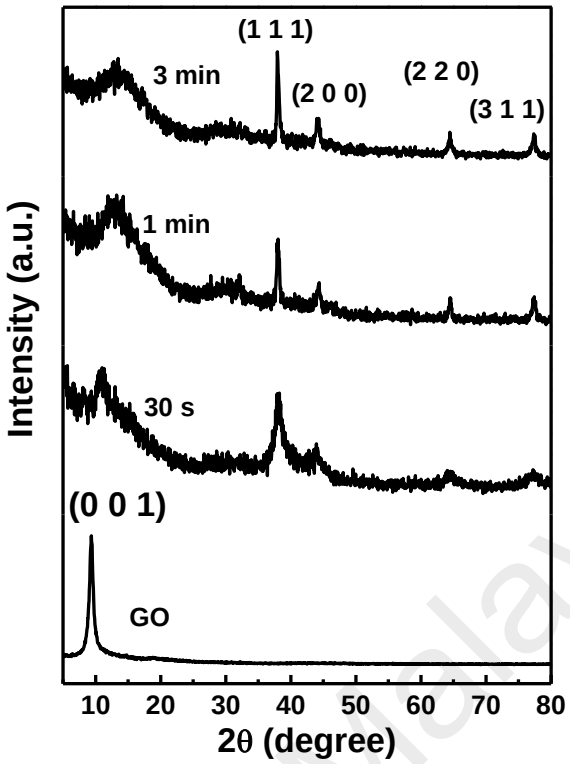

Figure 4.30: X-ray diffraction patterns of GO and rGO-Ag nanocomposite prepared at 30 s, 1 min and 3 min of microwave irradiation times.

Figure 4.31 shows the Raman spectra of GO and rGO-Ag (30 s, 1 min and 3 min) nanocomposites. Two characteristics peaks are generally known D and G bands of GO. The D band is assigned to the breathing mode of Ag_{1g} symmetry involving phonons near the K zone boundary and the G band corresponds to the E_{2g} mode of sp^2-bonded carbon atoms (Ferrari & Robertson, 2000).

The D and G bands of GO were appeared at 1350 and 1597 cm^{-1}, respectively with the intensity ratio, I_D/I_G, of 0.99. In comparison with GO, the G band of rGO-Ag nanocomposite slightly shifted to the lower wavenumbers which, indicated the reduction in GO after the microwave irradiation treatment (Lambert et al., 2009). It was also clearly shown that the intensity ratio, I_D/I_G, for rGO-Ag nanocomposite increased with increasing the microwave irradiation time from 30 s to 3 min. The increased

intensity of the D band could be attributed to the formation sp^2 bonds and decreased disorder, originating from defects associated with vacancies, edge defects and amorphous carbon species during the microwave irradiation (Tuinstra & Koenig, 1970). In addition, the peak intensities of the D and G bands of rGO-Ag nanocomposite were significantly enhanced in comparison with GO. This phenomenon is due to the intense local electromagnetic fields of the AgNPs, which indicated the surface–enhanced Raman scattering (SERS) activity (Li & Liu, 2010).

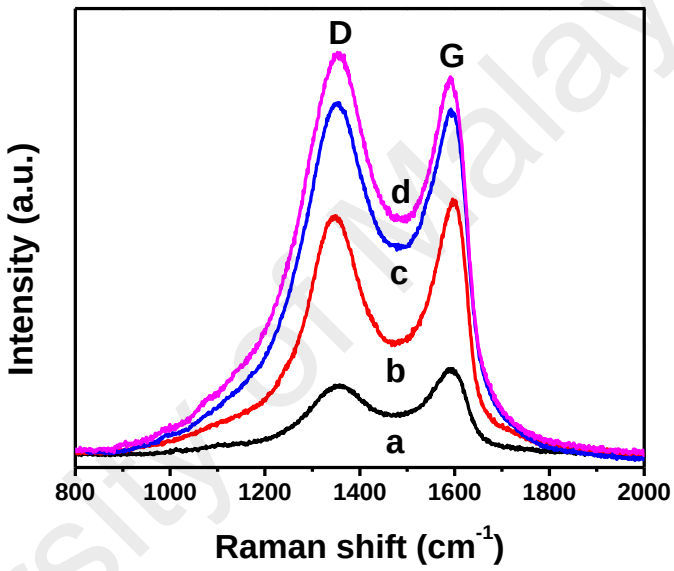

Figure 4.31: Raman spectra of GO (a), and rGO-Ag nanocomposites (b: 30 s, c: 1 min and d: 3 min.

The chemical analysis of the rGO-Ag nanocomposite was carried out by using XPS to further prove the reduction of GO after the microwave irradiation treatment on the rGO-Ag nanocomposite at different times (Figure 4.32). The core level spectra of C 1 s for GO and rGO-Ag nanocomposites and their peak positions were centered at 284.5, 286.3, 288.0and 289.2 eV which correspond to the C-C, C-O, C=O and O=C-O bonds, respectively. As depicted in the Figure 4.32, the peak intensity of the oxygenated carbon groups gradually decreased with an increased time of microwave irradiation, indicating

the successful reduction of GO to rGO in the rGO-Ag nanocomposite (Chen et al., 2010).

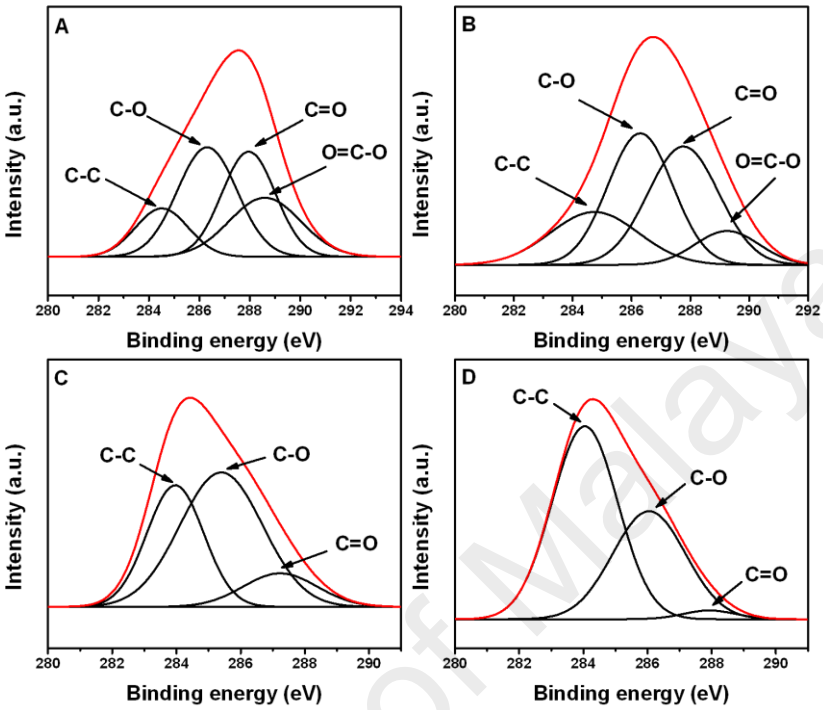

Figure 4.32: XPS of GO (A)and rGO-Ag nancomposites (B: 30s, C: 1 min and D: 3 min).

4.4.2.2 Electrochemical behavior of the rGO-Ag nanocomposite

Electrochemical impedance spectroscopy (EIS) measurement was studied to investigate the interfacial properties of the rGO-Ag nanocomposites modified electrode. The $[Fe(CN)_6]^{3-/4-}$ was chosen as a redox analyte to study the conducting behavior of the nanocomposite modified electrodes. Figure 4.33A displayed the Nyquist plots of bare GCE, GO and rGO-Ag nanocomposite modified GCEs for 2.5 mM $[Fe(CN)_6]^{3-/4-}$ in 0.1 M KCl. The Nyquist plot of GO modified GCE showed a semicircle with large diameter compared to the bare GCE, which indicated a large charge transfer resistance (R_{ct}).

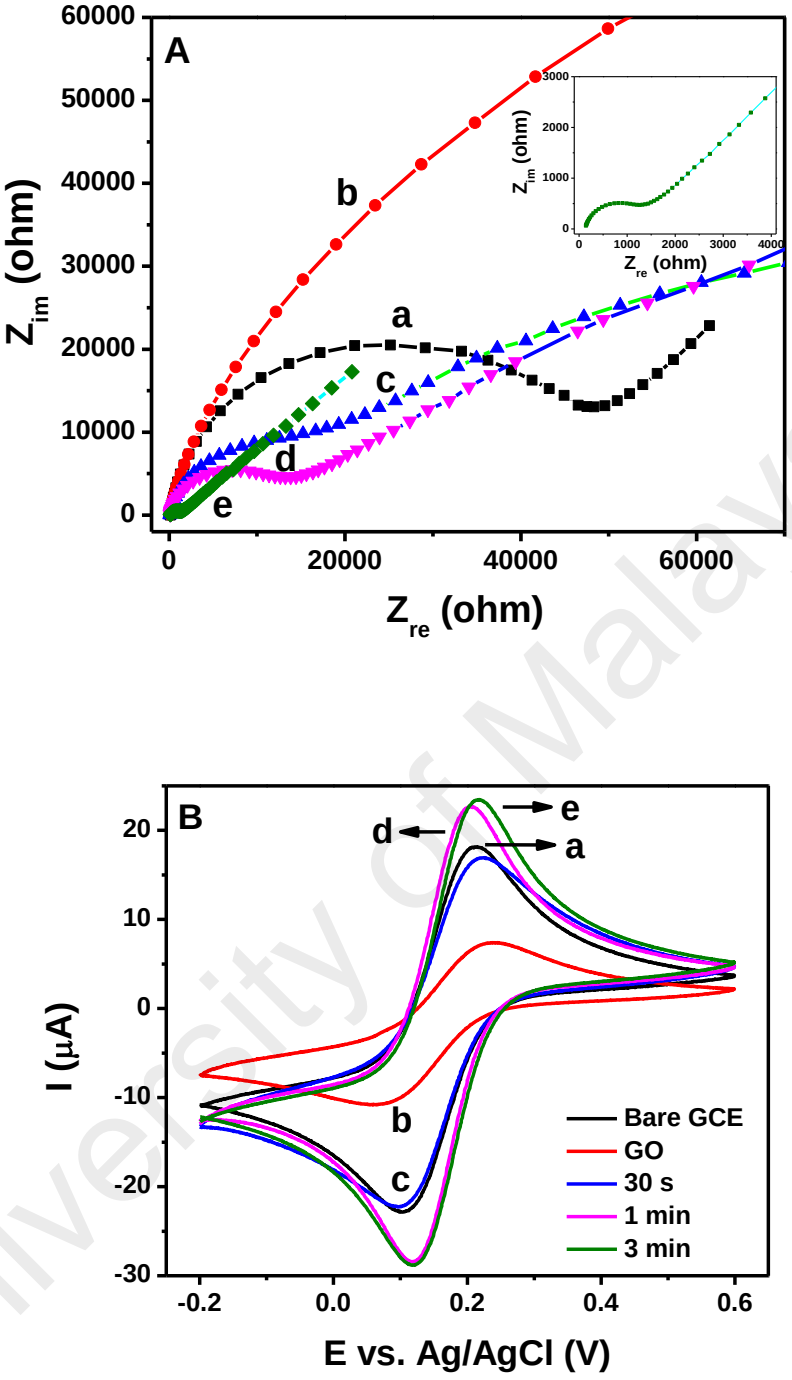

Figure 4.33: Nyquist plot for bare GCE (a) GO (b) and rGO-Ag nanocomposites (c: 30 s, d: 1 min and e: 3 min) modified electrode for 2.5 mM $K_3[Fe_3(CN)_6]$ in 0.1 M KCl. Inset shows the expanded view of "e" (A). Cyclic voltammograms recorded at bare GCE (a), GO (b) and rGO-Ag nanocomposites (c: 30 s, d: 1 min and e: 3 min) for 2.5 mM of $K_3[Fe_3(CN)_6]$ in 0.1 M KCl with a scan rate of 50 mV s^{-1} (B).

This could be attributed to the non-conducting behavior of GO at the modified electrode surface. The R_{ct} value highly decreased with the presence of conductive AgNPs in the nanocomposite. Moreover, the R_{ct} value decreased with increasing the microwave irradiation times, which indicated that the electron transfer process could be facilitated by the formation of highly conductive rGO and hence, enhanced the efficacy of AgNPs performance. The Bode phase plots recorded for the nanocomposite modified electrodes in the frequency range of 0.01-10000 Hz (Figure 4.34). The phase peaks appeared at a frequency range of 100-1000 Hz explaining the charge transfer resistance properties of the nanocomposite modified electrodes (Matemadombo & Nyokong, 2007). The rGO-Ag (3 min) nanocomposite showed a less intense peak compared to the other modified electrodes, which indicated a fast electron transfer process at the modified electrode. The phase angles for all the modified electrodes were less than 90^o at higher frequency suggested that the electrodes did not possess the capacitor properties (Matemadombo & Nyokong, 2007).

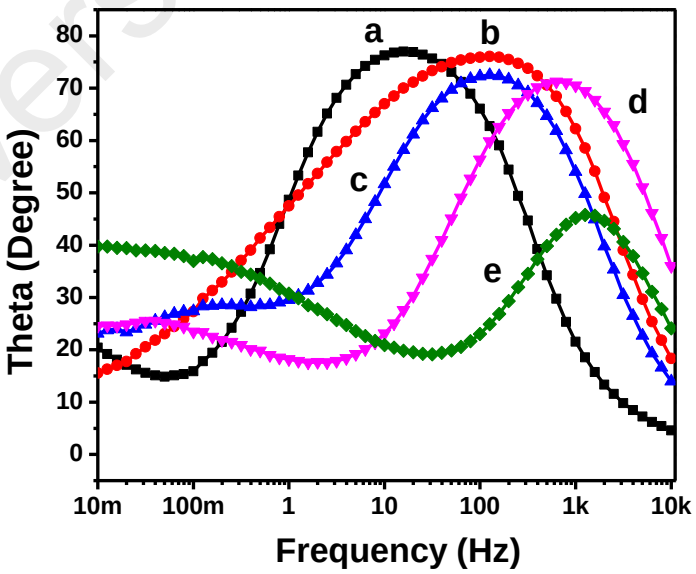

Figure 4.34: Bode impedance plot obtained for bare GCE (a), GO (b) and rGO-Ag nanocomposites (c: 30 s, d: 1 min and e: 3 min) modified electrode for 2.5 mM $K_3[Fe(CN)_6]$ in 0.1 M KCl.

The cyclic voltammetric responses recorded for $[Fe(CN)_6]^{-3/-4}$ redox analyte at the nanocomposite modified electrodes are shown in Figure 4.33B. The bare GCE, GO, rGO-Ag nanocomposites prepared at 30 s, 1 min and 3 min of microwave irradiation times displayed a reversible electrochemical responses with a peak-to-peak separation of 71, 100 73, 68 and 69 mV. The GO modified electrode showed a reversible voltammetric signal with a very low peak currents and large peak-to-peak separation. This observation revealed the kinetic hindrance of GO modified electrode on the electron transfer process. However, the rGO-Ag nanocomposites displayed a comparable peak-to-peak separation with GCE and enhanced peak currents except the rGO-Ag (30 s) modified electrode. By introducing the AgNPs, the redox current response with reversibility was enormously enhanced in the presence of rGO matrix because of the better kinetics of electron transfer process. The current enhancement was attributed to the conducting properties of AgNPs and carbon layer present at the electrode surface. The rGO-Ag nanocomposite acted as a new active electrode, which made a good electrical contact with the GCE surface. The EIS and cyclic voltammetric studies suggested that the present nanocomposite modified electrode could be used for electrocatalytic reduction of 4-NP.

4.4.2.3 Electrochemical reduction of 4-NP

The electrocatalytic reduction of 4-NP was chosen for the electrocatalytic application of the rGO-Ag nanocomposite modified electrode. In retrospect, all the modified electrodes investigated in this work showed a catalytic current response for the reduction of 4-NP (Figure 4.35). The rGO-Ag (3 min) nanocomposite displayed the enhanced catalytic current of -27.3 μA at the over potential of -0.52 V for addition of 100 μM 4-NP. The GO, rGO-Ag (30 s) and rGO-Ag (1 min) modified electrode showed lesser catalytic currents of -9.49, -15.0 and -20.5μA, respectively at more negative potentials for the reduction of same concentration of 4-NP. The enhanced performance

of rGO-Ag (3 min) nanocomposite could be attributed to the uniformly formed poly-dispersed spherical AgNPs and highly reduced GO. However, the rGO-Ag (3 min) nanocomposite did not show any current response in the absence of 4-NP.

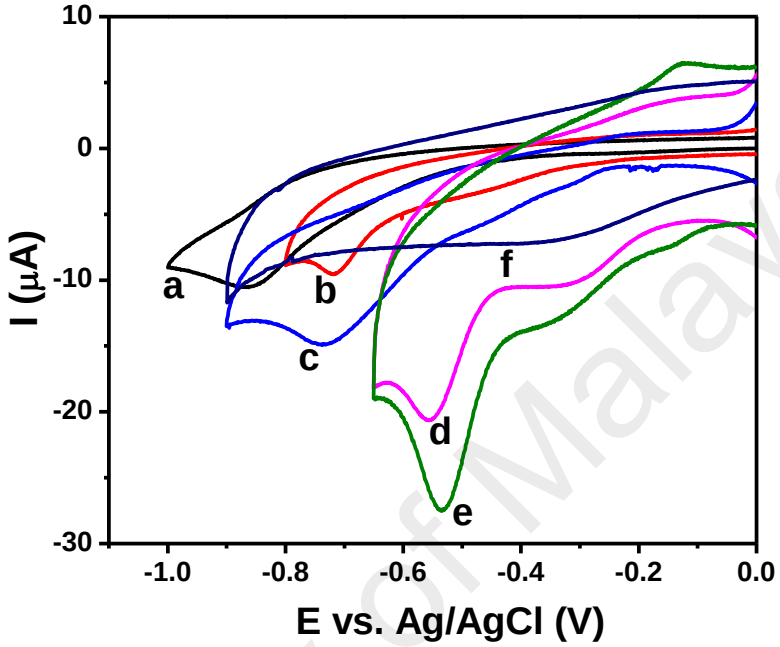

Figure 4.35: Cyclic voltammograms collected at bare GCE (a), GO (b) and rGO-Ag nanocomposites (c: 30 s, d: 1 min, and e: 3 min) modified electrodes in the presence of 100 µM 4-NP in 0.1 M phosphate buffer (pH 6) with a scan rate of 50 mV s^{-1}. 'f' is the cyclic voltammogram of rGO-Ag (3 min) nanocomposite modified electrode without 4-NP.

The pH dependence of the peak current and peak potential of cyclic voltammogram of 4-NP reduction at the rGO-Ag (3 min) nanocomposite modified electrode was studied by changing the pH of the phosphate buffer. The reduction peak potential was shifted towards a higher negative values when the pH was increased from 2 to 9 with the addition 100µM of 4-NP (Figure 4.36). Inset of Figure 4.36 shows the corresponding calibration plot of the reduction peak potential versus pH.

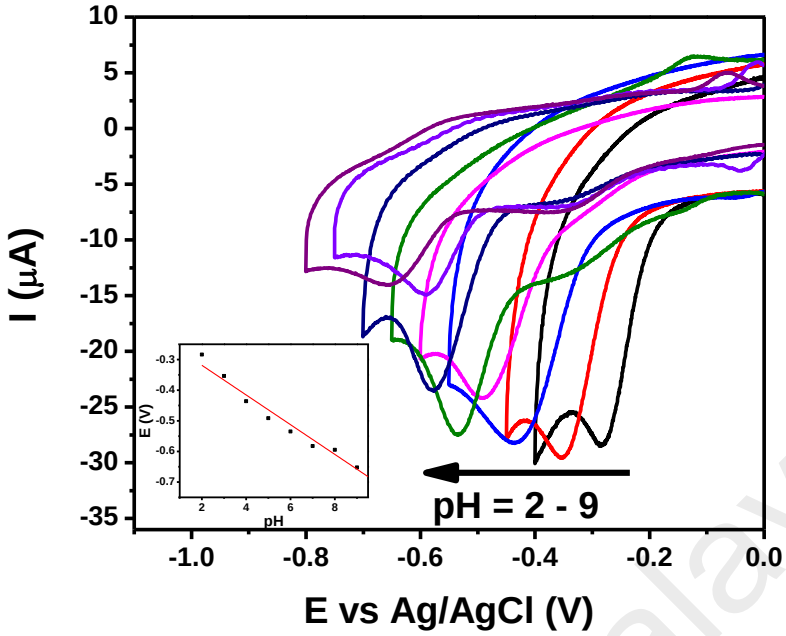

Figure 4.36: Cyclic voltammograms of rGO-Ag nanocomposite modified electrode in the presence of 100 μM 4-NP in 0.1 M phosphate buffer with different pH levels (pH = 2 – 9). Inset shows the plot of peak potential versus pH.

The shift in the peak potential with respect to the increase in the pH of buffer indicated that the 4-NP reduction at the rGO-Ag (3 min) nanocomposite modified electrode involved a proton-coupled reaction. The peak current increased with increasing the scan rate for the reduction of 100 μM 4-NP in 0.1 M phosphate buffer (pH 6) (Figure 4.37A). The plot of peak currents versus scan rates showed a linear relationship (Figure 4.37B) which indicated that the reduction of 4-NP at the rGO-Ag nanocomposite modified electrode was controlled by the adsorption process. The adsorption of 4-NP was facilitated because of the π-π interaction between the rGO and 4-NP.

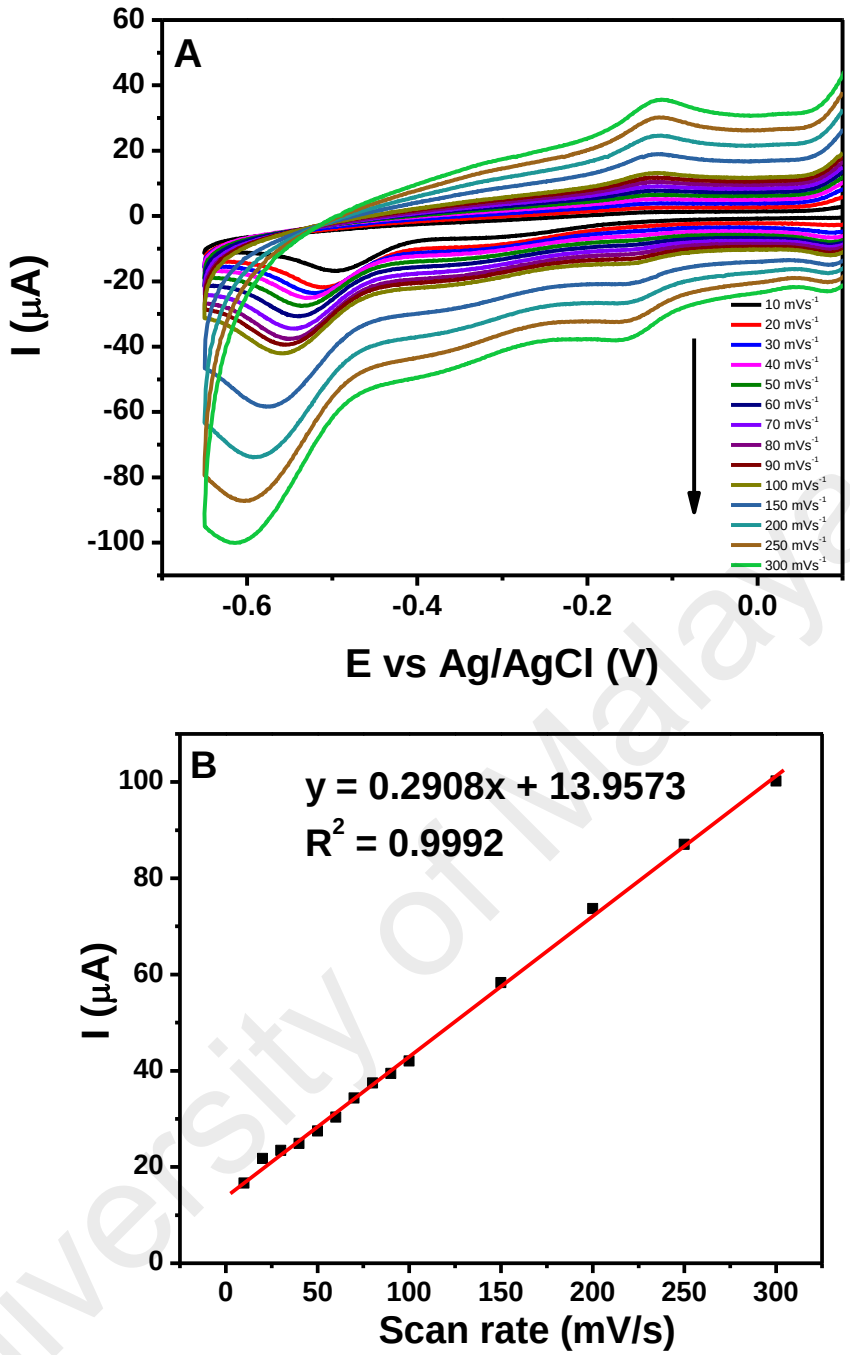

Figure 4.37: Cyclic voltatammograms obtained at rGO-Ag (3 min) nanocomposite modified electrode with different scan rates in the presence of 100 µM 4-NP in 0.1 M phosphate buffer (pH 6) (A).Calibration plot of peak current versus scan rate (B).

4.4.2.4 Amperometric detection of 4-NP

The amperometry *i-t* curve technique was used for the detection of flow concentrations of 4-NPand for the interference study. The current responses of the nanocomposite modified electrodes were recorded by the addition of different

concentrations of 4-NP in a homogenously stirred 0.1 M phosphate buffer at a regular time interval of 60 s. The rGO-Ag (3 min) nanocomposite modified electrode showed a good current responses for every injection of 4-NP with different concentration range (1, 10 and 100 μM) (Figure 4.38). The presence of Ag NPs with rGO layer at the modified electrode significantly enhanced the sensing ability toward the detection of 4-NP. The limit of detection was calculated to be 0.46, 1.02, 0.32 μM towards the detection of 4-NP. The amperometric *i-t* curve was recorded for the successive addition of 4-NP at concentration range 1-1200μM with the applied potential of -0.52 V and a multi-linear range was observed for the addition of different concentration ranges. A detailed comparison of the present electrochemical sensor performance with some of the previously reported sensors for the determination of 4-NP is summarized in Table 4.4.

Table 4.4: Comparison of the present sensor with some of the previously reported sensors for the electrochemical detection of 4-NP.

Type of Material	Analytical technique	Linear range (μM)	pH of the buffer	Limit of detection(μM)	Reference
GC-Co_3O_4 nanocubes	Square wave voltammetry	2 - 47	7.0	0.93	(Shahid et al., 2015)
GC-GO	Linear sweep voltammetry	0.1 - 120	4.8	0.02	(Junhua et al., 2012)
GC-graphene-Nf	Differential pulse voltammetry	10 – 620	7.0	0.6	(Arvinte et al., 2011)
AgA-PE	Differential pulse voltammetry	0.2 – 100	3.0	0.3	(Niaz et al., 2009)
Ag-chitosan	Square wave voltammetry	0.07 - 2	3.0	0.07	(De et al., 2014)
Ti-TiO_2-Au HRP-MB	Amperometry	0.3 - 140	7.0	0.11	(Kafi & Chen, 2009)
GC-nano-Cu_2O	Differential pulse voltammetry	1 – 400	6.0	0.5	(Yin et al., 2012)
mHAp/ECG/GC	Differential pulse voltammetry	0.2 - 994	5.0	0.27	(Bharath et al., 2015)

It is shown that the present rGO-Ag nanocomposite modified electrode is an excellent material for the detection of 4-NP. Selectivity study of the rGO-Ag nanocomposite for the detection of 4-NP was investigated by injecting the other interferents in the same solution and the current responses were noticed. Figure 4.39 displays the amperometry *i-t* curve response for the additions of 4-NP and the interferents in a stirred 0.1 M phosphate buffer. Bromophenol blue, 2-amino-4-nitrophenol, 2-chlorophenol and 2,4-dinitrophenol were added one by one after the few additions of 4-NP (1μM) and no enhancement in the current responses were observed even with the 50-fold higher concentration. With the injection of 4-NP in the same solution generated almost the same magnitude of the current response. These observations showed that the rGO-Ag nanocomposite exhibited good selectivity towards the detection of 4-NP even in the presence of a excess other interferent molecules.

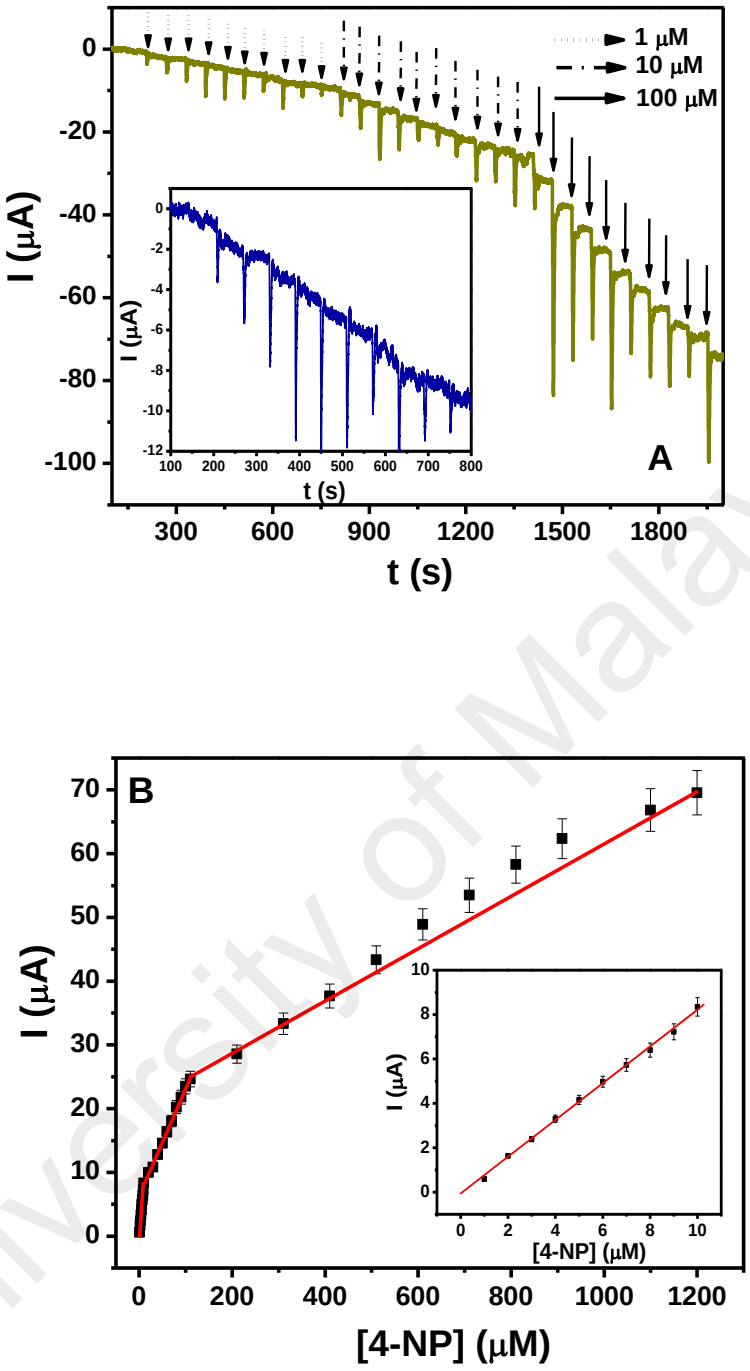

Figure 4.38: Amperometri i-t curves obtained at rGO-Ag nanocomposite modified electrode for the addition of 4-NP in the range 1 – 1200 μM in 0.1 M phosphate buffer (pH 6) at a regular interval of 60 s (A). Applied potential was –0.52 V. Calibration plot of current versus concentration of 4-NP (B). Insets show the expanded view of the first 10 additions (1-10 μM).

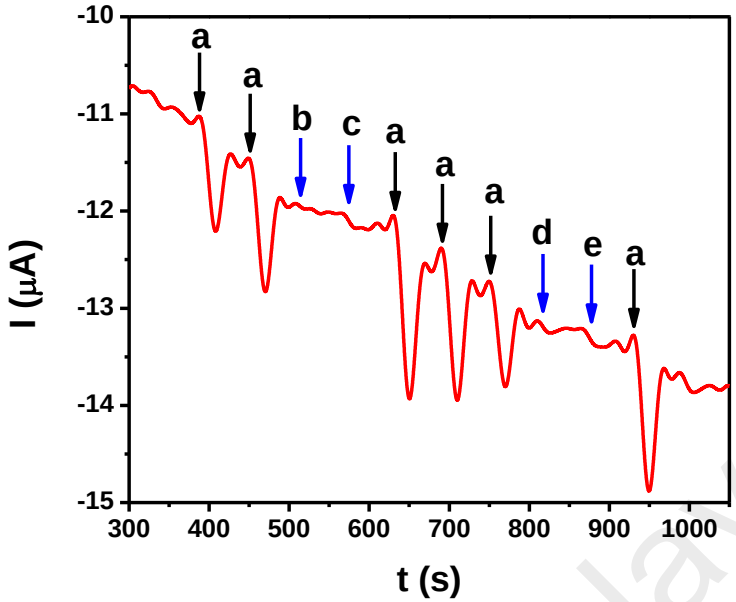

Figure 4.39: Amperometric i-t curve responses obtained at rGO-Ag nanocomposite modified electrode for the successive addition of 1 μM 4-NP (a) and each 50 μM of bromophenol blue (b), 2-amino-4-nitrophenol (c), 2-chlorophenol (d) and 2,4-dinitrophenol (e) in phosphate buffer (pH 6) at a regular time interval of 60 s. Applied potential was -0.52 V.

4.4.2.5 Applicability in Real Sample Analysis

The practical applicability of the rGO-Ag (3 min) nanocomposite to real sample analysis was evaluated for the detection of 4-NP by using tap water, river water and lake water. The water samples were filtered and used for the detection of 4-NP. Different concentrations of 4-NP were spiked and good recoveries were found (Table 4.5). The observed results showed that the rGO-Ag nanocomposite could be used for the determination of 4-NP in natural water samples.

Table 4.5: Measurement results of 4-NP in different real samples

Samples	Added (μM)	Found (μM)	Recovery (%)
	10	9.647	96.47
Tap water	30	29.874	99.58
	50	47.132	94.26
	10	9.602	96.02
River water	30	30.021	100.07
	50	48.963	97.92
	10	9.871	98.71
Lake water	30	28.534	95.11
	50	50.101	100.20

4.4.3 Conclusion

We have successfully synthesized the rGO-Ag nanocomposite using microwave irradiation and studied the electrocatalytic reduction of 4-NP. The crystalline AgNPs were observed with the increased reduction of GO after the irradiation time of 3 min. The EIS study showed the higher electron transfer process at the rGO-Ag nanocomposite modified electrode. The enhanced electrocatalytic activity was observed with the rGO-Ag (3 min) nanocomposite modified electrode compared to the other controlled modified electrodes for the reduction of 4-NP. The amperometrric i-t curve displayed a multi-linear relationship in the concentration range of 1–1200 μM with the LOD of 0.32 μM towards the detection of 4-NP. The nanocomposite exhibited a good selectivity in for 4-NP the presence of some of its structural analogues. It could be used in the validation of 4-NP in real samples and the satisfactory recoveries were found.

CHAPTER 5:
SUMMARY AND FUTURE WORK

As a conclusion of this study, sonochemical and microwave techniques have been developed and considered easy to be handled, simple, less toxic because it does not include toxic reducing and stabilizing agent to synthesize rGO and rGO-Ag nanocomposite for different sensor applications.

Silver nanoparticle (AgNP) that decorated the surface of reduced graphene oxide was successfully grown by using silver ammonia complex as a precursor. It was found that silver ammonia complex plays an important role in forming high-distributed AgNPs under small and narrow size distribution. The collected nanocomposite exhibited a notable optical sensing towards Hg in the presence of other common heavy metal ions, with LOD of 0.59 μM. This sample essentially provides an easy, environmental friendly, and low cost preparation of AgNPs based on nanocomposite assay in the spectrophotometer determination of mercury ion.

The exposure of aqueous solution containing graphene oxide and silver ammonia complex is an effective strategy in preparing graphene oxide decorated with AgNPs without requiring any toxic reducing agents. It was discovered that silver ammonia complex plays an important role in the growth of AgNPs which is embedded on the graphene oxide layer. The GO-Ag nanocomposite modified GCE has the ability to exhibit excellent electrocatalytic activity on H_2O_2 reduction, which leads to a highly sensitive sensor with a linear range of 100 μM – 11 mM (R^2 = 0.988) and LOD of 28.3 μM. Furthermore, the prepared nanocomposite also exhibited good selectivity among the common interference such as DA, AA, UA, and glucose.

The work was continued by studying the performance of reduced graphene oxide decorated with silver nanoparticle which is prepared through microwave irradiation for

SERS and spectrophotometric determination of dopamine. The existence of AgNPs on the GO plays an important role in determining DA because it facilitated the silver-dopamine interaction and consequently reduced DA concentration. The nanocomposite showed an excellent sensor performance in both SERS and spectrophotometric determination on DA. An enhanced determination as low as 1 μM was shown by SERS while the LOD of the spectrophotometric determination was calculated as 66.0 nM.

Finally, the study sought to focus on rGO-Ag nanocomposite that have prepared by microwave irradiation, which aimed to further enhance the electrocatalytic reduction of 4-NP. As confirmed by EIS, the incorporation of crystalline Ag NPs on graphene layer after 3 minutes of irradiation influenced the electrocatalytic activity due to the high electron transfer. To the best our knowledge, the greatly improved electrocatalytic reduction of 4-NP with LOD of 0.32 μM was achieved by measuring the amperometric i-t curve in the range of 1-1200μM. It was also shown to be applicable in real samples measurement.

5.1 Future Work

Based on the finding acquired in this study, it has opened several avenues that are worth to be investigated for future development of graphene oxide/graphene-silver nanocomposite for sensor applications.

Among the focus of this study is the use of silver complex. However, little effort has been made to understand the mechanism behind the enhancement property caused by the presence of silver complex and graphene. The work presented in Chapter 4.1, 4.2, 4.3, and 4.4 can be further extended to understand the interactions of graphene layer with different types of material such as metal complexes of Ni, Zn, and Cu in aqueous and other organic solvents. It would be interesting to study how various metal-

complexes interact with the graphene layer due to the fact that the atomic structure of these materials is totally different from graphene.

One of the ultimate goals of graphene/metal nanocomposites is to produce a highly homogenous dispersion in aqueous. In future studies, nanocomposite should be investigated in different areas of application such as energy storage (supercapacitor and solar cells) because the material can be easily deposited on the substrate. The homogenous silver nanoparticle will have a bigger surface area by electrochemically deposited the ITO, which will produce more effective electron movement.

REFERENCES

Abdel-Mohsen, A. M., Hrdina, R., Burgert, L., Krylová, G., Abdel-Rahman, R. M., Krejčová, A.,, Steinhart, M. & Beneš, L. (2012). Green synthesis of hyaluronan fibers with silver nanoparticles. *Carbohydrate Polymers*, *89*, 411–422.

Abdelhamid, H. N., & Wu, H.-F. (2015). Reduced graphene oxide conjugate thymine as a new probe for ultrasensitive and selective fluorometric determination of mercury(II) ions. *Microchimica Acta*, *182*, 1609–1617.

Agnihotri, S., Mukherji, S., & Mukherji, S. (2014). Size-controlled silver nanoparticles synthesized over the range 5–100 nm using the same protocol and their antibacterial efficacy. *Royal Society of Chemistry Advances*, *4*, 3974–3983.

Albert, G. C., Cook, C. M., Prato, F. S., & Thomas, a. W. (2009). Deep brain stimulation, vagal nerve stimulation and transcranial stimulation: An overview of stimulation parameters and neurotransmitter release. *Neuroscience & Biobehavioral Reviews*, *33*, 1042–1060.

Amini, M. K., Khezri, B., & Firooz, a. R. (2008). Development of a highly sensitive and selective optical chemical sensor for batch and flow-through determination of mercury ion. *Sensors and Actuators, B: Chemical*, *131*, 470–478.

An, S. J., Zhu, Y., Lee, S. H., Stoller, M. D., Emilsson, T., Park, S., Velamakanni, A., An, J., & Ruoff, R. S. (2010). Thin film fabrication and simultaneous anodic reduction of deposited graphene oxide platelets by electrophoretic deposition. *The Journal of Physical Chemistry Letters*, *1*, 1259–1263.

Anbazhagan, V., Ahmed, K. B. A., & Janani, S. (2014). Synthesis of catalytically active silver nanoparticles using lipid derived signaling molecule, N-steroylethanolamine: Promising antibacterial agent and selective colorimetric sensor for mercury ion. *Sensors and Actuators, B: Chemical*, *200*, 92–100.

Annadhasan, M., Muthukumarasamyvel, T., Sankar Babu, V. R., & Rajendiran, N. (2014). Green synthesized silver and gold nanoparticles for colorimetric detection of Hg^{2+} , Pb^{2+} , and Mn^{2+} in aqueous medium. *ACS Sustainable Chemistry &*

Engineering, *2*, 887–896.

Arvinte, A., Mahosenaho, M., Pinteala, M., Sesay, A. M., & Virtanen, V. (2011). Electrochemical oxidation of p-nitrophenol using graphene-modified electrodes, and a comparison to the performance of MWNT-based electrodes. *Microchimica Acta*, *174*, 337–343.

Bae, S., Kim, H., Lee, Y., Xu, X., Park, J. S., Zheng, Y., Balakrishnan, J., Lei, T., Kim, H. R., Song, Y. I., Kim. Y. J., Kim, K. S., Ozyilmaz, B., Ahn, J. H., Hong, B. H., & Iijima, S. (2010). Roll-to-roll production of 30-inch graphene films for transparent electrodes. *Nature Nanotechnology*, *5*, 574–578.

Bartlett, P. N., Birkin, P. R., Wang, J. H., Palmisano, F., & De Benedetto, G. (1998). An enzyme switch employing direct electrochemical communication between horseradish peroxidase and a poly(aniline) Film. *Analytical Chemistry*, *70*, 3685–3694.

Bharath, G., Veeramani, V., Chen, S. M., Madhu, R., Raja, M. M., Balamurugan, A., Mangalaraj, D., Viswanathan, C., & Ponpandian, N. (2015). Edge-carboxylated graphene anchoring magnetite-hydroxyapatite nanocomposite for an efficient 4-nitrophenol sensor. *RSC Advances*, *5*, 13392–13401.

Blake, P., Brimicombe, P. D., Nair, R. R., Booth, T. J., Jiang, D., Schedin, F., Ponomarenko, L. A., Morozov, S. V., Gleeson, H. F., Hill, E. W., Geim, A. K., & Novoselov, K. S. (2008). Graphene-based liquid crystal device. *Nano Letters*, *8*, 1704–1708.

Brodie, B. C. (1859). On the atomic weight of graphite. *Philosophical Transactions of the Royal Society of London*, *149*, 249–259.

Bu, Y., & Lee, S. (2012). Influence of dopamine concentration and surface coverage of Au shell on the optical properties of Au, Ag, and Ag core Au shell nanoparticles. *ACS Applied Materials and Interfaces*, *4*, 3923–3931.

Celebi, K., Cole, M. T., Teo, K. B. K., & Park, H. G. (2012). Observations of early stage graphene growth on copper. *Electrochemical and Solid-State Letters*, *15*, K1-K4.

Chang, B. Y. S., Huang, N. M., An'amt, M. N., Marlinda, A. R., Norazriena, Y., Muhamad, M. R., Chia, C. H. (2012). Facile hydrothermal preparation of titanium dioxide decorated reduced graphene oxide nanocomposite. *International Journal of Nanomedicine*, *7*, 3379–3387.

Chang, H., & Wu, H. (2013). Graphene-based nanocomposites: Preparation, functionalization, and energy and environmental applications. *Energy & Environmental Science*, *6*, 3483-3507.

Chen, L., Chan, L., Fu, X., & Lu, W. (2013). Highly sensitive and selective colorimetric sensing of Hg2+ based on the morphology transition of silver nanoprisms. *ACS Applied Materials and Interfaces*, *5*, 284–290.

Chen, L., Tang, Y., Wang, K., Liu, C., & Luo, S. (2011). Direct electrodeposition of reduced graphene oxide on glassy carbon electrode and its electrochemical application. *Electrochemistry Communications*, *13*, 133–137.

Chen, S., Yuan, R., Chai, Y., & Hu, F. (2013). Electrochemical sensing of hydrogen peroxide using metal nanoparticles: a review. *Microchimica Acta*, *180*, 15–32.

Chen, S., Zhu, J., Huang, H., Zeng, G., Nie, F., & Wang, X. (2010). Facile solvothermal synthesis of graphene-MnOOH nanocomposites. *Journal of Solid State Chemistry*, *183*, 2552–2557.

Chen, W., Yan, L., & Bangal, P. R. (2010). Preparation of graphene by the rapid and mild thermal reduction of graphene oxide induced by microwaves. *Carbon*, *48*, 1146–1152.

Chen, X., & Schluesener, H. J. (2008). Nanosilver: A nanoproduct in medical application. *Toxicology Letters*, *176*, 1-12.

Chen, Y., Yao, L., Deng, Y., Pan, D., Ogabiela, E., Cao, J., Adeloju, S. B., & Chen, W. (2015). Rapid and ultrasensitive colorimetric detection of mercury(II) by chemically initiated aggregation of gold nanoparticles. *Microchimica Acta*, *182*, 2147–2154.

Cheng, Y., Yin, L., Lin, S., Wiesner, M., Bernhardt, E., & Liu, J. (2011). Toxicity reduction of polymer-stabilized silver nanoparticles by sunlight. *Journal of*

Physical Chemistry C, *115*, 4425–4432.

Clarkson, T. W., Magos, L., & Myers, G. J. (2003). The toxicology of mercury--current exposures and clinical manifestations. *The New England Journal of Medicine*, *349*, 1731–1737.

Cui, K., Song, Y., Yong Yao, Huang, Z., & Wang, L. (2008). A novel hydrogen peroxide sensor based on Ag nanoparticles electrodeposited on DNA-networks modified glassy carbon. *Electrochemistry Communications*, *10*, 663–667.

Cuong, T. V., Pham, V. H., Chung, J. S., Shin, E. W., Yoo, D. H., Hahn, S. H., Huh, J. S., Rue, G. H., Kim, E. J., Hur, S. H., & Kohl, P. A. (2010). Solution-processed ZnO-chemically converted graphene gas sensor. *Materials Letters*, *64*, 2479–2482.

Darroudi, M., Khorsand Zak, A., Muhamad, M. R., Huang, N. M., & Hakimi, M. (2012). Green synthesis of colloidal silver nanoparticles by sonochemical method. *Materials Letters*, *66*, 117–120.

Das, M. R., Sarma, R. K., Saikia, R., Kale, V. S., Shelke, M. V., & Sengupta, P. (2011). Synthesis of silver nanoparticles in an aqueous suspension of graphene oxide sheets and its antimicrobial activity. *Colloids and Surfaces B: Biointerfaces*, *83*, 16–22.

De, L. C. A., Silva, P. S. D., & Spinelli, A. (2014). Chitosan-stabilized silver nanoparticles for voltammetric detection of nitrocompounds. *Sensors and Actuators B: Chemical*, *196*, 39–45.

Du, D., Liu, J., Zhang, X., Cui, X., & Lin, Y. (2011). One-step electrochemical deposition of a graphene-ZrO_2 nanocomposite: Preparation, characterization and application for detection of organophosphorus agents. *Journal of Materials Chemistry*, *21*, 8032-8037.

Du, J., Yue, R., Ren, F., Yao, Z., Jiang, F., Yang, P., & Du, Y. (2013). Simultaneous determination of uric acid and dopamine using a carbon fiber electrode modified by layer-by-layer assembly of graphene and gold nanoparticles. *Gold Bulletin*, *46*, 137–144.

Eda, G., & Chhowalla, M. (2010). Chemically derived graphene oxide: Towards large-

area thin-film electronics and optoelectronics. *Advanced Materials*, *22*, 2392–2415.

Eda, G., Fanchini, G., & Chhowalla, M. (2008). Large-area ultrathin films of reduced graphene oxide as a transparent and flexible electronic material. *Nature Nanotechnology*, *3*, 270–274.

El-Safty, S. A., & Shenashen, M. A. (2012). Mercury-ion optical sensors. *TrAC Trends in Analytical Chemistry*, *38*, 98–115.

Evtugyn, G. A., Shamagsumova , R. V., Sitdikov, R. R., Stoikov, I. I., Antipin, I. S., Ageeva, M. V., & Hianik, T. (2011). Dopamine sensor based on a composite of silver nanoparticles implemented in the electroactive matrix of calixarenes. *Electroanalysis*, *23*, 2281–2289.

Farhadi, K., Forough, M., Molaei, R., Hajizadeh, S., & Rafipour, A. (2012). Highly selective Hg^{2+} colorimetric sensor using green synthesized and unmodified silver nanoparticles. *Sensors and Actuators B: Chemical*, *161*, 880–885.

Fernández-Merino, M. J., Guardia, L., Paredes, J. I., Villar-Rodil, S., Solís-Fernández, P., Martínez-Alonso, A., & Tascón, J. M. D. (2010). Vitamin C is an ideal substitute for hydrazine in the reduction of graphene oxide suspensions. *The Journal of Physical Chemistry C*, *114*, 6426–6432.

Ferrari, A., & Robertson, J. (2000). Interpretation of Raman spectra of disordered and amorphous carbon. *Physical Review B*, *61*, 14095–14107.

Frederix, F., Friedt, J. M., Choi, K. H., Laureyn, W., Campitelli, A., Mondelaers, D., Maes, G., & Borghs, G. (2003). Biosensing based on light absorption of nanoscaled gold and silver particles. *Analytical Chemistry*, *75*, 6894–6900.

Fu, C., Kuang, Y., Huang, Z., Wang, X., Du, N., Chen, J., & Zhou, H. (2010). Electrochemical co-reduction synthesis of graphene/Au nanocomposites in ionic liquid and their electrochemical activity. *Chemical Physics Letters*, *499*, 250–253.

Gao, W., Alemany, L. B., Ci, L., & Ajayan, P. M. (2009). New insights into the structure and reduction of graphite oxide. *Nature Chemistry*, *1*, 403–408.

Gao, Z., Liu, N., Wu, D., Tao, W., Xu, F., & Jiang, K. (2012). Graphene-CdS composite, synthesis and enhanced photocatalytic activity. *Applied Surface Science*, *258*, 2473–2478.

Geim, A. K., & Novoselov, K. S. (2007). The rise of graphene. *Nature Materials*, *6*, 183–191.

Geng, J., Jia, X. D., & Zhu, J. J. (2011). Sonochemical selective synthesis of ZnO/CdS core/shell nanostructures and their optical properties. *CrystEngComm*, *13*, 193-198.

Ghosh, S. K., & Pal, T. (2007). Interparticle coupling effect on the surface plasmon resonance of gold nanoparticles: From theory to applications. *Chemical Reviews*, *107*, 4797–4862.

Gogotsi, Y. (2011). Controlling Graphene Properties Through Chemistry. *The Journal of Physical Chemistry Letters*, *2*, 2509–2510.

Golsheikh, A. M., Huang, N. M., Lim, H. N., & Zakaria, R. (2014). One-pot sonochemical synthesis of reduced graphene oxide uniformly decorated with ultrafine silver nanoparticles for non-enzymatic detection of H_2O_2 and optical detection of mercury ions. *RSC Advances*, *4*, 36401-36411.

Guascito, M. R., Filippo, E., Malitesta, C., Manno, D., Serra, A., & Turco, A. (2008). A new amperometric nanostructured sensor for the analytical determination of hydrogen peroxide. *Biosensors and Bioelectronics*, *24*, 1057–1063.

Guinea, F., Katsnelson, M. I., & Geim, A. K. (2009). Energy gaps and a zero-field quantum Hall effect in graphene by strain engineering. *Nature Physics*, *6*, 30–33.

Guo, H. L., Wang, X. F., Qian, Q. Y., Wang, F. B., & Xia, X. H. (2009). A green approach to the synthesis of graphene nanosheets. *ACS Nano*, *3*, 2653–2659.

Guo, Y., Wang, Z., Qu, W., Shao, H., & Jiang, X. (2011). Colorimetric detection of mercury, lead and copper ions simultaneously using protein-functionalized gold nanoparticles. *Biosensors and Bioelectronics*, *26*, 4064–4069.

Hambali, N. A., Yahaya, H., Mahmood, M. R., Terasako, T., & Hashim, A. M. (2014).

Synthesis of zinc oxide nanostructures on graphene/glass substrate by electrochemical deposition: effects of current density and temperature. *Nanoscale Research Letters*, *9*, 609-615.

Hanaoka, S., Lin, J. M., & Yamada, M. (2001). Chemiluminescent flow sensor for H_2O_2 based on the decomposition of H_2O_2 catalyzed by cobalt(II)-ethanolamine complex immobilized on resin. *Analytica Chimica Acta*, *426*, 57–64.

Hass, J., de Heer, W. A., & Conrad, E. H. (2008). The growth and morphology of epitaxial multilayer graphene. *Journal of Physics: Condensed Matter*, *20*, 323202-323229.

Hatamie, S., Ahadian, M. M., Ghiass, M. A., Iraji Z. A., Saber, R., Parseh, B., Oghabian, M. A., & Shanehsazzadeh, S. (2016). Graphene/cobalt nanocarrier for hyperthermia therapy and MRI diagnosis, *Colloids and Surfaces B: Biointerfaces, 146*, 271–279.

He, B. S., Song, B., Li, D., Zhu, C., Qi, W., Wen, Y., Wang, L., Song, S., Fang, H., & Fan, C. (2010). A graphene nanoprobe for rapid, sensitive, and multicolor fluorescent DNA analysis. *Advanced Functional Materials*, *20*, 453–459.

How, G. T. S., Pandikumar, A., Ming, H. N., & Ngee, L. H. (2014). Highly exposed {001} facets of titanium dioxide modified with reduced graphene oxide for dopamine sensing. *Scientific Reports*, *4*, 5044-5052.

Hu, A., Chen, X., Tang, Q., & Zeng, B. (2014). Hydrothermal controlled synthesis of Fe3O4 nanorods/graphene nanocomposite for high-performance lithium ion batteries. *Ceramics International*, *40*, 14713–14725.

Huang, N. M., Lim, H. N., Chia, C. H., Yarmo, M. A., & Muhamad, M. R. (2011). Simple room-temperature preparation of high-yield large-area graphene oxide. *International Journal of Nanomedicine*, *6*, 3443–3448.

Ikhsan, N. I., Rameshkumar, P., & Huang, N. M. (2016). Controlled synthesis of reduced graphene oxide supported silver nanoparticles for selective and sensitive electrochemical detection of 4-nitrophenol. *Electrochimica Acta*, *192*, 392–399.

Izrini, N., Rameshkumar, P., & Pandikumar, A. (2015). Facile synthesis of graphene

oxide–silver nanocomposite and its modified electrode for enhanced electrochemical detection of nitrite ions. *Talanta*, *144*, 908–914.

Jain, J., Arora, S., Rajwade, J. M., Omray, P., Khandelwal, S., & Paknikar, K. M. (2009). Silver nanoparticles in therapeutics: Development of an antimicrobial gel formulation for topical use. *Molecular Pharmaceutics*, *6*, 1388–1401.

Jana, N. R., Sau, T. K., & Pal, T. (1999). Growing small silver particle as redox catalyst. *The Journal of Physical Chemistry B*, *103*, 115–121.

Jayabal, S., Sathiyamurthi, R., & Ramaraj, R. (2014). Selective sensing of Hg^{2+} ions by optical and colorimetric methods using gold nanorods embedded in a functionalized silicate sol–gel matrix. *Journal of Materials Chemistry A*, *2*, 8918-8925.

Jia, W., Guo, M., Zheng, Z., Yu, T., Rodriguez, E. G., Wang, Y., & Lei, Y. (2009). Electrocatalytic oxidation and reduction of H_2O_2 on vertically aligned Co_3O_4 nanowalls electrode: Toward H_2O_2 detection. *Journal of Electroanalytical Chemistry*, *625*, 27–32.

Jiang, B. B., Wei, X. W., Wu, F. H., Wu, K. L., Chen, L., Yuan, G. Z., Dong, C., & Ye, Y. (2014). A non-enzymatic hydrogen peroxide sensor based on a glassy carbon electrode modified with cuprous oxide and nitrogen-doped graphene in a nafion matrix. *Microchimica Acta*, *181*, 1463–1470.

Jiang, Y., Chen, D., Song, J., Jiao, Z., Ma, Q., Zhang, H., Cheng, L., Zhao, B., & Chu, Y. (2013). A facile hydrothermal synthesis of graphene porous NiO nanocomposite and its application in electrochemical capacitors. *Electrochimica Acta*, *91*, 173–178.

Jin, S., Chen, M., Dong, H., He, B., Lu, H., Su, L., Dai, W., Zhang, Q., & Zhang, X. (2015). Stable silver nanoclusters electrochemically deposited on nitrogen-doped graphene as efficient electrocatalyst for oxygen reduction reaction. *Journal of Power Sources*, *274*, 1173–1179.

Kafi, A. K. M., & Chen, A. (2009). A novel amperometric biosensor for the detection of nitrophenol. *Talanta*, *79*, 97–102.

Karuppiah, C., Palanisamy, S., Chen, S. M., Veeramani, V., & Periakaruppan, P. (2014). A novel enzymatic glucose biosensor and sensitive non-enzymatic hydrogen peroxide sensor based on graphene and cobalt oxide nanoparticles composite modified glassy carbon electrode. *Sensors and Actuators, B: Chemical*, *196*, 450–456.

Kauppila, J., Kunnas, P., Damlin, P., Viinikanoja, A., & Kvarnström, C. (2013). Electrochemical reduction of graphene oxide films in aqueous and organic solutions. *Electrochimica Acta*, *89*, 84–89.

Kaur, B., Pandiyan, T., Satpati, B., & Srivastava, R. (2013). Simultaneous and sensitive determination of ascorbic acid, dopamine, uric acid, and tryptophan with silver nanoparticles-decorated reduced graphene oxide modified electrode. *Colloids and Surfaces B: Biointerfaces*, *111*, 97–106.

Kelly, K. L., Coronado, E., Zhao, L. L., & Schatz, G. C. (2003). The optical properties of metal nanoparticles: The influence of size, shape, and dielectric environment. *The Journal of Physical Chemistry B*, *107*, 668–677.

Khorsand, Z. A., Majid, W. H. A., Wang, H. Z., Yousefi, R., Golsheikh, A. M., & Ren, Z. F. (2013). Sonochemical synthesis of hierarchical ZnO nanostructures. *Ultrasonics Sonochemistry*, *20*, 395–400.

Kim, G. P., Nam, I., Park, S., Park, J., & Yi, J. (2013). Preparation via an electrochemical method of graphene films coated on both sides with NiO nanoparticles for use as high-performance lithium ion anodes. *Nanotechnology*, *24*, 475402-475410.

Kim, H., Dugerjav, O., Lkhagvasuren, A., & Seo, J. M. (2016). Charge neutrality of quasi-free-standing monolayer graphene induced by the intercalated Sn layer. *Journal of Physics D: Applied Physics*, *49*, 135307-135314.

Kim, K. S., Zhao, Y., Jang, H., Lee, S. Y., Kim, J. M., Kim, K. S., Ahn, J. H., Kim, P., Choi, J. Y., & Hong, B. H. (2009). Large-scale pattern growth of graphene films for stretchable transparent electrodes. *Nature*, *457*, 706–710.

Kim, Y. T., Han, J. H., Hong, B. H., & Kwon, Y. U. (2010). Electrochemical Synthesis of CdSe quantum-Dot arrays on a graphene basal plane using mesoporous silica

thin-film templates. *Advanced Materials*, *22*, 515–518.

Kochmann, S., Hirsch, T., & Wolfbeis, O. S. (2012). Graphenes in chemical sensors and biosensors. *TrAC - Trends in Analytical Chemistry*, *39*, 87–113.

Kudin, K. N., Ozbas, B., Schniepp, H. C., Prud'homme, R. K., Aksay, I. a, & Car, R. (2008). Raman spectra of graphite oxide and functionalized graphene sheets. *Nano Letters*, *8*, 36–41.

Kumar, S. V., Huang, N. M., Lim, H. N., Zainy, M., Harrison, I., & Chia, C. H. (2013). Preparation of highly water dispersible functional graphene/silver nanocomposite for the detection of melamine. *Sensors and Actuators, B: Chemical*, *181*, 885–893.

Kurowska, E., Brzózka, a., Jarosz, M., Sulka, G. D., & Jaskuła, M. (2013). Silver nanowire array sensor for sensitive and rapid detection of H_2O_2. *Electrochimica Acta*, *104*, 439–447.

Kurt, B. Z., Durmus, Z., & Durmus, A. (2016). Preparation and characterization of platinum (Pt) and palladium (Pd) nanoparticle decorated graphene sheets and their utilization for the elimination of basic fuchsin and indigo carmine dyes. *Solid State Sciences*, *51*, 51–58.

Lambert, T. N., Chavez, C. a, Hernandez-sanchez, B., Lu, P., Bell, N. S., Ambrosini, A., Friedman, T., Boyle, T. J., Wheeler, D. R., & Huber, D. L. (2009). Synthesis and characterization of titania - graphene nanocomposites. *Journal of Physical Chemistry C*, *113*, 19812–19823.

Lee, Y. J., Park, J. Y., Kim, Y., & Ko, J. W. (2011). Amperometric sensing of hydrogen peroxide via highly roughened macroporous gold-platinum nanoparticles electrode. *Current Applied Physics*, *11*, 211–216.

Li, D., Müller, M. B., Gilje, S., Kaner, R. B., & Wallace, G. G. (2008). Processable aqueous dispersions of graphene nanosheets. *Nature Nanotechnology*, *3*, 101–105.

Li, J., Kuang, D., Feng, Y., Zhang, F., Xu, Z., & Liu, M. (2012). A graphene oxide-based electrochemical sensor for sensitive determination of 4-nitrophenol. *Journal of Hazardous Materials*, *201-202*, 250–259.

Li, J., & Liu, C. (2010). Ag/graphene heterostructures: Synthesis, characterization and optical properties. *European Journal of Inorganic Chemistry*, *2010*, 1244–1248.

Li, X., Heryadi, D., & Gewirth, A. A. (2005). Electroreduction activity of hydrogen peroxide on Pt and Au electrodes. *Langmuir*, *21*, 9251–9259.

Li, Y., Lu, Q., Wu, S., Wang, L., & Shi, X. (2013). Hydrogen peroxide sensing using ultrathin platinum-coated gold nanoparticles with core@shell structure. *Biosensors and Bioelectronics*, *41*, 576–581.

Li, Y., Tang, L., & Li, J. (2009). Preparation and electrochemical performance for methanol oxidation of pt/graphene nanocomposites. *Electrochemistry Communications*, *11*, 846–849.

Li, Y., Zhang, Y., Zhong, Y., & Li, S. (2015). Enzyme-free hydrogen peroxide sensor based on Au@Ag@C core-double shell nanocomposites. *Applied Surface Science*, *347*, 428–434.

Lian, W., Wang, L., Song, Y., Yuan, H., Zhao, S., Li, P., & Chen, L. (2009). A hydrogen peroxide sensor based on electrochemically roughened silver electrodes. *Electrochimica Acta*, *54*, 4334–4339.

Lightcap, I. V., Kosel, T. H., & Kamat, P. V. (2010). Anchoring semiconductor and metal nanoparticles on a two-dimensional catalyst mat. storing and shuttling electrons with reduced graphene oxide. *Nano Letters*, *10*, 577–583.

Lim, J. W., & Kang, I. J. (2013). Chitosan-gold nano composite for dopamine analysis using raman scattering. *Bulletin of the Korean Chemical Society*, *34*, 237–242.

Liu, J., Fu, S., Yuan, B., Li, Y., & Deng, Z. (2010). Toward a universal "adhesive nanosheet" for the assembly of multiple nanoparticles based on a protein-induced reduction/decoration of graphene oxide. *Journal of the American Chemical Society*, *132*, 7279–7281.

Liu, S., Tian, J., Wang, L., & Sun, X. (2011). A method for the production of reduced graphene oxide using benzylamine as a reducing and stabilizing agent and its subsequent decoration with Ag nanoparticles for enzymeless hydrogen peroxide detection. *Carbon*, *49*, 3158–3164.

Liu, Y., Sun, G., Jiang, C., Zheng, X. T., Zheng, L., & Li, C. M. (2013). Highly sensitive detection of hydrogen peroxide at a carbon nanotube fiber microelectrode coated with palladium nanoparticles. *Microchimica Acta*, *181*, 63–70.

Liu, Z., Du, J., Qiu, C., Huang, L., Ma, H., Shen, D., & Ding, Y. (2009). Electrochemical sensor for detection of p-nitrophenol based on nanoporous gold. *Electrochemistry Communications*, *11*, 1365–1368.

Lu, Z., Guo, C. X., Yang, H. Bin, Qiao, Y., Guo, J., & Li, C. M. (2011). One-step aqueous synthesis of graphene-CdTe quantum dot-composed nanosheet and its enhanced photoresponses. *Journal of Colloid and Interface Science*, *353*, 588–592.

Lung H. H., B., Wu, F. Y., Lin, C. T., Khlobystov, A. N., & Li, L. J. (2013). Graphene-modified $LiFePO_4$ cathode for lithium ion battery beyond theoretical capacity. *Nature Communications*, *4*, 1687-1694.

Luo, J., Cong, J., Liu, J., Gao, Y., & Liu, X. (2015). A facile approach for synthesizing molecularly imprinted graphene for ultrasensitive and selective electrochemical detecting 4-nitrophenol. *Analytica Chimica Acta*, *864*, 74–84.

Lyon, J. L., & Stevenson, K. J. (2006). Picomolar peroxide detection using a chemically activated redox mediator and square wave voltammetry. *Analytical Chemistry*, *78*, 8518–8525.

Ma, L., Ye, J., Chen, W., Chen, D., & Yang Lee, J. (2014). Gemini surfactant assisted hydrothermal synthesis of nanotile-like MoS_2/graphene hybrid with enhanced lithium storage performance. *Nano Energy*, *10*, 144–152.

Madhu, R., Karuppiah, C., Chen, S.-M., Veerakumar, P., & Liu, S. B. (2014). Electrochemical detection of 4-nitrophenol based on biomass derived activated carbons. *Analytical Methods*, *6*, 5274-5280.

Maduraiveeran, G., & Ramaraj, R. (2007). Gold nanoparticles embedded in silica sol-gel matrix as an amperometric sensor for hydrogen peroxide. *Journal of Electroanalytical Chemistry*, *608*, 52–58.

Marcano, D. C., Kosynkin, D. V., Berlin, J. M., Sinitskii, A., Sun, Z., Slesarev, A., Alemany, L. B., Lu, W., & Tour, J. M. (2010). Improved synthesis of graphene

oxide. *ACS Nano*, *4*, 4806–4814.

Marlinda, a. R., Huang, N. M., Muhamad, M. R., An'Amt, M. N., Chang, B. Y. S., Yusoff, N., Harrison, I., Lim, H. N., Chia, C. H., & Kumar, S. V. (2012). Highly efficient preparation of ZnO nanorods decorated reduced graphene oxide nanocomposites. *Materials Letters*, *80*, 9–12.

Matemadombo, F., & Nyokong, T. (2007). Characterization of self-assembled monolayers of iron and cobalt octaalkylthiosubstituted phthalocyanines and their use in nitrite electrocatalytic oxidation. *Electrochimica Acta*, *52*, 6856–6864.

Matsubara, C., Kawamoto, N., & Takamura, K. (1992). Oxo[5, 10, 15, 20-tetra(4-pyridyl)porphyrinato]titanium(IV): An ultra-high sensitivity spectrophotometric reagent for hydrogen peroxide. *The Analyst*, *117*, 1781-1784.

Mcallister, M. J., Li, J., Adamson, D. H., Schniepp, H. C., Abdala, A. A., Liu, J., Alonso, M. H., Milius, D.L., Car, R., Prud'homme, R. K., & Aksay, I. A. (2007). Single sheet functionalized graphene by oxidation and thermal expansion of graphite. *Society*, *19*, 4396–4404.

Mehta, V. N., & Kailasa, S. K. (2015). Malonamide dithiocarbamate functionalized gold nanoparticles for colorimetric sensing of Cu^{2+} and Hg^{2+} ions. *Rsc Advances*, *5*, 4245–4255.

Min, S., Zhao, C., Chen, G., & Qian, X. (2014). One-pot hydrothermal synthesis of reduced graphene oxide/$Ni(OH)_2$ films on nickel foam for high performance supercapacitors. *Electrochimica Acta*, *115*, 155–164.

Morales Torres, S., Pastrana Martinez, L. M., Figueiredo, J. L., Faria, J. L., & Silva, A. M. T. (2012). Design of graphene-based TiO_2 photocatalysts - A review. *Environmental Science and Pollution Research*, *19*, 3676–3687.

Morones, J. R., Elechiguerra, J. L., Camacho, A., Holt, K., Kouri, J. B., Ramirez, J. T., Yacaman, M. J. (2005). The bactericidal effect of silver nanoparticles. *Nanotechnology*, *16*, 2346–2353.

Nagl, S., & Wolfbeis, O. S. (2007). Optical multiple chemical sensing: Status and current challenges. *The Analyst*, *132*, 507–511.

Nair, R. R., Blake, P., Grigorenko, A. N., Novoselov, K. S., Booth, T. J., Stauber, T., Peres, N. M. R. & Geim, A. K. (2008). Fine structure constant defines visual transperency of graphene. *Science*, *320*, 1308-1308.

Niaz, A., Fischer, J., Barek, J., Yosypchuk, B., & Bhanger, M. I. (2009). Voltammetric determination of 4-nitrophenol using a novel type of silver amalgam paste electrode. *Electroanalysis*, *21*, 1786–1791.

Nickel, U., Castell, A. Z., Poppl, K., & Schneider, S. (2000). Silver colloid produced by reduction with hydrazine as support for highly sensitive surface-enhanced Raman spectroscopy. *Langmuir*, *16*, 9087–9091.

Nie, S. (1997). Probing single molecules and single nanoparticles by surface-enhanced raman scattering. *Science*, *275*, 1102–1106.

Noor, A. M., Rameshkumar, P., Huang, N. M., & Wei, L. S. (2016). Visual and spectrophotometric determination of mercury (II) using silver nanoparticles modified with graphene oxide. *Microchimica Acta*, *183*, 597-603.

Novoselov, K. S., Geim, A. K., Morozov, S. V., Jiang, D., Zhang, Y., Dubonos, S. V., Firsov, A.A., & Firsov, A. A. (2004). Electric field effect in atomically thin carbon films. *Science*, *306*, 666–669.

Novoselov, K. S., Geim, A. K., Morozov, S. V, Jiang, D., Katsnelson, M. I., Grigorieva, I. V, Dubonos, S. V., & Firsov, A. A. (2005). Two-dimensional gas of massless Dirac fermions in graphene. *Nature*, *438*, 197–200.

Nurzulaikha, R., Lim, H. N., Harrison, I., Lim, S. S., Pandikumar, A., Huang, N. M., Lim, S. P., & Ibrahim, I. (2015). Graphene/SnO_2 nanocomposite-modified electrode for electrochemical detection of dopamine. *Sensing and Bio-Sensing Research*, *5*, 42–49.

Pandikumar, A., Soon How, G. T., See, T. P., Omar, F. S., Jayabal, S., Kamali, K. Z., Yusoff, N., Jamil, A., Ramaraj, R., John, S. A., Lim, H. N., & Huang, N. M. (2014). Graphene and its nanocomposite material based electrochemical sensor platform for dopamine. *RSC Advances*, *4*, 63296–63323.

Paredes, J. I., Rodil, S. V., Alonso A. M., & Tascon, J. M. D. (2008). Graphene oxide

dispersions in organic solvents. *Langmuir*, *24*, 10560–10564.

Pavithra, C. L. P., Sarada, B. V, Rajulapati, K. V, Rao, T. N., & Sundararajan, G. (2014). A new electrochemical approach for the synthesis of copper-graphene nanocomposite foils with high hardness. *Scientific Reports*, *4*, 4049-4056.

Pol, V. G., Srivastava, D. N., Palchik, O., Palchik, V., Slifkin, M. A., Weiss, A. M., & Gedanken, A. (2002). Sonochemical deposition of silver nanoparticles on silica spheres. *Langmuir*, *18*, 3352–3357.

Qin, L., Li, X., Kang, S. Z., & Mu, J. (2015). Gold nanoparticles conjugated dopamine as sensing platform for SERS detection. *Colloids and Surfaces. B, Biointerfaces*, *126*, 210–216.

Qiu, Y., Wang, Z., Owens, A. C. E., Kulaots, I., Chen, Y., Kane, A. B., & Hurt, R. H. (2014). Antioxidant chemistry of graphene-based materials and its role in oxidation protection technology. *Nanoscale*, *6*, 11744–11755.

Radhakrishnan, S., Krishnamoorthy, K., Sekar, C., Wilson, J., & Kim, S. J. (2014). A highly sensitive electrochemical sensor for nitrite detection based on Fe_2O_3 nanoparticles decorated reduced graphene oxide nanosheets. *Applied Catalysis B: Environmental*, *148-149*, 22–28.

Ramesha, G. K., & Sampath, N. S. (2009). Electrochemical reduction of oriented graphene oxide films: An in situ Raman spectroelectrochemical study. *Journal of Physical Chemistry C*, *113*, 7985–7989.

Rameshkumar, P., Manivannan, S., & Ramaraj, R. (2013). Silver nanoparticles deposited on amine-functionalized silica spheres and their amalgamation-based spectral and colorimetric detection of Hg(II) ions. *Journal of Nanoparticle Research*, *15*, 1639-1649.

Rameshkumar, P., Viswanathan, P., & Ramaraj, R. (2014). Silicate sol-gel stabilized silver nanoparticles for sensor applications toward mercuric ions, hydrogen peroxide and nitrobenzene. *Sensors and Actuators, B: Chemical*, *202*, 1070–1077.

Raoof, J. B., Kiani, A., Ojani, R., Valiollahi, R., & Rashid-Nadimi, S. (2010). Simultaneous voltammetric determination of ascorbic acid and dopamine at the

surface of electrodes modified with self-assembled gold nanoparticle films. *Journal of Solid State Electrochemistry*, *14*, 1171–1176.

Raoof, J. B., Ojani, R., Hasheminejad, E., & Rashid-Nadimi, S. (2012). Electrochemical synthesis of Ag nanoparticles supported on glassy carbon electrode by means of p-isopropyl calix[6]arene matrix and its application for electrocatalytic reduction of H_2O_2. *Applied Surface Science*, *258*, 2788–2795.

Reddy, S., Kumara Swamy, B. E., & Jayadevappa, H. (2012). CuO nanoparticle sensor for the electrochemical determination of dopamine. *Electrochimica Acta*, *61*, 78–86.

Reina, A., Jia, X., Ho, J., Nezich, D., Son, H., Bulovic, V., Dresselhaus, M. S., & Kong, J. (2009). Large area, few-layer graphene films on arbitrary substrates by chemical vapor deposition. *Nano Letters*, *9*, 30–35.

Santhiago, M., Henry, C. S., & Kubota, L. T. (2014). Low cost, simple three dimensional electrochemical paper-based analytical device for determination of p-nitrophenol. *Electrochimica Acta*, *130*, 771–777.

Schniepp, H. C., Li, J. L., McAllister, M. J., Sai, H., Herrera-Alonson, M., Adamson, D. H., Prud'homme, R. K., Car, R., Saville, D. A., & Aksay, I. A. (2006). Functionalized single graphene sheets derived from splitting graphite oxide. *Journal of Physical Chemistry B*, *110*, 8535–8539.

Sevim, M., Francia, C., Amici, J., Vankova, S., Şener, T., & Metin, Ö. (2016). Bimetallic MPt (M: Co, Cu, Ni) alloy nanoparticles assembled on reduced graphene oxide as high performance cathode catalysts for rechargable lithium-oxygen batteries. *Journal of Alloys and Compounds*, *683*, 231–240.

Shahid, M. M., Rameshkumar, P., & Huang, N. M. (2015). Morphology dependent electrocatalytic properties of hydrothermally synthesized cobalt oxide nanostructures. *Ceramics International*, *41*, 13210–13217.

Shahid, M. M., Rameshkumar, P., Pandikumar, A., Lim, H. N., Ng, Y. H., & Huang, N. M. (2015). An electrochemical sensing platform based on a reduced graphene oxide–cobalt oxide nanocube@platinum nanocomposite for nitric oxide detection. *Journal of Materials Chemistry A*, *3*, 14458–14468.

Shen, J., Shi, M., Yan, B., Ma, H., Li, N., & Ye, M. (2011). One-pot hydrothermal synthesis of Ag-reduced graphene oxide composite with ionic liquid. *Journal of Materials Chemistry*.

Shi, Y., Liu, Z., Zhao, B., Sun, Y., Xu, F., Zhang, Y., Wen, Z., Yang, H., & Li, Z. (2011). Carbon nanotube decorated with silver nanoparticles via noncovalent interaction for a novel nonenzymatic sensor towards hydrogen peroxide reduction. *Journal of Electroanalytical Chemistry*, *656*, 29–33.

Shin, H. J., Kim, K. K., Benayad, A., Yoon, S. M., Park, H. K., Jung, I. S., Jin, M. H., Jeong, H. K., Kim, J. M., Choi, J. Y., & Lee, Y. H. (2009). Efficient reduction of graphite oxide by sodium borohydride and its effect on electrical conductance. *Advanced Functional Materials*, *19*, 1987–1992.

Si, Y., & Samulski, E. T. (2008). Synthesis of water soluble graphene. *Nano Letters*, *8*, 1679–1682.

Stankovich, S., Dikin, D. A., Piner, R. D., Kohlhaas, K. A., Kleinhammes, A., Jia, Y., Wu, Y., Nguyen, S. T. & Ruoff, R. S. (2007). Synthesis of graphene-based nanosheets via chemical reduction of exfoliated graphite oxide. *Carbon*, *45*, 1558–1565.

Staudenmaier, L. (1898). Verfahren zur darstellung der graphitsäure. *Berichte Der Deutschen Chemischen Gesellschaft*, *31*, 1481–1487.

Tang, J., Chen, Q., Xu, L., Zhang, S., Feng, L., Cheng, L., Xu, H., Liu, Z., & Peng, R. (2013). Graphene oxide−silver nanocomposite as a highly effective antibacterial agent with species-specific mechanisms. *ACS Applied Materials & Interfaces*, *5*, 3867-3874.

Tang, Y., Huang, R., Liu, C., Yang, S., Lu, Z., & Luo, S. (2013). Electrochemical detection of 4-nitrophenol based on a glassy carbon electrode modified with a reduced graphene oxide/Au nanoparticle composite. *Analytical Methods*, *5*, 5508-5514.

Teo, P. S., Lim, H. N., Huang, N. M., Chia, C. H., & Harrison, I. (2012). Room temperature in situ chemical synthesis of Fe_3O_4/graphene. *Ceramics International*, *38*, 6411–6416.

Thavanathan, J., Huang, N. M., & Thong, K. L. (2013). Colorimetric detection of DNA hybridization based on a dual platform of gold nanoparticles and graphene oxide. *Biosensors & Bioelectronics*, *55C*, 91–98.

Tian, J., Liu, S., Zhang, Y., Li, H., Wang, L., Luo, Y., Asiri, A. M., Youbi, A. O. A., & Sun, X. (2012). Environmentally friendly, one-pot synthesis of Ag nanoparticle-decorated reduced graphene oxide composites and their application to photocurrent generation. *Inorganic Chemistry*, *51*, 4742–4746.

Tien, H. W., Huang, Y. L., Yang, S. Y., Wang, J. Y., & Ma, C. C. M. (2011). The production of graphene nanosheets decorated with silver nanoparticles for use in transparent, conductive films. *Carbon*, *49*, 1550–1560.

Toh, S. Y., Loh, K. S., Kamarudin, S. K., & Daud, W. R. W. (2014). Graphene production via electrochemical reduction of graphene oxide: Synthesis and characterization. *Chemical Engineering Journal*, *251*, 422–434.

Tripathy, S. K., Mishra, A., Jha, S. K., Wahab, R., & Al-Khedhairy, A. A. (2013). Synthesis of thermally stable monodispersed Au@SnO_2 core-shell structure nanoparticles by a sonochemical technique for detection and degradation of acetaldehyde. *Analytical Methods*, *5*, 1456–1462.

Tuinstra, F., & Koenig, L. (1970). Raman spectrum of graphite. *The Journal of Chemical Physics*, *53*, 1126–1130.

Van Bommel, A. J., Crombeen, J. E., & Van Tooren, A. (1975). LEED and Auger electron observations of the SiC(0001) surface. *Surface Science*, *48*, 463–472.

Van Noorden, R. (2012). Production: Beyond sticky tape. *Nature*, *483*, 32–33.

Vijay Kumar, S., Huang, N. M., Lim, H. N., Marlinda, A. R., Harrison, I., & Chia, C. H. (2013). One-step size-controlled synthesis of functional graphene oxide/silver nanocomposites at room temperature. *Chemical Engineering Journal*, *219*, 217–224.

Wang, J., Sun, H. Bin, Pan, H. Y., Ding, Y. Y., Wan, J. G., Wang, G. H., & Han, M. (2016). Detection of hydrogen peroxide at a palladium nanoparticle-bilayer graphene hybrid-modified electrode. *Sensors and Actuators, B: Chemical*, *230*,

690–696.

Wang, Q. H., Jin, Z., Kim, K. K., Hilmer, A. J., Paulus, G. L. C., Shih, C. J., Ham, M. H., Yamagishi, J. D. S., Watanabe, K., Taniguchi, T., Kong, J., Herrero, P. J., & Strano, M. S. (2012). Understanding and controlling the substrate effect on graphene electron-transfer chemistry via reactivity imprint lithography. *Nature Chemistry*, *4*, 724–732.

Wang, S., Zhang, Y., Ma, H. L., Zhang, Q., Xu, W., Peng, J., Li, J., Yu, Z. Z., & Zhai, M. (2013). Ionic-liquid-assisted facile synthesis of silver nanoparticle-reduced graphene oxide hybrids by gamma irradiation. *Carbon*, *55*, 245–252.

Wang, X., Tabakman, S. M., & Dai, H. (2008). Atomic layer deposition of metal oxides on pristine and functionalized graphene. *Journal of the American Chemical Society*, *130*, 8152–8153.

Wang, Y., Li, Y., Tang, L., Lu, J., & Li, J. (2009). Application of graphene-modified electrode for selective detection of dopamine. *Electrochemistry Communications*, *11*, 889–892.

Welch, C. M., Banks, C. E., Simm, a. O., & Compton, R. G. (2005). Silver nanoparticle assemblies supported on glassy-carbon electrodes for the electro-analytical detection of hydrogen peroxide. *Analytical and Bioanalytical Chemistry*, *382*, 12–21.

Wu, S., & Meng, S. (2005). Preparation of ultrafine silver powder using ascorbic acid as reducing agent and its application in MLCI. *Materials Chemistry and Physics*, *89*, 423–427.

Wu, S., Yin, Z., He, Q., Lu, G., Yan, Q., & Zhang, H. (2011). Nucleation mechanism of electrochemical deposition of Cu on reduced graphene oxide electrodes. *Journal of Physical Chemistry C*, *115*, 15973–15979.

Wu, Z. S., Ren, W., Gao, L., Liu, B., Jiang, C., & Cheng, H. M. (2009). Synthesis of high-quality graphene with a pre-determined number of layers. *Carbon*, *47*, 493–499.

Wu, Z. S., Ren, W., Gao, L., Zhao, J., Chen, Z., Liu, B., Tang, D., Yu, B., Jiang, C., &

Cheng, H. M. (2009). Synthesis of graphene sheets with high electrical conductivity and good thermal stability by hydrogen arc discharge exfoliation. *ACS Nano*, *3*, 411–417.

Xie, G., Cheng, J., Li, Y., Xi, P., Chen, F., Liu, H., Hou, F., Shi, Y., Huang, L., Xu, Z., Bai, D., & Zeng, Z. (2012). Fluorescent graphene oxide composites synthesis and its biocompatibility study. *Journal of Materials Chemistry, 22*, 9308-9314.

Xu, C., Yuan, R., & Wang, X. (2014). Selective reduction of graphene oxide. New *Carbon Materials*, *29*, 61-66.

Xu, X., Zhang, H., Shi, H., Ma, C., Cong, B., & Kang, W. (2012). Determination of three major catecholamines in human urine by capillary zone electrophoresis with chemiluminescence detection. *Analytical Biochemistry*, *427*, 10–17.

Xue, L., Shen, C., Zheng, M., Lu, H., Li, N., Ji, G., Pan, L., & Cao, J. (2011). Hydrothermal synthesis of graphene-ZnS quantum dot nanocomposites. *Materials Letters*, *65*, 198–200.

Yang, J., & Gunasekaran, S. (2013). Electrochemically reduced graphene oxide sheets for use in high performance supercapacitors. *Carbon*, *51*, 36–44.

Yang, S. T., Chen, S., Chang, Y., Cao, A., Liu, Y., & Wang, H. (2011). Removal of methylene blue from aqueous solution by graphene oxide. *Journal of Colloid and Interface Science*, *359*, 24–29.

Yang, X., Bai, J., Wang, Y., Jiang, X., & He, X. (2012). Hydrogen peroxide and glucose biosensor based on silver nanowires synthesized by polyol process. *The Analyst*, *137*, 4362–4367.

Yao, Y., Xu, C., Miao, S., Sun, H., & Wang, S. (2013). One-pot hydrothermal synthesis of Co(OH)2 nanoflakes on graphene sheets and their fast catalytic oxidation of phenol in liquid phase. *Journal of Colloid and Interface Science*, *402*, 230–236.

Yin, H., Zhou, Y., Ai, S., Ma, Q., Zhu, L., & Lu, L. (2012). Electrochemical oxidation determination and voltammetric behaviour of 4-nitrophenol based on Cu_2O nanoparticles modified glassy carbon electrode. *International Journal of Environmental Analytical Chemistry*, *92*, 742–754.

Yin, Z., Wu, S., Zhou, X., Huang, X., Zhang, Q., Boey, F., & Zhang, H. (2010). Electrochemical deposition of ZnO nanorods on transparent reduced graphene oxide electrodes for hybrid solar cells. *Small (Weinheim an Der Bergstrasse, Germany)*, *6*, 307–312.

Yu, G., Hu, L., Vosgueritchian, M., Wang, H., Xie, X., McDonough, J. R., Cui, X., Cui, Y., & Bao, Z. (2011). Solution-processed graphene/MnO_2 nanostructured textiles for high-performance electrochemical capacitors. *Nano Letters*, *11*, 2905–2911.

Yu, Q., Lian, J., Siriponglert, S., Li, H., Chen, Y. P., & Pei, S. S. (2008). Graphene segregated on Ni surfaces and transferred to insulators. *Applied Physics Letters*, *93*, 113103-113105.

Yusoff, N., Huang, N. M., Muhamad, M. R., Kumar, S. V., Lim, H. N., & Harrison, I. (2013). Hydrothermal synthesis of CuO/functionalized graphene nanocomposites for dye degradation. *Materials Letters*, *93*, 393–396.

Zainy, M., Huang, N. M., Vijay Kumar, S., Lim, H. N., Chia, C. H., & Harrison, I. (2012). Simple and scalable preparation of reduced graphene oxide–silver nanocomposites via rapid thermal treatment. *Materials Letters*, *89*, 180–183.

Zangeneh Kamali, K., Pandikumar, A., Sivaraman, G., Lim, H. N., Wren, S. P., Sun, T., & Huang, N. M. (2015). Silver@graphene oxide nanocomposite-based optical sensor platform for biomolecules. *RSC Advances*, *5*, 17809–17816.

Zeng, Y., Zhou, Y., Zhou, T., & Shi, G. (2014). A novel composite of reduced graphene oxide and molecularly imprinted polymer for electrochemical sensing 4-nitrophenol. *Electrochimica Acta*, *130*, 504–511.

Zhang, D., Hu, B., Guan, D., & Luo, Z. (2016). Essential roles of defects in pure graphene/Cu_2O photocatalyst. *Catalysis Communications*, *76*, 7–12.

Zhang, H., Sun, J. T., Yang, H., Li, L., Fu, H., Meng, S., & Gu, C. (2016). Tunable magnetic moment and potential half-metal behavior of Fe-nanostructure-embedded graphene perforation. *Carbon*, *107*, 268–272.

Zhang, N., Qiu, H., Liu, Y., Wang, W., Li, Y., Wang, X., & Gao, J. (2011). Fabrication of gold nanoparticle/graphene oxide nanocomposites and their excellent catalytic performance. *Journal of Materials Chemistry*, *21*, 11080–11083.

Zhang, X., Ning, J., Li, X., Wang, B., Hao, L., Liang, M., Jin, M., & Zhi, L. (2013). Hydrogen-induced effects on the CVD growth of high-quality graphene structures. *Nanoscale*, *5*, 8363–8366.

Zhang, Y., Li, B., & Chen, X. (2010). Simple and sensitive detection of dopamine in the presence of high concentration of ascorbic acid using gold nanoparticles as colorimetric probes. *Microchimica Acta*, *168*, 107–113.

Zhang, Y., Liu, S., Wang, L., Qin, X., Tian, J., Lu, W., Chang, G., Sun, X. (2012). One-pot green synthesis of Ag nanoparticles-graphene nanocomposites and their applications in SERS, H_2O_2 , and glucose sensing. *RSC Advances*, *2*, 538–545.

Zhao, H., Fu, H., Tian, C., Ren, Z., & Tian, G. (2010). Fabrication of silver nanoparticles/single-walled carbon nanotubes composite for surface-enhanced Raman scattering. *Journal of Colloid and Interface Science*, *351*, 343–347.

Zheng, L., Cheng, X., Cao, D., Wang, G., Wang, Z., Xu, D., Xia, C., Shen, L., Yu, Y., & Shen, D. (2014). Improvement of Al_2O_3 films on graphene grown by atomic layer deposition with pre-H_2O treatment. *ACS Applied Materials and Interfaces*, *6*, 7014–7019.

Zhou, X., Huang, X., Qi, X., Wu, S., Xue, C., Boey, F. Y. C., Yan, Q., Chen, P., & Zhang, H. (2009). In situ synthesis of metal nanoparticles on single-layer graphene oxide and reduced graphene oxide surfaces, *The Journal of Physical Chemistry C*, 113, 10842–10846.

Zhu, C., Guo, S., Fang, Y., & Dong, S. (2010). Reducing sugar: New functional molecules for the green synthesis of graphene nanosheets. *ACS Nano*, *4*, 2429–2437.

Zhu, C., Guo, S., Fang, Y., Han, L., Wang, E., & Dong, S. (2011). One-step electrochemical approach to the synthesis of graphene/MnO_2 nanowall hybrids. *Nano Research*, *4*, 648–657.

Zhu, Y., Murali, S., Cai, W., Li, X., Suk, J. W., Potts, J. R., & Ruoff, R. S. (2010). Graphene and graphene oxide: Synthesis, properties, and applications. *Advanced Materials*, *22*, 3906–3924.

LIST OF PUBLICATIONS AND PAPERS PRESENTED

Publications

[1] **An'amt Mohamed Noor**, Perumal Rameshkumar, Lee Seong Wei and Huang Nay Ming. (2016). Visual and spectrophotometric determination of mercury(II) using silver nanoparticles modified with graphene oxide. *Microchimica Acta*, 183, 597-603.

[2] **An'amt Mohamed Noor**, Muhammad Mehmood Shahid, Perumal Rameshkumar and Huang Nay Ming. (2016). A glassy carbon electrode modified with graphene oxide and silver nanoparticles for amperometric determination of hydrogen peroxide. *Microchimica Acta*, 183, 911-916.

[3] **An'amt Mohamed Noor**, Perumal Rameshkumar, Norazriena Yusoff, Huang Nay Ming, Mohd Shaiful Sajab. (2016). Microwave synthesis of reduced graphene oxide decorated with silver nanoparticles for electrochemical determination of 4-nitrophenol. *Ceramics International*, 42, 18813-18820.

Paper presented in international conference:

1. **An'amt Mohamed Noor** and Huang Nay Ming, " Rapid Heat Treatment Synthesis of Reduced Graphene Oxide Uniformly Decorated with Nickel Oxide Nanoparticles for Antioxidant Activities" in 2nd Edition Smart Materials & Surfaces Conference, SMS Korea 2016, 23-25 March 2016, Incheon, Korea.